DYNAMIC INTERACTION IN ELEVATED BRIDGE SYSTEM AND ITS EVALUATION BY PARALLEL PSEUDO-DYNAMIC TEST

A thesis submitted to the Faculty of Engineering of Kyoto University in partial fulfillment of the requirements for the Degree of Doctor of Engineering

by
Kazutoshi Nagata

July 2004

Abstract

An Elevated bridge so called viaduct is a structural system consisting of foundation, pier, bearing and superstructure. This structural system has played an important role in the construction of roadways as well as railways in urban areas. During the Hyogoken-Nanbu Earthquake, which was a near field earthquake, highway networks such as the Hansin Expressway were severely damaged by the strong ground motion. Even though there have been significant developments in the design of earthquake-resistant structures, the damages sustained by the Hyogoken-Nanbu Earthquake have motivated engineers to take into consideration the interaction of each structural component on the performance of the overall structural system. In this study, the seismic response of elevated bridges and the methods for evaluating this response were assessed with consideration paid to the dynamic interaction of each component of the elevated bridge system.

First, the dynamic interaction of an elevated bridge system consisting of steel and RC piers was investigated, where the elevated bridge was simply modeled by a series of mass-spring-dashpot systems. The restoring force characteristics, such as bilinear, trilinear, or a combination of these simple models, were utilized in this study. Furthermore, the strength-degrading trilinear restoring force characteristics for steel piers considering the local buckling of stiffened steel panels, and the stiffness-degrading trilinear restoring force characteristics for RC piers considering cracking and yielding were used. In addition, the dimensions of the bridge pier model in this analysis were determined according to the RC piers and steel piers of an existing elevated bridge system of the Kobe Line of the Hanshin Expressway. It was demonstrated by the numerical simulation that in a hybrid system with steel and RC piers whose restoring force characteristics generally differ from each other, the joint response among their adjacent members may be considerably different from their independent responses. Namely, steel and RC piers are mutually influenced; the joint response depends on the combination of restoring force characteristics. Therefore, an earthquake-resistant design should be made by balancing the strength and ductility of each pier with a consideration of the redistribution of the seismic forces acting on superstructures. Consequently, structural elements such as girders, piers and bearings should be designed by considering their inter-dependency on the overall response.

Secondly, special emphasis was placed on the nonlinear dynamic interaction of the foundation-structure system. The equation of motion for such a structural system was simply modeled by a three degree-of-freedom system allowing for the sway of the superstructure, and the sway and rocking of the foundation, in which restoring force characteristics were modeled by a bilinear relation. The effects of both the yielding strength and the tangential second stiffness of the bilinear restoring force on the structural damage were assessed. It was concluded from the parametric analysis varying yield restoring force and tangent stiffness in the plastic range that damages tend to be localized to the weakest degree-of-freedom of

the structural system and that there is significant interaction between the response of the superstructure and the rocking of foundation.

Thirdly, the effect of beam-column interaction on the frame-type steel pier was investigated, since steel rigid-frame piers were damaged by local buckling of the beam web plates and column flange plates as well as brittle cracking at the beam-column connections during the 1995 Hyogoken-Nanbu Earthquake. In order to understand the horizontal load carrying capacity and ductility of such piers, that is, in order to understand the in-plane collapse mechanism, a static loading test and a finite element analysis were carried out. A pseudo-dynamic test was also carried out to assess the seismic performance of such piers. It was found that a steel rigid-frame pier can have the stiffness as high as the initial elastic one until two plastic hinges are formed, and that the ultimate state may be obtained when four plastic hinges are formed.

In addition, studied are the strength interactions of structural elements under a biaxial loading condition and their effects on the seismic response of structures were studied. In order to assess such an interaction; i.e., the elasto-plastic response of steel box piers subjected to strong ground motions in two horizontal directions, a pseudo-dynamic test was carried out. In addition, elasto-plastic finite displacement analyses were carried out to further clarify the complex behavior. Moreover, a simple elasto-plastic response method of analyzing the spring-mass system while considering the correlation of strength in two orthogonal directions was proposed. It was found that the strength and ductility of steel piers under biaxial loading conditions may be reduced, and thus the displacement response may tend to increase, compared to those under a uniaxial loading condition. It was also verified that the proposed simple analysis method can be used to evaluate the seismic response of a structural system under 3-D earthquake loads.

Finally, in order to assess the dynamic interaction of a structural system with multi-degrees-of-freedom, a versatile evaluation method was proposed, namely, a parallel pseudo-dynamic testing system using the Internet. At first, an error propagation in response evaluation by the proposed system was assessed, where the system has been established by connecting experimental stations located at Osaka City University and Kyoto University through the Internet. Then, the feasibility of the proposed system for the international connection of testing and computing facilities was assessed. For this purpose, a link was established among Korea Advanced Institute of Science and Technology (KAIST) in Korea, the State University of New York at Buffalo in the U.S.A., Monash University in Australia, and Osaka City University and Kyoto University in Japan. Moreover, among Osaka City University, KAIST and Kyoto University, international collaborative testing was carried out using this proposed method. The results demonstrated that the proposed system was very effective and the network security can be accomplished in high level for carrying out the response evaluation.

Acknowledgments

The author is deeply grateful and indebted to his academic advisor, Professor Eiichi Watanabe, Chair of Structural Engineering in the Department of Civil and Earth Resources Engineering, Kyoto University, for his crucial guidance, encouragement and support throughout this study. Sincere thanks are also extended to Professor Hirokazu Iemura of the Department of Urban Management and Associate Professor Kunitomo Sugiura of the Department of Urban and Environmental Engineering for their detailed review of this dissertation.

The author also wishes to express his grateful appreciation to Professor Toshiyuki Kitada of Osaka City University, Professor Chung-Bang Yun of Korea Advanced Institute of Science and Technology, Professor George C. Lee and Professor Andrei M. Reinhorn of State University of New York at Buffalo and Professor Xiao-Ling Zhao of Monash University for their kind cooperation in allowing me to use the experimental facilities and computer networks of their institutions for developing the parallel pseudo-dynamic test using the Internet.

Special thanks are also due to Associate Professor Tomoaki Utsunomiya of Kyoto University for his consistent support, and to Associate Professor Takashi Yamaguchi of Osaka City University for his valuable advice and continuous encouragement. Acknowledgment goes to Dr. Shigeki Okashiro of NEWJEC, Dr. Yukihide Kajita of National Defense Academy, and Dr. Yasuo Kitane of Simpson Gumpertz & Heger Inc. for their useful assistance.

Behavior of steel rigid-frame piers was investigated with Hanshin Expressway Public Corporation. The author is grateful to excellent engineers of Hanshin Expressway Public Corporation. The author wishes to extend appreciation to Mr. Yasuhiro Miyasaka and Mr. Kiyoshi Fujino for manufacturing the specimens and apparatus of loading test. The author also wishes to extend appreciation to Dr. Kazuhisa Niwa of JIP Techno Science Corporation for the development of the program for a parallel pseudo-dynamic test.

The author is thankful to Mr. Dong-Uk Park of Korea Advanced Institute of Science and Technology for his kind cooperation. The author is also thankful for the perfect assistance of the former graduate students of the Structural Engineering Laboratory, Yoshikazu Suzuka, Ryo Kunishi, Hideyuki Suzuki, Masaki Takei, Kiyoto Nakamura and Kazuki Hiroshima, and to Isao Tamura, Takashi Okafuji, Taku Okamoto and Takato Ozeki et al. of the Structural Engineering Laboratory for their help.

Finally, the author expresses his deep appreciation to his parents, Mr. Tazo Nagata and Mrs. Keiko Nagata, for their infinite affection and complete devotion for the completion of this dissertation. This dissertation is dedicated to my family.

Table of Contents

Chapter 1

Introduction

1.1 Characteristics of the Hyogoken-Nanbu Earthquake

The Hyogoken-Nanbu Earthquake occurred at 5:46 AM on 17 January 1995, Japanese time. The hypocenter was estimated to be just below the northern part of Awaji Island. The earthquake was caused by a series of movements of active faults running below the northern part of Awaji Island and the Hanshin (Kobe to Osaka) Area (Abiko Research Laboratory, 1995; Nakamura et al., 1995, 1995). The 7.2-magnitude shock inflicted unprecedented damage on a wide area from the northern part of Awaji Island to the Hanshin Area. The Meteorological Agency graded the maximum seismic intensity as 7 on the Japanese scale of 7, making it the worst earthquake natural disaster in Japanese history (Taisei Corporation, 1995). The lives of about 6,300 people were lost, and about 200,000 houses and office buildings were destroyed with a total economic loss estimated at US $100 billion.

The features of the motion of this earthquake are described in the following (Hanshin Expressway Public Corporation, 1997). Fig. 1.1 shows the ground acceleration records and acceleration response spectrum (damping factor h=0.05) of the NS, EW and UD components recorded at Kobe Marine Meteorological Observatory (Ground Type I), JR-Takatori station (Ground Type II) and Higashi Kobe Bridge (Ground Type III). The maximum acceleration of 818 gal (cm/s^2) in the NS component at the Kobe Marine Meteorological Observatory confirms that the Hyogoken-Nanbu Earthquake is the largest earthquake ever experienced by a highly populated city in Japan. The maximum acceleration response spectrum of all observation points is more than 1,000 gal (cm/s^2), and the structures in the natural period zone were subjected to an extremely large inertial force. Fig. 1.2 shows a displacement trace of the bidirectional horizontal ground motions at each of the three points mentioned above. It can be seen that the direction of earthquake motion changed each moment, and the main direction of the shaking was in the northwest-southeast direction (perpendicular to the direction of most of the lifeline systems).

1.2 General Remarks on Structural Damage

The collapse of road and railway viaducts and other major infrastructural components during the Hyogoken-Nanbu Earthquake was an unprecedented shock (Inside Newsletter, 1995). The probable

frequency of a large near-field earthquake occurring in the Hanshin Area was thought to be one in every 500 or 1,000 years. Most of the severely damaged structures were found to have been designed and constructed before modern earthquake-resistant design codes were established. For example, the Kobe Line (Route 3) of the Hanshin Expressway came into service during the period between 1966 and 1970, whereas the provisions for modern earthquake-resistant design in the Japanese specifications for the highway bridges were made in 1971, 1980 and 1990 (Nakamura et al., 1995). Shown in Table 1.1 and 1.2 are the results of a damage study on the Kobe Line of the Hanshin Expressway (Committee on Roadway Bridges by the Hyogoken-Nanbu Earthquake, 1995, 1995). The Sanyo New Line (Shinkansen) was also designed according to the older specifications for Shinkansen implemented in 1966. These infrastructures had been basically designed to be earthquake-resistant using the seismicity coefficient method assuming an elastic acceleration response of only 200-300 gal. The specifications (JRA, 1990, 1990, 1994) were implemented considering new findings from damages sustained during large historical earthquakes, such as the Miyagiken-Oki earthquake. Compared with these infrastructures, most of the main structural frames of the bridges on Bay Line (Route 5) of the Hanshin Expressway were relatively undamaged (Table 2) (Committee on Roadway Bridges by the Hyogoken-Nanbu Earthquake, 1995).

An exceptional case was the Nishinomiya Harbor Bridge, running in the EW direction, where the simply-supported steel box girder of the eastern side span (52m) adjacent to the main span of a Nielsen arch bridge (span length 252m) fell to the ground due to the horizontal movement of the eastern foundation and pier of the main span, presumably due to liquefaction, as shown in Photo 1.1.

1.3 Damage to Steel Bridges

For the first time in history, steel bridge piers suffered significant damage due to an earthquake (Nakamura et al., 1995; Obayashi Technical Research Institute, 1995; Takenaka Corporation, 1995; Yamaguchi, 1993). Concrete piers have been commonly constructed all over Japan; however, steel piers have been constructed only in limited regions, such as in large Japanese cities where the construction sites rest on soft alluvial deposits. Fortunately, most of these cities have not yet experienced a large earthquake since the Great Kanto earthquake in 1923. From the results of field investigations, typical damage to the steel bridge piers may be classified as: (a) local buckling; (b) brittle crack failure; or (c) low-cycle fatigue failure. Each type of damage is briefly described below.

The first type of damage, namely local buckling of steel bridge piers, was seen for the first time in the Hyogoken-Nanbu Earthquake. Photo 1.2 shows a case of local buckling of a rectangular cross-section of bridge piers, while Photo 1.3 shows a case of local buckling of the circular cross-section of

bridge piers, or so-called ‘elephant-foot’ buckling. Most of the steel bridge piers were composed of thin-walled cross-sections such as stiffened panels and cylindrical shells, and such thin plate/shell elements may undergo local buckling in response to bending-induced compression. Although it remains a subject controversy whether or not a main cause of elephant-foot buckling is the impulsive vertical shock induced by the near-field earthquake, alternating buckling of outer thin walls due to bending has been verified to be predominant by a static loading test in the laboratory on scaled bridge pier models (Yamaguchi, 1993). In particular, an axisymmetric buckling shape of the elephant-foot type for circular cross-sections can be easily misattributed to the impulsive force in the vertical direction. If this were the case, buckling should have occurred only at the cross-sections of thinner walls, but this did not always occur.

The second type of damage, brittle crack failure of microscopic dimension, has sometimes been witnessed on bridges under daily traffic loads. Also, cracks were reported to have occurred in the connections of steel bridges and buildings due to large earthquakes in the past. However, during the Hyogoken-Nanbu Earthquake, such damage was more prevalent and of larger dimensions. Photo 1.4 shows a case of brittle crack of a bridge pier of the rigid frame-type. The damage to the upper corner of the pier may be attributed to the simultaneous action of liquefaction of the bridge foundation and an adverse combination of big-impact ground velocities in the horizontal and vertical directions at freezing temperatures. Similar cracks have also been reported in the columns of high-rise apartment buildings (Takenaka Corporation, 1995). These types of damage require engineers to urgently develop welding details to protect against excessive deformation of corners.

The third type of damage, low-cycle fatigue failure, may be considered intermediary between the first and the second type. This is characterized by alternatively local buckling accompanied by the occurrence of tensile cracks. Photo 1.5 provides an example. Although steel is a ductile material, excessive plastic deformation makes steel brittle. Therefore, structural details should also be developed to prevent such accumulation of plastic deformation due to local buckling.

In addition to the above-mentioned damage to bridge piers, the following damages were also reported:

(a) Damage to bearing devices, seismic connectors of girders and expansion joints (Photo 1.6).
(b) Excessive horizontal bending deformation of girder ends (e.g., knee-braced) (Photo 1.7).
(c) Buckling of girders due to the collapse of supporting piers (Photo 1.8).
(d) Damage to superstructures due to bouncing and stamping on hard obstacles (Photo 1.9).
(e) Buckling of struts connecting arch ribs (Photo 1.10).
(f) Loosening of cables in Nielsen arch bridges at the anchor sockets (Photo 1.11).
(g) Bidirectional ‘x-shaped’ panel shear buckling in beam members of frame-type bridge piers (Photo

1.12).

(h) Plastic elongation of anchor bolts connecting steel bridge piers and anchor frames at the footing.

(i) Sliding of bolted connections.

(j) Cracks in bearing piles beneath the footings.

1.4 State of the Art on Dynamic Interaction of Elevated Bridge Systems and Seismic Design

Although elevated bridges are an important part of the infrastructure of the transportation network system both for the daily use of citizens and for supporting economic activities, these functions were instantly cut by the severe damage to bridges following the Hyogoken-Nanbu Earthquake. In the urgent report after the disaster, Iemura and Izuno (Nakamura, et al., 1995) focused on the interaction between piers. Fujino also emphasized that the seismic design of structures must be applied globally and interactively to the whole system, rather than individually to single components (Nikkei Construction, 1995). Moreover, Imoto described the necessity of seismic design in consideration of the interaction of bridge systems based on analyses of the damage to steel bridges in the report of the meeting of the Kansai branch of the Japan Society of Civil Engineers (Toki, et al., 1996).

In 1923, Japan became the first country to adopt the seismic coefficient method (Seismic intensity: 0.1) for the seismic design of elevated bridges. Ever since, whenever earthquake damage has occurred, the seismic coefficient method has been modified, and the seismic intensity has been changed. Seismic design that accounted for nonlinear behavior was finally adopted in 1990 (JRA, 1990). Although the dynamic analysis of elevated bridges was prescribed in the revision of the seismic design specifications after the Hyogoken-Nanbu Earthquake, dynamic interaction is not clearly described in the present seismic design specifications for Highway Bridges (JRA, 1996). Therefore, research on various dynamic interactions of the structural system has been carried out after the earthquake disaster as summarized below.

Research on the dynamic interaction of an elevated bridge system has been carried out as shown in the following. Fujino et al. (1997) demonstrated the optimal design of bearings in a bridge system using a simple linear two-degrees-of-freedom bridge model, and also investigated the optimal allocation method of damage to a bridge system under very severe ground motion. Izuno et al. (1997) carried out numerical simulations to clarify the effect of an adjacent RC pier on the seismic response of a steel pier. An optimal damage-allocation method that considered the seismic performance of the total structural system was proposed by Shoji et al. (1997). Optimization of passive energy dissipation devices, such as isolator bearings, to improve the seismic performance of elevated bridges was also studied by Abe et al. (1998).

Seismic interaction between a long-span bridge and an adjacent approach bridge was examined by Izuno et al. (1999). Nakajima et al. (2000, 2001) investigated the dynamic response behavior of a viaduct system designed by the seismic coefficient method during a severe earthquake. In addition, the relative velocity response and the seismic collision velocity between the adjacent bridges were studied by Takeno et al. (2001).

Housner and Merritt et al. (1954, 1956) were the first to analyze the ground beneath a building as a coiled spring. This was the first research about the dynamic interaction of a soil-foundation-structure system (Sato et al., 1989). Other authors have since investigated this dynamic interaction further (Toki, 1981). However, the dynamic interaction of the soil-foundation-structure system is not dealt with precisely in the Japanese Seismic Design Specification for Highway Bridges. After the Hyogoken-Nanbu Earthquake, clarifying the dynamic interaction of the soil-foundation-structure system for elevated bridges was considered one of the most urgent tasks. The strength-demand spectrum taking into account the soil-structure interaction was studied by Toki et al. (1998). Yabe et al. (1999) examined the effect of the yield-strength ratio of the column and pile foundation on the plastic deformation of a pile foundation. Nakajima (1999) investigated the damping characteristics of a pier-foundation-soil system with consideration paid to the material damping of the pier and energy radiation from the foundation to the ground. Nonlinear seismic response of a pile foundation and its push-over analysis was assessed by Yabe et al. (1999). The seismic behavior of steel bridge piers or multi-span continuous bridges with steel piers considering soil-structure interaction was evaluated by Kasai et al. (2000, 2002). The response spectrum considering the dynamic interaction of the foundation-soil-structure system was studied by Yamashita (2001). A nonlinear seismic response analysis of the dynamic soil-structure interaction was carried out by Kimura et al. (2001), and the elasto-plastic dynamic analysis of steel bridge piers in consideration of plate buckling and ground behavior was carried out by Nara et al. (2002).

Steel piers can be roughly classified as either single-column piers or rigid-frame piers. Before the Hyogoken-Nanbu Earthquake, although numerous researches on the strength and ductility of single-column piers had been carried out, few studies were performed on rigid-frame piers, since these piers were considered statically indeterminate structures that they were likely to have high deformability. However, during the 1995 Hyogoken-Nanbu Earthquake, many steel rigid-frame piers were damaged by local buckling and brittle crack failure due to cyclic loading, and thus research into their failure has become crucial. This research can be classified into four general areas as follows.

(a) Strength and ductility (Usami et al.,1999; Nishikawa et al., 1999; Yamada et al., 2000; Suzuki et al., 2000; Kitamura et al., 2002; Ozawa et al., 2002).

(b) Seismic response behavior (Miki et al., 1997, 1999, 2000, 2001; Kodama et al., 2000).

(c) Behavior of the beam-to-column connection (Miki et al., 1997; Aoki et al., 1997; Yamaguchi et al., 2000).

(d) Seismic design method (Shiraki et al., 2000; Nakajima et al., 1998; Morishita et al., 2000; Ikeda et al., 1998).

In general, the ability of bridges to withstand strong earthquakes may be assessed in both the direction of the bridge axis and the direction perpendicular to the bridge axis. Building structures are also assessed by applying the design earthquake loads independently to two directions orthogonal each other. After the Hyogoken-Nanbu Earthquake, the Architectural Institute of Japan started to investigate the spatial response of building structures, including the torsional response caused by the incoincidence of gravity center and stiffness center, such as in buildings with irregularly located columns (AIJ, 1998). On the other hand, for seismic design specifications in other countries, the CQC (Complete Quadratic Combination), 30 percent Rule, or 40 percent Rule may be found in the American specifications (AASHTO, 1996). However, these rules were developed based on the elastic response of structures, such as the random vibration theory. There has been little research on the behavior of steel piers subjected to strong ground motions in two horizontal directions. The effects of multidirectional displacement paths on the cyclic behavior of rectangular hollow steel columns were investigated statically by Watanabe et al., 2000. Elasto-plastic three-dimensional dynamic response analyses of bridge piers modeled on a rigid-body spring have also been conducted (Oide et al., 2000)

Structural design is often carried out through such a complex analysis to assure safety against excessive loading. However, there are still many problems in the mathematical modeling of nonlinear structural behavior, so an experimental evaluation procedure may be inevitable. A semi-analytical method of combining analysis with experiments, a process known as “hybrid testing”, has been developed (Hakuno et al., 1969). This method has been utilized particularly for the evaluation of the dynamic response of structures and is also referred to as “pseudo-dynamic testing” (Iemura, 1985; Nakashima et al., 1990-1993; Nishizawa et al., 1988, 1989; Saizuka et al., 1995; Sato et al., 1994; Takanashi et al., 1987; Usami et al., 1995; Watanabe et al., 1994). The advanced improvement of this testing system has been carried out. This system has played a large role in the elucidation of the nonlinear dynamic response of structures in civil and architectural engineering fields.

1.5 Objectives and Scope

An elevated bridge is a structural system consisting of foundations, piers, bearings and superstructures. During the Hyogoken-Nanbu Earthquake, the Hanshin Expressway was significantly damaged due to

strong ground motion in three dimensions, especially in the direction perpendicular to the highway network line. Therefore, in order to improve the seismic performance of elevated bridges, it is necessary to clarify the dynamic interaction among the parts of the structural system. In this study, the dynamic interaction of elevated bridges of the Hanshin Expressway was mainly assessed. More specifically, this study focuses on

(a) the assessment of the seismic behavior and dynamic interaction of an elevated bridge system;

(b) the evaluation of the nonlinear dynamic interaction of a foundation-structure system;

(c) the elucidation of the collapse processes and seismic performances of steel rigid-frame piers subjected to in-plane horizontal loads;

(d) the assessment of the seismic performance of steel bridge piers subjected to bidirectional horizontal ground motions; and

(e) the development of a parallel pseudo-dynamic testing system and evaluation of the seismic behavior of elevated bridges.

In Chapter 1, the Hyogoken-Nanbu Earthquake and the current status of the dynamic interaction and the seismic design of elevated bridges are described.

In Chapter 2, the dynamic interaction of an elevated bridge system consisting of steel and RC piers investigated by a bridge model made up of a series of mass-spring-dashpot systems is assessed. The restoring force characteristics of each structural element utilized in the analysis are either bilinear, trilinear, or a combination thereof. In particular, the bridge piers in this analysis are modeled according to the RC piers and steel piers of an existing elevated bridge system on the Kobe Line of the Hanshin Expressway. The strength-degrading trilinear restoring force characteristics for steel piers are used considering the local buckling of stiffened panels and stiffness-degrading tri-linear restoring force characteristics of RC piers considering cracking and yielding.

In Chapter 3, the effects of restoring the force characteristics of the nonlinear dynamic interaction of the foundation-structure system are studied. The bridge structural system is simply modeled by three degree-of-freedom systems allowing for the sway of the structure and the sway and rocking of the foundation, and its equation of motion is derived by considering bilinear restoring force characteristics. The equation of motion for a 3 DOF system is solved numerically by Newmark's β method in order to obtain the nonlinear dynamic response of a foundation-structure system subjected to strong ground motions. The effects of both the yielding strength and the tangential second stiffness of the bilinear restoring force on the structural damage are evaluated.

In Chapter 4, steel rigid-frame piers damaged by local buckling and brittle cracking during the 1995 Hyogoken-Nanbu Earthquake are discussed. In order to improve their seismic performance, it is necessary to clarify the relationship between the horizontal load carrying capacity and the ductility of such

piers. In this study, a static loading test was carried out to evaluate the in-plane collapse mechanism of such piers in conjunction with Finite Element Analysis. Pseudo-dynamic testing was also carried out to evaluate the in-plane seismic behavior of these piers.

In Chapter 5, the elasto-plastic response of steel box piers subjected to strong ground motions in two horizontal directions is assessed. First, pseudo-dynamic testing of box steel piers subjected to these strong ground motions was carried out. Secondly, elasto-plastic finite displacement analyses of box steel piers were carried out in order to confirm the validity of these experiments. And thirdly, an elasto-plastic seismic response analysis method for the spring-mass system that considers the correlation of the two directions was proposed.

In Chapter 6, a parallel pseudo-dynamic testing system is developed and at first assessed for error propagation in response evaluation. The system is established by connecting experimental stations located in Osaka City University and Kyoto University through the Internet. An international link to Korea, then the U.S.A., then Australia is assessed, and its feasibility is demonstrated through the help of Osaka City University and KAIST.

In Chapter 7, the conclusions made from this study are summarized and future research needs are discussed.

References

Abe, M. and Fujino, Y., (1998), “Optimal design of passive energy dissipation devices for seismic protection of bridges”, Journal of Structural Mechanics and Earthquake Engineering, JSCE, No.605/I-45, pp. 241-252 (in Japanese).

Abiko Research Laboratory, (1995), “Preliminary report on characteristics and damages investigation of the 1995 Hyogoken-Nanbu Earthquake”, Central Research Institute of Electric Power Industry, U94042 (in Japanese).

Architectural Institute of Japan, (1998), “Structural performances under multi-dimensional earthquake ground Motions”, Muruzen Co., Ltd. (in Japanese).

American Association of State Highway and Transportation Officials, (1996), “Standard specification for highway bridges”, 16th Edition.

Aoki, T., Hasegawa, K. and Yamada, M., (1997), “An experimental study on load-deflection behavior of steel box section beam-to-column connections under static repeated loading”, Journal of Structural Engineering, JSCE, Vol. 43A, pp.177-186 (in Japanese).

Committee on Roadway Bridges by the Hyogoken-Nanbu Earthquake, (1995), “Investigations on damages of roadway bridges by the Hyogoken-Nanbu Earthquake”, Draft of Interim Report (in Japanese).

Committee on Roadway Bridges by the Hyogoken-Nanbu Earthquake, (1995), “Investigations on damages of roadway bridges by the Hyogoken-Nanbu Earthquake” (in Japanese).

Fujino, Y. and Abe, M., (1997), “Optimization of elevated highway bridge system subjected to sever ground motion”, Proceedings of Nonlinear Numerical Analysis and Seismic Design of Steel Bridge Piers, pp.59-66 (in Japanese).

Hakuno, M., Shidawara, M. and Hara, T., (1969), “Dynamic destructive test of a cantilever beam, controlled by an analog computer”, Trans., Japan Society of Civil Engineers, No. 171, pp.1-9.

Housner, G. W., (1956), “Interaction of building and ground during an earthquake”, Bull. Seism. soc. Am., Vol. 47, No. 3, pp.179-186.

Iemura, H., (1985), “Development and future prospect of hybrid experiment”, Journal of Structural Engineering and Earthquake Engineering, JSCE, No.356/I-3, pp. 1-10 (in Japanese).

Ikeda, M., Yamada, M., Ichikawa, A., Yasunami, H. and Tominaga, T., (1998), “Study on seismic design method of steel rigid frame piers for railway”, Proceedings of the Second Symposium on Nonlinear Numerical Analysis and its Application to Seismic Design of Steel Structures, pp.143-150 (in Japanese).

Inside Newsletter, (1995), “The first 55 hours – Great Hanshin Earthquake”, Institute of Industrial Science, University of Tokyo (in Japanese).

Izuno, K. and Nakamura, K., (1997), “Effect of adjacent RC pier on seismic response of steel pier”, Proceedings of Nonlinear Numerical Analysis and Seismic Design of Steel Bridge Piers, pp.287-294 (in Japanese).

Izuno, K., Takeno, S. and Nakai, H., (1999), “A study on seismic interaction between long-span bridge and adjacent approach bridge”, Journal of Structural Mechanics and Earthquake Engineering, JSCE, No.633/I-49, pp. 169-180 (in Japanese).

Japan Road Association, (1990), “Specifications of roadway bridges and commentaries: I common and II steel bridges” (in Japanese).

Japan Road Association, (1990), “Specifications of roadway bridges and commentaries: V earthquake-resistant design” (in Japanese)

Japan Road Association, (1994), “SI common and III concrete bridges” (in Japanese).

Japan Road Association, (1996), “Specifications of roadway bridges and commentaries: V earthquake-resistant design” (in Japanese).

Kasai, A., Kawamura, Y. and Usami, T., (2000), “Seismic behavior of steel bridge piers considering soil-structure interaction”, Journal of Structural Engineering, JSCE, Vol. 46A, pp.745-756 (in Japanese).

Kasai, A., Usami, T. and Kawamura, Y., (2002), “Seismic behavior of multi-span continuous bridges with steel piers considering soil-structure interaction”, Proceedings of the Forth Symposium on Nonlinear Numerical Analysis and its Application to Seismic Design of Steel Structures, pp.49-54 (in Japanese).

Kimura, Y. and Kawano, K., (2001), “Fundamental study of nonlinear seismic response analysis on dynamic soil-structure interaction”, Journal of Structural Engineering, JSCE, Vol. 47A, pp.599-606 (in Japanese).

Kitamura, M., Goto, H., Shiraki, W. and Dogaki, M., (2002), “Evaluation earthquake resistance for steel piers with rigid frame by dynamic response”, Journal of Structural Engineering, JSCE, Vol. 48A, pp.267-275 (in Japanese).

Kodama, N. and Yoda, T., (2000), “Characteristics of load carrying capacity seismic response analysis of steel rigid frames ”, Proceedings of the Third Symposium on Nonlinear Numerical Analysis and its Application to Seismic Design of Steel Structures, pp.143-148 (in Japanese).

Merritt, R. G. and Housner, G. W., (1954), “Effect of foundation compliance on earthquake stresses in multistory buildings”, Bull. Seism. soc. Am., Vol. 44, No. 4, pp.551-569.

Miki, C., Aizawa, T. and Anami, K., (1997), “Aseismatic intensity of steel beam-to-column connections”, Proceedings of Nonlinear Numerical Analysis and Seismic Design of Steel Bridge Piers, pp.307-314 (in Japanese).

Miki, T., Kotoguchi, H. and Osada, Y., (1997), “Inelastic earthquake response and collapse modes of steel portal frames with variable cross-section”, Journal of Structural Engineering, JSCE, Vol. 43A, pp.205-216 (in Japanese).

Miki, T. and Yamada, O., (1999), “Inelastic earthquake response analysis of steel two-story frames with shear collapse in middle of beam”, Journal of Structural Engineering, JSCE, Vol. 45A, pp.227-234 (in Japanese).

Miki, T. and Yamada, O., (2000), “Collapse mechanism and inelastic earthquake response of steel portal frames with collapse of beam”, Journal of Structural Engineering, JSCE, Vol. 46A, pp.663-673 (in Japanese).

Miki, T., (2001), “Effect of strain rate on inelastic earthquake response of steel portal frames with shear collapse of beam”, Journal of Structural Engineering, JSCE, Vol. 47A, pp.771-782 (in Japanese).

Morishita, H., Takaku, T., Aoki, T., Fukumoto, Y., Okamoto, T. and Matsui, E., (2000), “Experimental study on strength and ductility of a rigid-frame steel pier with intermediate cross beam”, Journal of Structural Engineering, JSCE, Vol. 46A, pp.831-840 (in Japanese).

Nakajima, A. and Onodera, O., (1998), “A study on elasto-plastic behavior of steel portal frames under

sever earthquake and applicability of equal energy assumption to its seismic design", Proceedings of the Second Symposium on Nonlinear Numerical Analysis and its Application to Seismic Design of Steel Structures, pp.135-142 (in Japanese).

Nakajima, A., Kanamaru, K. and Doki, H., (1999), "Damping characteristics of pier-foundation-soil system during earthquake excitation", Journal of Structural Engineering, JSCE, Vol. 45A, pp.763-770 (in Japanese).

Nakajima, A., Shoji, Y. and Saiki, I., (2000), "Dynamic response behavior of viaduct system designed by seismic coefficient method under severe earthquake", Proceedings of the Third Symposium on Nonlinear Numerical Analysis and its Application to Seismic Design of Steel Structures, pp.225-232 (in Japanese).

Nakajima, A., Kudo, T., Shoji, Y. and Saiki, I., (2001), "Applicability of simplified models for simulating elasto-plastic dynamic behavior of viaduct systems", Journal of Structural Engineering, JSCE, Vol. 47A, pp.831-842 (in Japanese).

Nakamura, H., et al., (1995), "Investigations on disaster by the Great Hanshin Earthquake", Prompt Report, Japan Society of Civil Engineers (in Japanese).

Nakamura, H., et al., (1995), "Investigations on disaster by the Great Hanshin Earthquake", Second Report, Japan Society of Civil Engineers (in Japanese).

Nakashima, M., Ishida, M., and Ando, K., (1990), "Integration techniques for substructure pseudo dynamic test", Journal of Structural and Constructional Engineering, AIJ, No. 417, 107-117 (in Japanese).

Nakashima, M., Kato, H., and Takaoka, E., (1992), "Development of real-time pseudo dynamic testing", Earthquake Engrg. Struct. Dynamics, Vol.21, 79-92 (in Japanese).

Nakashima, M., Akazawa, T. and Sakaguti, O., (1993), "Integration method of controlling experimental error growth in substructure pseudo dynamic test", Journal of Structural and Constructional Engineering, AIJ, No.454, 61-71 (in Japanese).

Nara, S., Murakami, S. and Ishida, T., (2002), "Elasto-plastic dynamic analysis of steel bridge piers in consideration of plate buckling and ground behavior", Proceedings of the Forth Symposium on Nonlinear Numerical Analysis and its Application to Seismic Design of Steel Structures, pp.55-60 (in Japanese).

Nara, S., Murakami, S. and Ishida, T., (2002), "elasto-plastic dynamic analysis of steel bridge piers in consideration of plate buckling and ground behavior", Proceedings of the Forth Symposium on Nonlinear Numerical Analysis and its Application to Seismic Design of Steel Structures, pp.55-60 (in Japanese).

Nikkei Construction, (1995), "Great Hanshin Earthquake with which the civil engineering encountered

”, Nikkei Business Publications, Inc. (in Japanese).

Nishizawa, H., Tachibana, A. and Kaneta, K., (1988), "The on-line hybrid earthquake simulation system based on the digital differential analyzer and the digital actuator", Journal of Structural and Constructional engineering, AIJ, No. 385, 30-38 (in Japanese).

Nishizawa, H., Eguchi, S., and Kaneta, K., (1989), "An on-line hybrid earthquake response simulation system using a digital differential analyzer and digital actuators", Journal of Structural and Constructional Engineering, AIJ, No. 405, 51-61 (in Japanese).

Nishikawa, K., Murakoshi, J., Takahashi, M., Okamoto, T., Ikeda, S. and Morishita, H., (1999), “Experimental study on strength and ductility of steel portal frame bridge pier”, Journal of Structural Engineering, JSCE, Vol. 45A, pp.235-244 (in Japanese).

Obayashi Technical Research Institute, (1995), “Preliminary report on the 1995 southern Hyogo Prefecture Earthquake”, Second Report (in Japanese).

Oide, K., Nakajima, A. and Saiki, I., (2000), “Three dimensional dynamic response analysis of bridge piers by rigid-body spring model”, Journal of Structural Mechanics and Earthquake Engineering, JSCE, No.654/I-52, pp. 259-270 (in Japanese).

Ozawa, K., Wang, Q. and Goto, Y., (2002), “Pushover analysis of portal frame-type bridge piers by beam model considering local buckling of stiffened compression panel and shear deformation of corner panel zone”, Journal of Structural Engineering, JSCE, Vol. 48A, pp.99-107 (in Japanese).

Saizuka, K., Itoh, Y., Kiso, E. and Usami, T., (1995), “A consideration on procedures of hybrid earthquake response test taking account of the scale factor”, Journal of Structural Mechanics and Earthquake Engineering, JSCE, No.507/I-30, pp. 179-190 (in Japanese).

Sato, T. et al., (1989), “Methods for dynamic analyses”, Dynamic Analysis and Seismic Design, Vol. 2, Gihodo Shuppan Co., Ltd (in Japanese).

Sato, T., Toki, K. and Yoshikawa, M., (1994), “Hybrid experiment on nonlinear dynamic soil-structure interaction system”, Proceedings of the 43rd Nat. Cong. of Theoretical & Applied Mechanics, pp. 595-596 (in Japanese).

Shiraki, W., Yamamoto, Y., Matsumoto, S. and Dogaki, M., (2000), “Evaluation of a seismic reliability of steel piers with rigid portal frame based upon elasto-plastic finite displacement analysis”, Journal of Structural Engineering, JSCE, Vol. 46A, pp.403-411 (in Japanese).

Shoji, G., Fujino, Y. and Abe, M., (1997), “Optimal allocation of earthquake-induced damage for elevated highway bridges”, Journal of Structural Mechanics and Earthquake Engineering, JSCE, No.563/I-39, pp. 79-94 (in Japanese).

Suzuki, M., Aoki, T. and Matsui, E., (2000), “Seismic resistance capacity of retro fitted rigid frame steel

bridge pier", Proceedings of the Third Symposium on Nonlinear Numerical Analysis and its Application to Seismic Design of Steel Structures, pp.135-142 (in Japanese).

Suzuki, M., Aoki, T. and Nomura, K., (2000), "Experimental study on seismic resistance capacity of simply retrofitted rigid frame steel bridge pier", Journal of Structural Engineering, JSCE, Vol. 46A, pp.135-142 (in Japanese).

Taisei Corporation, (1995), "Preliminary report on the Hyogoken-Nanbu Earthquake – ground motion and structural damages", Second Report, Japan Society of Civil Engineers (in Japanese).

Takanashi, K., and Nakashima, M., (1987), "Japanese activities on on-line testing", Journal of Structural Engineering Mechanics, ASCE, Vol. 113, No. 7, 1014-1032.

Takenaka Corporation, (1995), "2nd report on Hanshin (Hyogoken-Nanbu) Earthquake" (in Japanese).

Takeno, S. and Izuno, K., (2001), "Estimation of relative velocity response considering pounding between adjacent bridges during earthquakes", Journal of Structural Mechanics and Earthquake Engineering, JSCE, No.668/I-54, pp. 163-175 (in Japanese).

Toki, K., (1981), "Seismic analyses for structures", New Style System Civil Engineering, Vol. 11.

Toki, K., Kiyono, J., Ishizaki, H. and Ono, Y., (1998), "Strength demand spectrum taking into account soil-structure interaction", Proceedings of the 10th Japan Earthquake Engineering Symposium, pp. 1861-1866 (in Japanese).

Toki, K. et al., (1996), "Interim report of committee on disaster by the Great Hanshin-Awaji Earthquake" (in Japanese).

Usami, T., Suzuki, T. and Itoh, Y., (1995), "Pseudo-dynamic tests of concrete-filled steel columns with prototype details", Journal of Structural Mechanics and Earthquake Engineering, JSCE, No.525/I-33, pp. 55-67 (in Japanese).

Usami, T., Saizuka K., Kiso, E. and Itoh, Y., (1995), "Pseudo-dynamic tests of steel bridge pier models under sever earthquake", Journal of Structural Mechanics and Earthquake Engineering, JSCE, No.519/I-32, pp. 101-113 (in Japanese).

Usami, T., Zheng, Y. and Ge, H., (1999), "A seismic performance evaluation procedure for steel framed bridge piers through a pushover analysis and an equivalent SDOF model", Journal of Structural Mechanics and Earthquake Engineering, JSCE, No.626/I-48, pp. 213-240 (in Japanese).

Watanabe, E., Sugiura, K., Utsunomiya, T. and Higuchi, Y., (1994), "Pseudo-dynamic testing considering rate-dependency of Materials", Proceedings of the 43rd Nat. Cong. of Theoretical & Applied Mechanics, pp. 577-580 (in Japanese).

Watanabe, E., Sugiura, K. and Oyawa, W. O., (2000), "Effects of multi-directional displacement paths on the cyclic behaviour of rectangular hollow steel columns", Journal of Structural Mechanics and

Earthquake Engineering, JSCE, No.647/I-51, pp. 79-95.

Yabe, M. and Kawashima, K., (1999), “Effect of the yield strength ratio between the column and pile foundation on the plastic deformation of pile foundation”, Journal of Structural Mechanics and Earthquake Engineering, JSCE, No.626/I-48, pp. 51-68 (in Japanese).

Yabe, M. and Kawashima, K., (1999), “Nonlinear seismic response of a pile foundation and its push-over analysis”, Journal of Structural Mechanics and Earthquake Engineering, JSCE, No.619/I-47, pp. 91-109 (in Japanese).

Yamaguchi, E., Ichikawa, A., Ikeda, M., Kubo, T. and Miki, C., (2000), “Effect of haunch at connection of steel moment frame subjected to cyclic loading”, Journal of Structural Engineering, JSCE, Vol. 46A, pp.119-125 (in Japanese).

Yamaguchi, T., (1993), “Fundamental study on earthquake resistant design of circular steel bridge piers”, Proceedings of 48th Annual Meeting, JSCE, pp. 356-357 (in Japanese).

Yamada, O. and Miki, T., (2000), “Collapse mechanism and earthquake response of two-story portal frames with collapse of beam by using partially tapered member”, Proceedings of the Third Symposium on Nonlinear Numerical Analysis and its Application to Seismic Design of Steel Structures, pp.149-156 (in Japanese).

Yamashita, N. and Harada, T., (2001), “A study of response spectrum considering dynamic soil structure interaction of foundation-soil-structure system”, Journal of Structural Engineering, JSCE, Vol. 47A, pp.591-598 (in Japanese).

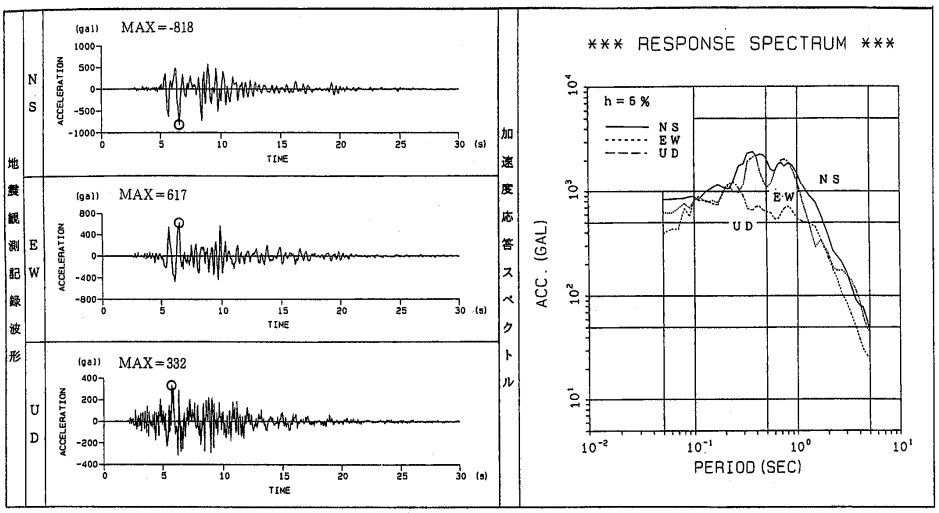

(a) Kobe Marine Meteorological Observatory (Ground Type I)

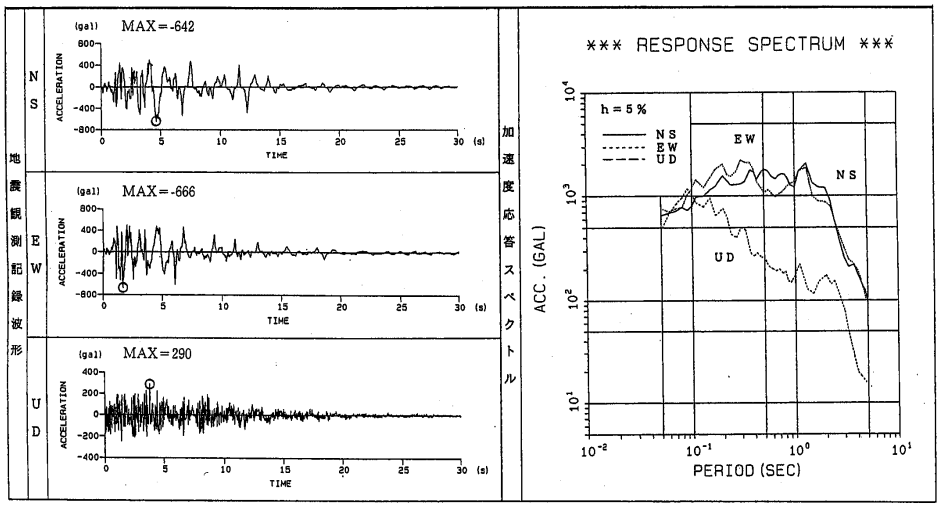

(b) JR-Takatori Station (Ground Type II)

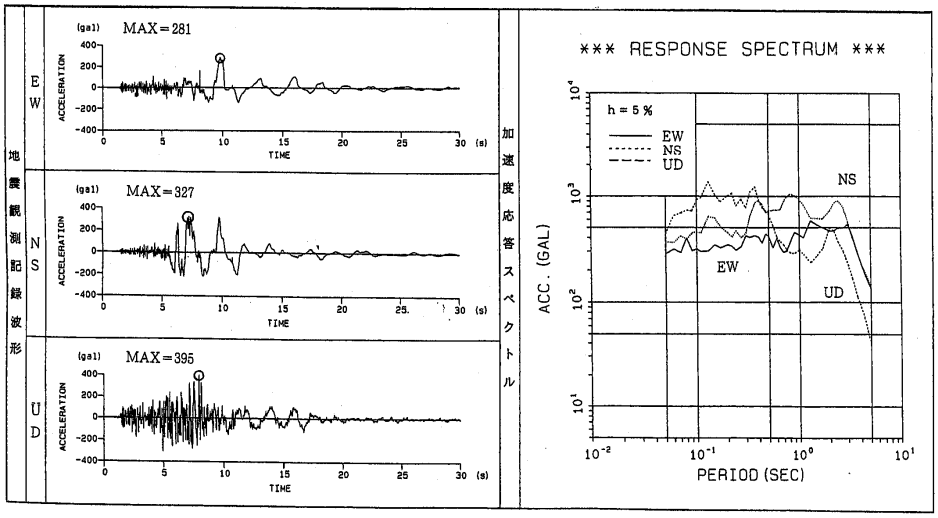

(c) Higashi Kobe Bridge (Ground Type III)

Fig. 1.1 Ground acceleration records and acceleration

Kobe Marine Meteorological Observatory

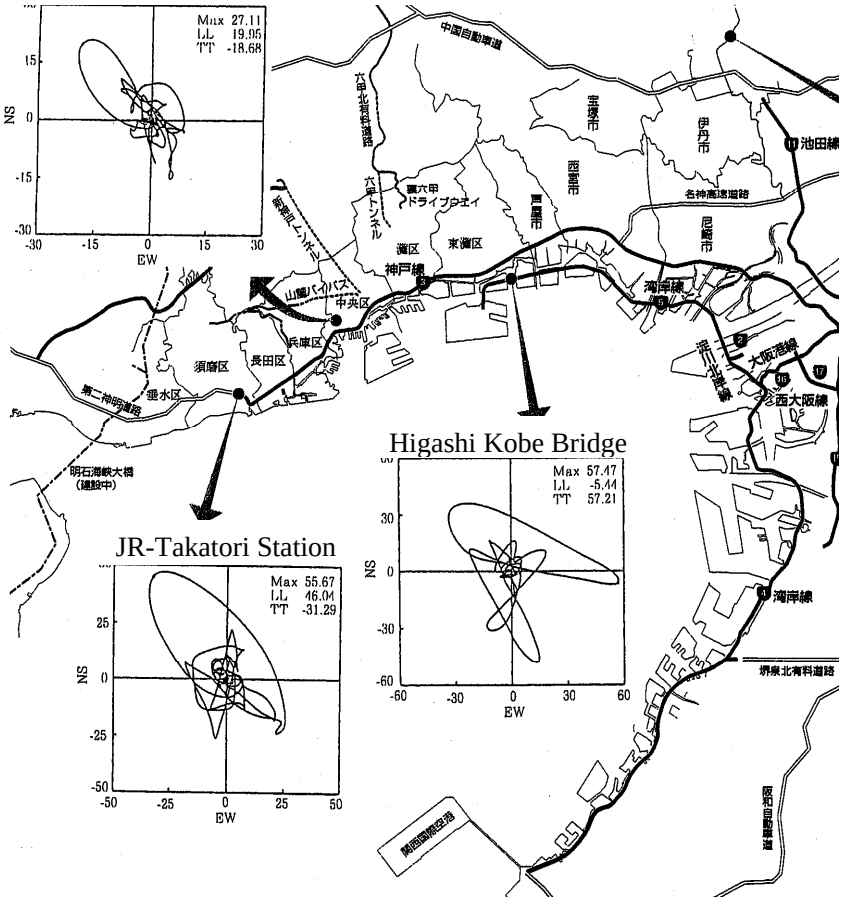

Fig. 1.2 Displacement trace of bi-directional horizontal ground

Table 1.1 Number of piers and girders damaged during the Hygoken-Nanbu earthquake: Kobe Line (route 3) of the Hanshin Expressway

Damage rank	Steel piers	Concrete piers	Steel and concrete bridge girders	Bearing system*
As (collapse)	3	65	29	—
A (serious)	8	84	64	220
B (moderate)	12	107	243	195
C (light)	112	246	215	206
D (none)	28	510	753	348
Total	163	1012	1304	969

*Number of bearing lines or number of bearing devices.

Table 1.2 Number of piers and girders damaged during the Hygoken-Nanbu earthquake: Bay Line (route 5) of the Hanshin Expressway

Damage rank	Steel piers	Concrete piers	Steel and concrete bridge girders	Bearing system*
As (collapse)	0	0	1	—
A (serious)	0	0	0	42
B (moderate)	13	1	8	78
C (light)	21	22	28	102
D (none)	109	200	425	229
Total	143	223	462	451

*Number of bearing lines or number of bearing devices.

Photo 1.1 A side-span of the Nishinomiya Harbor Bridge fell to the ground

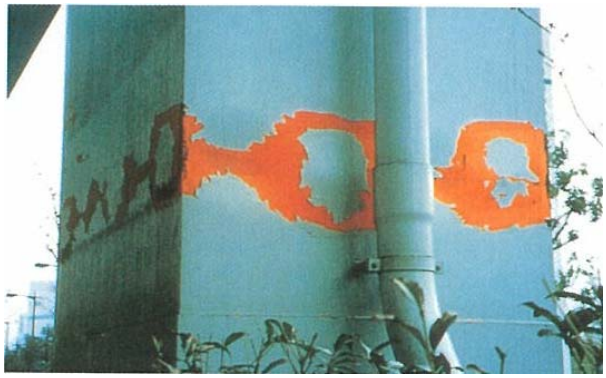

Photo 1.2 Buckling of steel pier with a box cross-section

Photo 1.3 Elephant-foot buckling of a steel bridge pier

Photo 1.4 A brittle crack in the beam-to-columr connection of a steel frame-type pier

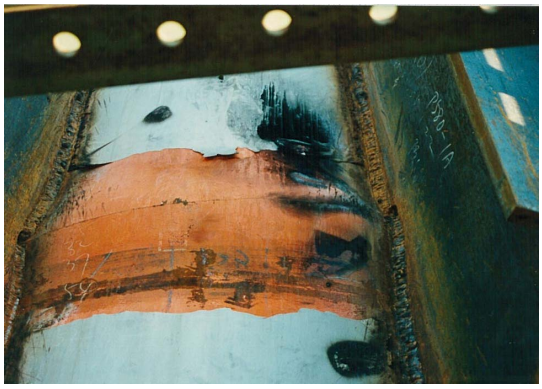

Photo 1.5 Low-cycle fatigue cracking due to excessive plastic buckling deformation of bridge pier

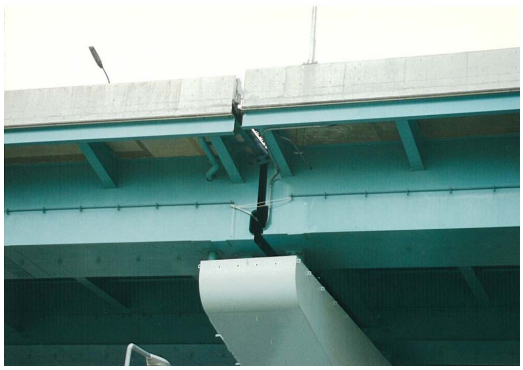

Photo 1.6 Plastic elongation of a seismic girder connector

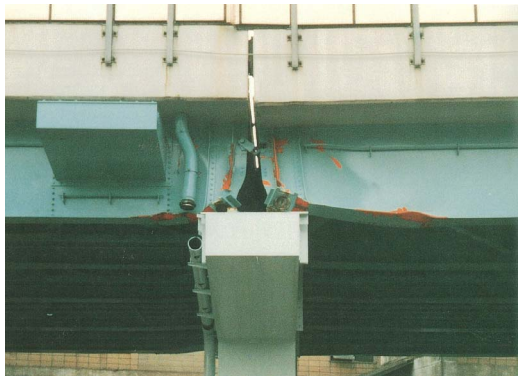

Photo 1.7 Excessive horizontal deformation of a girder end

Photo 1.8 Buckling of a steel box girder due to collapse of supporting bridge pier

Photo 1.9 Damage of an arch bridge by bounding and stamping on a jacking up mount

Photo 1.10 Buckling of struts connecting arch ribs due to the excessive displacement at bearing devices

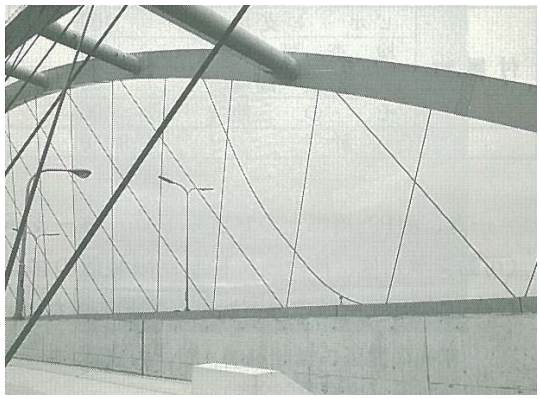

Photo 1.11 Loosening of a cable in a Nielsen arch bridge at the anchor socket

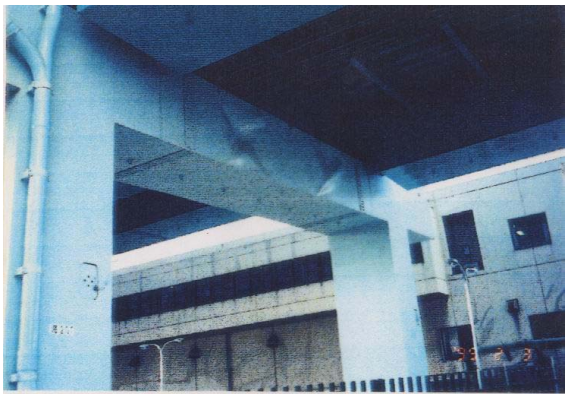

Photo 1.12 Bi-directional ‘x-shaped’ panel shear buckling in beam portion of a bridge pier

Chapter 2

Investigation of the Dynamic Interaction of Continuous Elevated Bridges

2.1 Introduction

The Hyogoken-Nanbu Earthquake, which occurred at Kobe and on Awaji Island on January 17, 1995, caused extensive damage to highway bridges. Several studies on this destruction have been made using detailed structural models, and most of the causes of the damage to highway bridges have been clarified (Hanshin Expressway Public Corporation, 1997; Japan Society of Civil Engineers, 1996; Kansai Branch of the Japan Society of Civil Engineers, 1998; Subcommittee on New Technology for Steel Structures of the Japan Society of Civil Engineers, 1996). Taking these studies into consideration, the Japanese Specifications for Highway Bridges were revised in 1996. According to the current Japanese Specifications for Highway Bridges Part V, Seismic Design, the vibration unit of the structure is determined based on the natural period of the part of the structure that includes its piers (Japan Road Association, 1996). If the dynamic response of the structure is simple, a static analysis is conducted in the design of an elevated bridge; if not, it is necessary to perform a response analysis by solving the equation of motion. Therefore, it is necessary to select a design vibration unit depending on the direction of the inertia force, the bridge style, the fixed conditions of the bearings and the vibration characteristic of piers. In the case of the excitation in the direction perpendicular to the bridge axis of a continuous elevated bridge, the design vibration unit consists of piers, foundations and superstructures in which the natural periods of adjacent piers are different. On the other hand, when the natural periods of adjacent piers are very close to each other, the design vibration unit consists of one pier and the superstructure only. In addition, an elevated bridge can be modeled by a pier and a girder. If the ratio of the minimum value to the maximum value of the natural periods of each part is smaller than 1.5, the effect of the difference of the natural periods on the response can be neglected.

Many structures sustained structural-joint damage in the Hyogoken-Nanbu Earthquake (Committee on Roadway Bridges by the Hyogoken-Nanbu Earthquake, 1995; Nakamura et al., 1995). Therefore, in this chapter, a continuous elevated bridge that consists of steel piers and RC piers was considered in order to assess the interaction of steel and RC piers on the overall response of elevated

bridges. Then, elevated bridges were modeled by a mass-spring-dashpot model, and an eigenvalue analysis and elasto-plastic response analysis were performed. Finally, the response characteristics of the continuous elevated bridge and the dynamic interaction resulting from a change in various parameters, the number of piers, the stiffness of the superstructure, etc., were investigated.

2.2 Modeling of Elevated Bridges and Analytical Procedure

In this study, the seismic response of continuous elevated bridges in the direction perpendicular to the bridge axis was investigated, with a focus on the continuous elevated bridge consisting of steel piers and RC piers, as shown in Fig. 2.1. To set up a more practical bridge model, the elevated highway bridges of the Hanshin Expressway (Kobe Route) damaged during the 1995 Hyogoken-Nanbu Earthquake, which consisted of a steel pier (Pier No. 353) and a RC pier (Pier No. 354), as shown in Fig. 2.2, were used as a reference. Table 2.1 shows the specific value of the structural elements of such an elevated bridge. The mass of the superstructure, the stiffness and the yield force of each pier and the force required to crack the RC pier based on the structural details specified in the design were determined. The girders were modeled simply as elastic shear elements in order to make clear the dynamic interaction between the steel pier and the RC pier. Therefore, the torsional response of the girders was not considered; in addition, the shear stiffness of the girders was assumed to be equivalent to the horizontal stiffness of the steel pier.

2.2.1 Modeling of Elevated Bridges

The elevated bridge system is modeled as a mass-spring-dashpot system to assess the dynamic interaction between different kinds of piers, namely only a response in one direction.

(a) Standard Model

A standard model is first considered, such as clarifying the dynamic interaction between the piers. This model consists of the piers and the girders, as shown in Fig. 2.3(a) and (d). Most of the damage to the elevated bridges during the 1995 Hyogoken-Nanbu Earthquake occurred at the piers and bearings. In order to identify the cause of the damage, it is necessary to determine the seismic response of the elevated bridge as a structural system. Therefore, the bearings are also modeled as a structural element, just like the piers. However, because our purpose is to clarify the effect of the restoring force characteristics of the piers on the overall seismic response of the bridge system, the bearing model is not modeled in the standard. The foundation was also not modeled.

(b) Model including the bearing

This model is considered in order to assess the effect of the restoring force characteristics of the bearings on the dynamic interaction among the piers. After the 1995 Hyogoken-Nanbu Earthquake, “menshin” bearings (base isolation) were installed on new and existing bridges. It was thought that the restoring force characteristics of the menshin bearings would affect the seismic response of the continuous elevated bridges. So, a bearing model was added to the standard model, as shown in Fig. 2.3(b) and (d). The dynamic properties of the menshin bearings were expressed in the spring and the dashpot. The dimensions and specific properties of the bearings are summarized in Tables 2.2 and 2.3, respectively.

(c) Model including the foundation

This model was used to assess the effect of the restoring force characteristics of the foundation on the dynamic interaction between the piers. So, the foundation model is added to the standard model, as shown in Fig. 2.3(c) and (d). The motions of the foundation, such as the sway motion and rocking motion, were incorporated, and these degree of freedom were also modeled by the spring and the dashpot. The dimensions and the specific properties of the foundation are shown in Table 2.4.

2.2.2 Analytical Procedure

(a) Eigenvalue analysis

An eigenvalue analysis of the standard model was carried out to identify the basic vibration behavior of the elevated bridges. By changing the number of piers, the stiffness of the piers and the girders, and the combination of the pier types, the fundamental vibration characteristics were assessed. Damping was not considered in this eigenvalue analysis, because the effect of damping can be comparatively small on the natural period and the vibration mode of the elevated bridges.

(b) Elasto-plastic time history response analysis

A time history response analysis was performed on each of the structural models by using Newmark’s β method (β =1/6). The time increment was set at 0.002 sec. It is assumed that the girder behave elastically in this analysis. Tables 2.1, 2.3 and 2.4 show the damping constant used in this analysis. The damping coefficient of each structural element is determined by the mass, the stiffness and the damping constant of each structural element. The input ground motion is the one which was recorded at the Kobe Marine Observatory (N-S component) during the Hyogoken-Nanbu Earthquake. Figs. 2.4(a) and (b) show the Fourier amplitude spectrum and the acceleration response spectrum, respectively. The main characteristics

of this ground motion are as follows.

(i) The maximum acceleration is 818 gal, which is one of the strongest ground motions in Japan.

(ii) The duration of the main vibration is very short.

(iii) The predominant period is about 0.7 sec, which is a typical natural period of bridge piers.

First, the elastic and the elasto-plastic response analysis were preformed for the basic vibration unit, which consists of a steel/RC pier and the girder supported by piers. Then, the seismic response of the basic vibration unit was clarified. Next, the elastic and the elasto-plastic response analysis were carried out for the model with changes in several parameters, i.e., the number of the piers, the stiffness of the piers, the stiffness of the girders and the combination of the pier types. Then, the seismic response of the continuous elevated bridge and the dynamic interaction between the steel pier and the RC pier were assessed. Moreover, the elastic and the elasto-plastic analysis were also conducted for the model with consideration for the degrees of freedom of the bearings/foundation. Finally, the manner in which the structural elements, such as the bearings and the basement, affect the overall response of the continuous elevated bridges was examined.

The restoring force characteristics of each structural element considered in this study can be summarized as follows. Two types of restoring force characteristics of the steel pier were employed. One was the trilinear model, which represents the degradation after the local buckling occurs at the base of the pier column, as shown in Fig. 2.5(a) (Watanabe et al., 1996). The other is the bilinear model without degradation, but with hardening after yielding, as shown in Fig. 2.5(c). On the other hand, in the case of the RC pier, a degrading trilinear model, which was able to model the degradation of the stiffness caused by the cyclic loading, was used, as shown in Fig. 2.5(b) (Architectural Institute of Japan, 1990). In the case of the bearings, either a linear elastic model or a bilinear model that can represent the energy absorption by the hysteresis loop was employed. The proof force of the bearing was assumed to be 23% of the loading-carrying capacity of the steel pier or 52% of that of the RC pier, as shown in Tables 2.1 and 2.3.

2.3 Results of Analysis and Discussion

2.3.1 Eigenvalue Analysis

The natural period and the mode of the vibration from the first mode to the fifth mode obtained from the eigenvalue analysis are shown in Fig. 2.6. The mode of the vibration is normalized by the maximum amplitude.

(a) Effect of number of degrees of freedom

Figs. 2.6(a) and 2.6(b) show the natural period and the vibration mode of the continuous elevated bridge which consists of either 24 steel piers or 24 RC piers. In the case of the steel piers, the first natural period is 0.720(sec). In the case of the RC piers, it is 0.612(sec). These periods are identical to the natural periods of a single steel pier or single RC pier. Therefore, all 24 piers vibrate at the same phases.

(b) Effect of combinations of the different types of piers

Fig. 2.6(c) shows the natural period and the vibration mode of the continuous elevated bridge that has 24 piers, but for which 12 of the piers are steel and 12 are RC. The amplitude of the vibration of the RC piers is very small in the first and second vibration modes. In other words, only the steel piers vibrate in these vibration modes. Then, the amplitude of the vibration of the RC piers becomes larger when the fourth and larger mode is picked up. This is why the natural period of the fourth vibration mode is close to that of the single RC pier. Therefore, the vibration characteristics of the continuous elevated bridge that consists of different types of piers differs from that of the continuous elevated bridge that consists of the same type of piers.

(c) Effect of number of degrees-of-freedom characteristics of the continuous elevated bridge with different numbers of piers

An eigenvalue analysis was conducted for the continuous elevated bridge by changing the number of piers. The following three cases were considered: (i) a case with 6 steel piers and 6 RC piers (Case A); (ii) a case with 12 steel piers and 12 RC piers (Case B); and (iii) a case with 24 steel piers and 24 RC piers (Case C). Figs. 2.6 (c), (e) and (e) show the results of these cases, respectively. In all three cases, only steel piers had a displacement amplitude of vibration. Next, in the vibration mode of the large order, the whole continuous elevated bridge showed an equivalent displacement amplitude in Case A and Case B. On the other hand, in Case C, most of the RC piers had a small displacement amplitude, even though the vibration mode becomes the fifth order. Accordingly, the vibration characteristics made a difference when the number of piers that compose the continuous elevated bridge was changed.

(d) Effect of the stiffness of girders

The stiffness of the girders affects the magnitude of shear deformation between adjacent piers in the horizontal direction. In addition, the fixture of the horizontal movement and rotation of girder ends at a bearing also affect the girder deformation. However, little is known about the effect of such a fixture of girder ends at a bearing on the stiffness of the girder. Therefore, an eigenvalue analysis was performed by changing the stiffness of the girder such to 0.1 times, 1.0 times, and 10.0 times the standard value (433

kN/cm). The numerical results are shown in Figs. 2.6 (f), (c) and (g). In the case that the stiffness of the girder is 0.1 times that of the standard value, only steel piers have a displacement amplitude, while the RC piers have little displacement amplitude. Next, in the case that the stiffness of the girder is the same as the standard value, the RC piers have a displacement amplitude except for the first mode of the vibration. Finally, in the case that the stiffness of the girder is 10 times the standard value, the whole continuous elevated bridge has a displacement amplitude that is equal in all modes of the vibration. This indicates that the vibration characteristics make a difference by changing the stiffness of the girders, and that it is clear to have rigid body movement when the stiffness of the girder becomes larger regardless of the stiffness of the piers.

(e) Effect of irregular location of particular piers in the bridge system

Two steel piers are located at the center of 22 the group of RC piers. Fig. 2.6(h) shows the natural period and the vibration mode. Two steel piers and a few RC piers adjacent to them have a displacement amplitude in the first mode of vibration. On the other hand, the whole continuous elevated bridge vibrates in the second or larger mode of vibration. Consequently, the vibration characteristics make a difference by changing the combination of the pier types.

The results of the eigenvalue analysis can be summarized as follows. The ratio of the natural period of the steel pier to that of the RC pier is 1.17. Although the ratio of the natural period is less than 1.5, it is clearly observed that the vibration characteristics vary according to the number of piers, the stiffness of the girders and the combination of the pier types. Consequently, it is necessary to pay attention to the vibration unit in the seismic design method.

2.3.2 Natural Period of Piers and Vibration Characteristics of Continuous Elevated Bridges

First, the elastic and the elasto-plastic response analysis were performed to obtain the vibration characteristics of a steel pier and a RC pier as a basic vibration unit. The time history of the displacement and the maximum displacement of the steel pier and the RC pier are shown in Fig. 2.7 and Table 2.5, respectively. It can be found from the numerical results that the maximum displacement of the steel pier is larger than that of the RC pier and the residual deformation of the steel pier is large in the case of the elasto-plastic analysis. Therefore, it is thought that the dynamic interaction arises at the boundary area between the steel piers and the RC piers. In addition, the ductility ratio of the steel pier, which means the ratio of the maximum displacement to the yield displacement, is 3.38, whereas for the RC pier, the plastic

ratio is 4.85. In this section, the time history analysis of the seismic response of a continuous elevated bridge consisting of steel and RC piers is conducted. The analytical results are assessed by using the maximum displacement of the superstructure of the top of each pier.

(a) Effect of pier types

The response analysis is conducted for the continuous elevated bridge which consists of 12 steel piers and 12 RC piers. The maximum displacement of each superstructure obtained from the elastic and the elasto-plastic analysis is shown in Fig. 2.8. The maximum displacement of the continuous elevated bridge becomes similar to that of the steel pier or the RC pier around the 10th pier from the particular pier where the steel piers and the RC piers locate side by side. Therefore, the effect of the dynamic interaction between the piers is significant at this location. In other words, the effect is very small when the different types of piers are constructed separately. Accordingly, it is thought that we need to pay attention to determine the prescription of the performance requirement where the different types of piers are placed.

(b) Effect of the number of piers

The elasto-plastic analysis is conducted by changing the number of piers. There are three numerical cases: (i) a case with 6 steel piers and 6 RC piers (Case A); (ii) a case with 12 steel piers and 12 RC piers (Case B); and (iii) a case with 24 steel piers and 24 RC piers (Case C).

Fig. 2.9 shows the maximum displacement of the superstructure at the pier locations. The maximum displacement at the steel piers of the continuous elevated bridge which is adjacent to RC piers becomes smaller than that of the steel pier as a basic vibration unit. On the other hand, the maximum displacement at the RC piers becomes larger. The effect of the dynamic interaction between the piers can be found only at the piers above steel and RC piers are located side by side as stated above. Therefore, the number of piers is not very important for the design of continuous elevated bridges.

(c) Effect of girder stiffness

The elasto-plastic analysis is performed by changing the stiffness of the girder to 0.1 times, 1.0 times, and 10.0 times the reference value (433 kN/cm). Fig. 2.10 shows the maximum displacement of the superstructure at the pier locations. The mode of rigid body motion of superstructure is appeared when the stiffness of the girder is 10 times the standard value. Therefore, the effect of the dynamic interaction increases with increasing girder stiffness.

(d) Effect of pier location

Two steel piers are located in the middle of other 22 RC piers. The maximum displacement of the superstructure is shown in Fig. 2.11. As can be seen, the displacement at the steel pier is much larger than that of the RC pier in the elastic response. But, these values are almost the same as the displacement of the steel pier and the RC pier as a basic vibration unit. And the displacement of the RC piers adjacent to steel piers is larger than that of the RC piers at the end, whereas, in the elasto-plastic analysis, the displacement at the steel piers becomes smaller than that of the steel pier as the basic vibration unit. On the other hand, the displacement of the RC piers adjacent to steel piers becomes larger. This result is similar to the result obtained from the continuous elevated bridge which consists of 12 steel piers and 12 RC piers, as mentioned previously, in Fig. 2.8.

(e) Effect of pier retrofitting

After the 1995 Hyogoken-Nanbu Earthquake, the hollow sections at the base of steel piers were filled with concrete to prevent the piers from local buckling. This retrofitting changed the restoring force characteristics of the steel piers. Therefore, the restoring force characteristics of the retrofitted steel pier are modeled as a bilinear response, because the strength does not degrade due to the filled concrete. A seismic response analysis of the continuous elevated bridge consisting of 12 steel piers and 12 RC piers was performed. Fig. 2.12 shows the maximum displacement response of each superstructure. Compared with the results in Fig. 2.7, the maximum displacement of most of the steel piers decreases slightly. On the other hand, the displacement of the RC piers adjacent to steel piers increases slightly. Consequently, the vibration characteristics of elevated bridges should be reinvestigated even if a slight change in the restoring force characteristics due to retrofitting occurs.

(f) Effect of the bearings

Two restoring force characteristic models of the bearing are prepared. One was a linear model and the other a bilinear model, i.e., a model with a seismic isolation bearing installed. A base-isolated continuous elevated bridge with 12 steel piers and 12 RC piers was considered. Fig. 2.13 shows the maximum displacement of each superstructure. The maximum displacement in the linear model is larger than that in the bilinear model at most of the pier locations. However, at piers that are located adjacent to a pier of different type, the maximum displacement in the linear model is smaller than that in the bilinear model. Therefore, it is not necessarily the case that the seismic isolation bearing reduces the maximum displacement of all the piers. In other words, it is necessary to properly determine the stiffness of each bearing based on the design principle that distributes the inertia force so as to make a design the reasonable size of bearing as well as piers.

The results of the seismic response analysis can be summarized as follows. As in the eigenfrequency analysis, the vibration changes in characteristics are clarified as for the number of piers, the stiffness of the girders and the combination of the pier types change. Especially, the maximum displacement of the piers whose different types of piers are located adjacently is different from that of the pier as a basic vibration unit. Consequently, it is necessary to investigate these phenomena in detail when elevated bridges which consist of different types of piers are designed.

2.3.3 Effect of Stiffness and Strength of Adjacent Piers

In the previous section, a numerical analysis was performed only in the case that the ratio of the natural period of the steel pier to that of the RC pier was 1.15. It is supposed that the vibration characteristics of continuous elevated bridges which consist of different types of piers varies depending on the natural period of each pier. In this section, three kinds of ratios of the natural period of the steel pier to that of the RC pier are considered. In the first case (Case A), the natural period of the steel pier (Ts) is longer than that of the RC pier (Tc), that is, the ratio is set to be 1.17 (Ts/Tc=1.17). In the second case (Case B), Ts is equal to Tc; that is, the ratio is set to be 1.00. In the final case (Case C), Ts is shorter than Tc; that is, the ratio is set to be 0.832. In these three cases, the natural period of the RC pier remains constant, but the natural period of the steel pier is changed by varying the stiffness of the steel pier. An eigenfrequency analysis and a seismic response analysis were conducted for each of these three cases.

(a) Results of eigenfrequency analysis and discussion

Fig. 2.14 shows the natural period of the continuous elevated bridge system for all the cases. In Case A and Case C, the interval of the natural period of the elevated bridge between each mode becomes longer than that of Case B. Furthermore, the first mode of the natural period of the elevated bridge is almost equal to the larger natural period of the steel pier and the RC pier.

(b) Results of elastic response analysis and discussions

Fig. 2.15 shows the maximum displacement of the elevated bridge. such as that of Case B, the maximum displacements of all the piers are almost the same and the displacement response can be given. Therefore, it is possible to neglect the dynamic interaction between the piers by reducing the difference of the natural periods of the elevated bridge which consists of the different types of piers, while in Case A and Case C, the maximum displacement of the piers adjacent to different types of piers may not be the same as that of the pier by a basic vibration unit. Moreover, it is found that the maximum displacement of the continuous

elevated bridge becomes close to that of the 10th pier from the location where the steel piers and the RC piers are adjacent.

(c) Results of elasto-plastic analysis and discussion

Fig. 2.16 shows the results of the elasto-plastic analysis of the elevated bridge. In this analysis, the maximum displacement of the piers where different types of piers are adjacent differs from that of the pier by the basic vibration unit in all three cases. More precisely, the maximum displacement of the steel piers becomes smaller than that of the vibration unit, on the other hand, while that of the RC piers becomes larger than that of the vibration unit. This is because the restoring force characteristics of the steel pier are different from that of the RC pier, as shown in Fig. 2.5, so that the effect of the dynamic interaction of the piers may be reduced. Therefore, it is necessary to have natural periods for the different types of the piers; in other words, the difference in the restoring force characteristics should be minimized.

2.3.4 Effect of the Plasticity of the Foundation

Three levels of the yield force of the foundations which are installed under the RC piers were prepared. The reference value was two times the maximum force obtained by the elastic analysis for the standard acceleration (Soil Profile I). Therefore, the yield force levels were set to be the same as the reference value, 0.80 times the reference value, and 0.60 times the reference value. Assessed is the RC pier adjacent to the steel pier. Fig. 2.17 shows the maximum displacement at all the locations of the superstructure. It is found from the numerical results that the maximum displacement of the RC piers is reduced with decreasing yield force, while the maximum displacement of the steel pier which is next to the RC pier increases. This is why the inertia force of the superstructures is distributed to each pier due to the plasticity of the foundation. Therefore, it is also necessary to consider the yield force of the foundation in the design of elevated bridges.

2.4 Concluding Remarks

In this chapter, the seismic response characteristics were discussed in terms of the dynamic interaction of the continuous elevated bridge consisting of different types of piers, i.e., steel piers and RC piers. The conclusions and the directions for future research can be summarized as follows:

1) The vibration mode of the continuous elevated bridge consisting of different types of piers is completely different from that of the continuous elevated bridge consisting of only one type of pier. Therefore, if elevated bridges consist of piers which have different characteristics of restoring force, it

is necessary to perform the seismic design for a whole elevated bridge as a vibration unit.

2) As for the elevated bridge consisting of steel and RC piers, the effect of the dynamic interaction becomes significant up to about the 10th pier from the boundary of dissimilar piers (i.e., the boundary between the adjacent steel and RC pier).
3) The vibration mode varies according to the scale of the elevated bridge, that is, the number of piers and the stiffness of the girders. In addition, not only the stiffness of the girders but also the arrangement of the bearings must be accounted for.

The damage mechanism and the restoring force characteristics of steel piers and RC piers are generally different from each other. However, the current design specifications are determined without having the consistency of the limit state of steel piers and RC piers. Therefore, the limit states of steel piers and RC piers must be taken into consideration when continuous elevated bridges are designed. Moreover, it is necessary to establish a new design method in which an elevated bridge is regarded as a structural system which consists of various type of structural elements. In this chapter, the elevated bridge was replaced with a simple model in order to clarify its dynamic interaction. In the future, it will be necessary to investigate the dynamic interaction quantitatively in order to develop a practical design procedure using a more detailed analytical model.

References

Architectural Institute of Japan, (1990), “Ultimate strength and deformation capacity of buildings in seismic design (1990)”, pp. 423-425 (in Japanese).

Committee on Roadway Bridges by the Hyogoken-Nanbu Earthquake, (1995), “Investigations on damages of roadway bridges by the Hyogoken-Nanbu Earthquake”, Draft of Interim Report (in Japanese).

Hanshin Expressway Public Corporation, (1997), “The great earthquake is overcome - Diary on seismic disaster restoration construction -”, (in Japanese).

Japan Society of Civil Engineers, (1996), “Proposal collection on criterion of earthquake resistance” (in Japanese).

Japan Road Association, (1996), “Specification of highway bridges, Part V, Seismic Design”, Maruzen (in Japanese).

Kansai branch of Japan Society of Civil Engineers, (1998), “Lesson from great seismic disaster – Report of great Hanshin-Awaji Earthquake investigation committee –” (in Japanese).

Nakamura, H. et al., (1995), “Investigations on disaster by the Great Hanshin Earthquake”, Prompt Report, Japan Society of Civil Engineers (in Japanese).

Subcommittee on new technology for steel structures of Japan Society of Civil Engineers, (1996), “Final report on researches on seismic design” (in Japanese).

Watanabe, E., Maekawa, Y., Sugiura, K. and Kitane, Y., (1996), “Damages and seismic performance of steel bridges”, Civil Engineering, JSCE, pp. 54-62 (in Japanese).

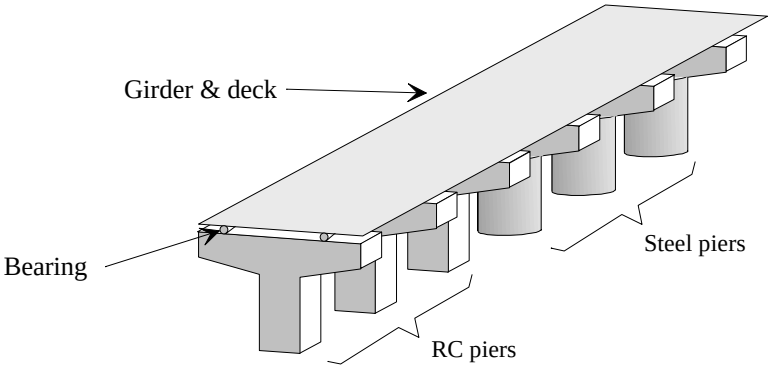

Fig. 2.1 Elevated bridge system consisting of steel and RC piers

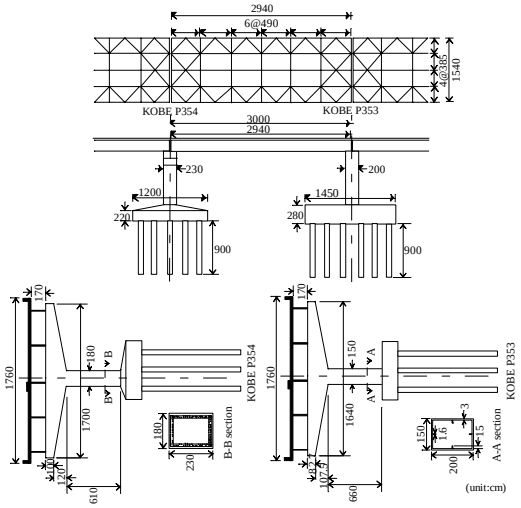

Fig. 2.2 Existing elevated bridge (Hanshin Expressway (Kobe route))

Table 2.1 Structural parameters of girder and piers

		Girder	Steel pier	RC pier
Weight (tonf)		528	30	225.7
Spring constant (tonf/cm)		43.3	43.3	81
Damping factor (%)		3	5	5
Restoring force (tonf)	Crack	—	—	56.7
	Yield	—	339.4	152.5

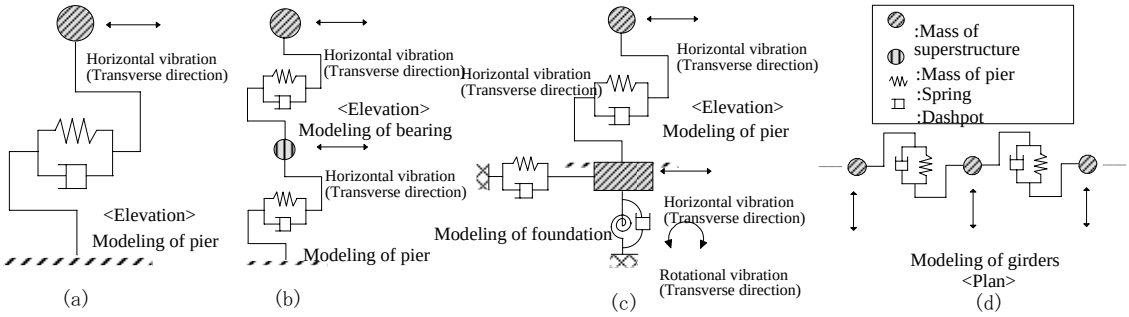

Fig. 2.3 Modeling of elevated bridge by mass-spring-dashpot

Table 2.2 Shape and size of bearing

Plane shape	62cm×62cm
Effective shape	60cm×60cm
Thickness of rubber	1.4cm×8Layres
Number of Bearing	5

Table 2.3 Structural parameters of bearing

Spring constant (tonf/cm)	48.5
Damping factor (%)	0
Yield restoring force (tonf)	79

Table 2.4 Structural dimensions and parameters of foundation

Weight		315(tonf)
Length in bridge axis		700(cm)
Length in the direction perpendicular to bridge axis		900(cm)
Rotation inertia		5.37×10^{4}(tonf·cm·s^{2})
Damping factor	Sway	0.1
	Rocking	0.1
Spring constant	Sway	2.22×10^{3}(tonf/cm)
	Rocking	4.49×10^{8}(tonf·cm)

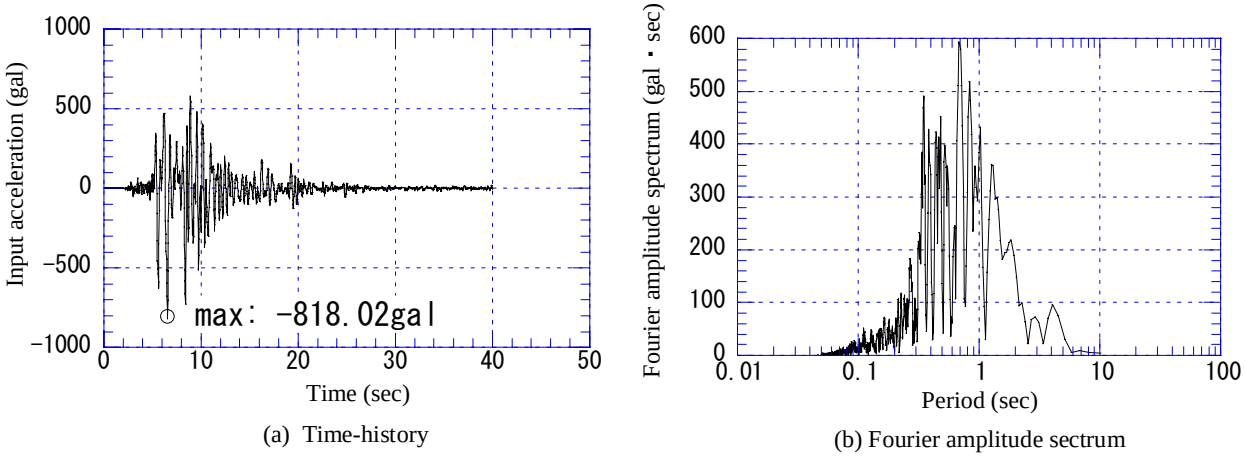

(a) Time-history

(b) Fourier amplitude sectrum

Fig. 2.4 Input ground motion

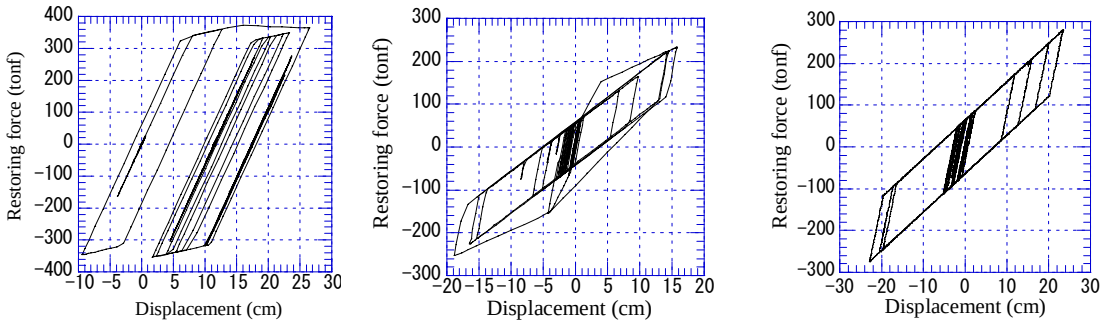

(a) Degrading tri-linear model

(b) Stiffness-degrading tri-linear model

(c) Bi-linear model

Fig. 2.5 Example of restoring force characteristics of piers

Natural period (sec)

1st order	2nd order	3rd order	4th order	5th order
0. 720	0. 714	0. 697	0. 671	0. 640

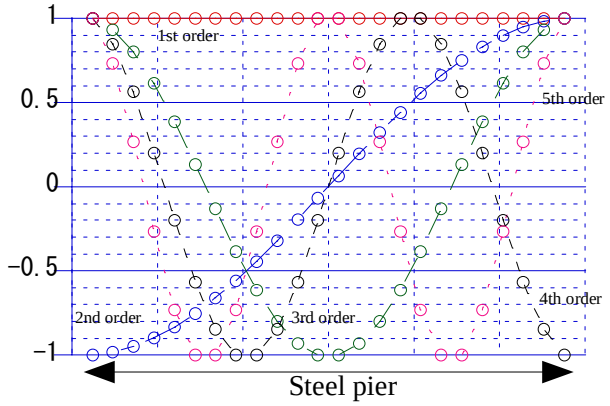

(a) 24 steel piers

Natural period (sec)

1st order	2nd order	3rd order	4th order	5th order
0. 612	0. 609	0. 601	0. 589	0. 573

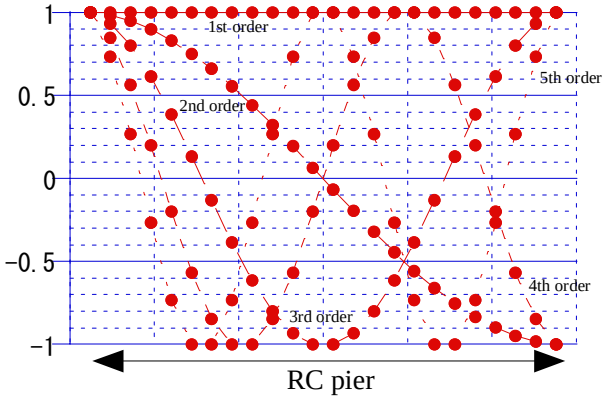

(b) 24 RC piers

Natural period (sec)

1st order	2nd order	3rd order	4th order	5th order
0. 715	0. 681	0. 629	0. 609	0. 592

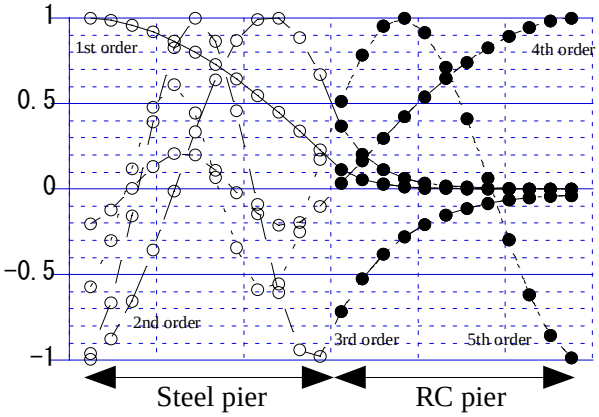

(c) 12 steel piers and 12 RC piers

Natural period (sec)

1st order	2nd order	3rd order	4th order	5th order
0. 705	0. 624	0. 597	0. 547	0. 501

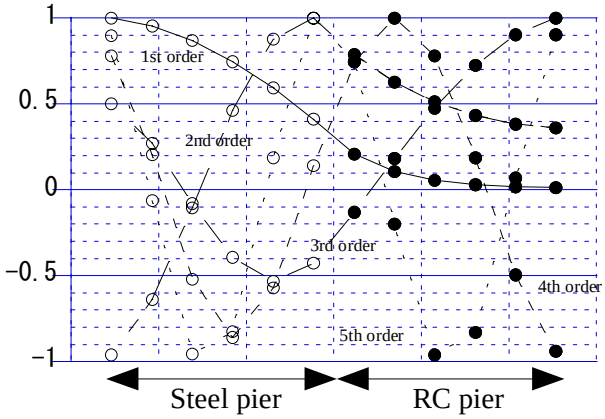

(d) 6 steel piers and 6 RC piers

Natural period (sec)

1st order	2nd order	3rd order	4th order	5th order
0. 719	0. 708	0. 689	0. 663	0. 634

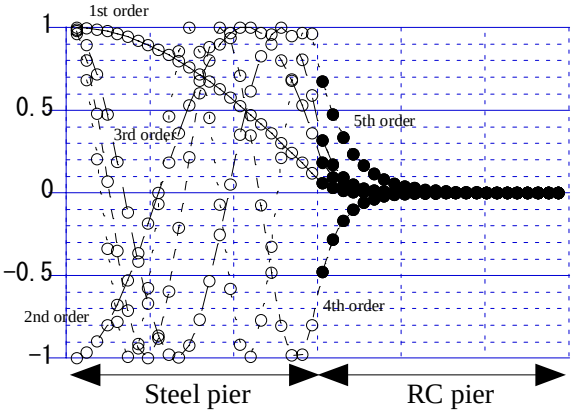

(e) 24 steel piers and 24 RC piers

Natural period (sec)

1st order	2nd order	3rd order	4th order	5th order
0. 719	0. 707	0. 696	0. 683	0. 669

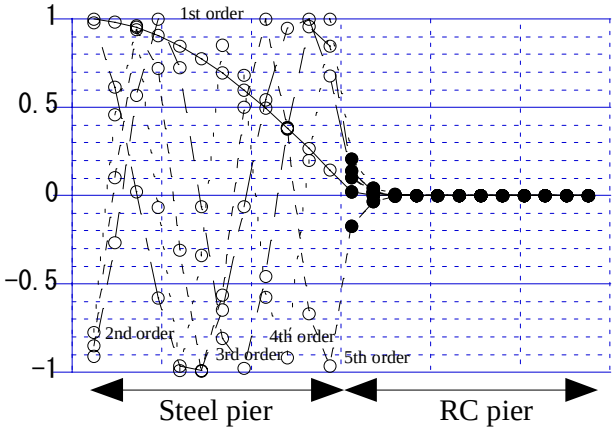

(f) Stiffness of girder (Stiffness: 0.1 times)

Fig. 2.6 Results of eigenfrequency analysis

Natural period (sec)

1st order	2nd order	3rd order	4th order	5th order
0. 691	0. 600	0. 537	0. 454	0. 385

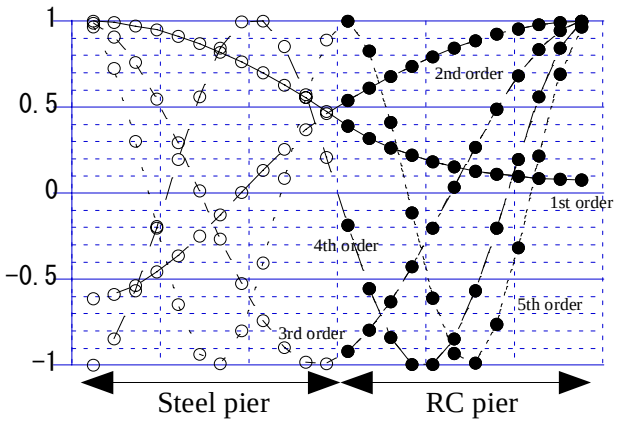

(g) Stiffness of girder (Stiffness: 10 times)

Natural period (sec)

1st order	2nd order	3rd order	4th order	5th order
0. 633	0. 609	0. 607	0. 589	0. 578

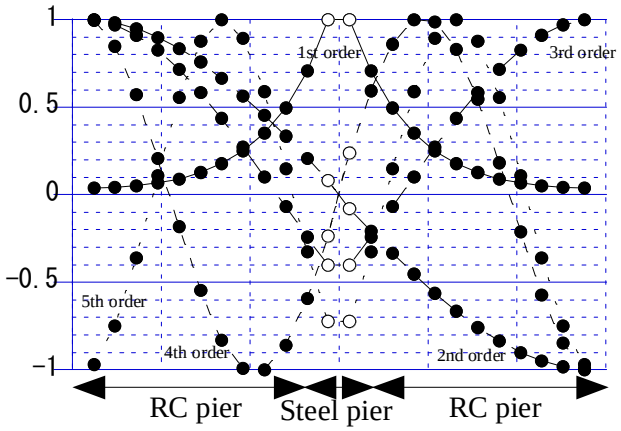

(h) 2 steel piers are arranged in the center of 22 RC piers

Fig. 2.6 Results of eigenfrequency analysis（continued）

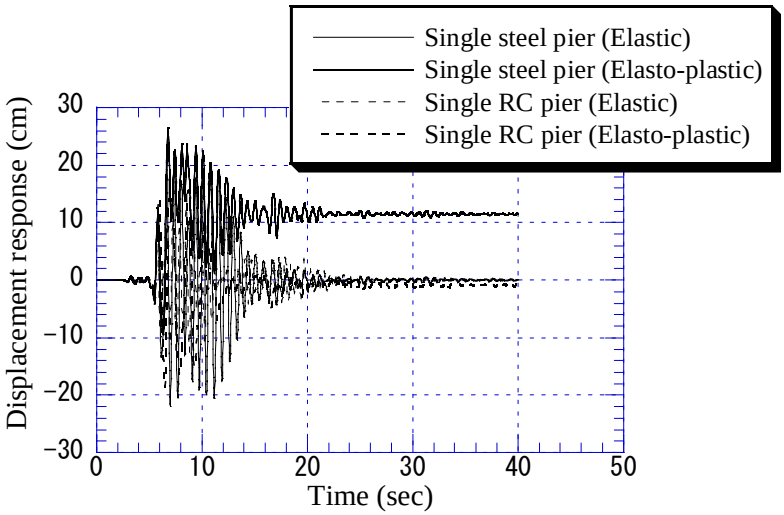

Fig. 2.7 Time history of displacement response

Table 2.5 Maximum displacement response of piers

		Yield displacement (cm)	Maximum displacement response (cm)	Ductility factor
Steel pier	Elastic	—	22.0	—
	Elasto-plastic	7.84	26.5	3.38
RC pier	Elastic	—	15.4	—
	Elasto-plastic	3.88	18.8	4.85

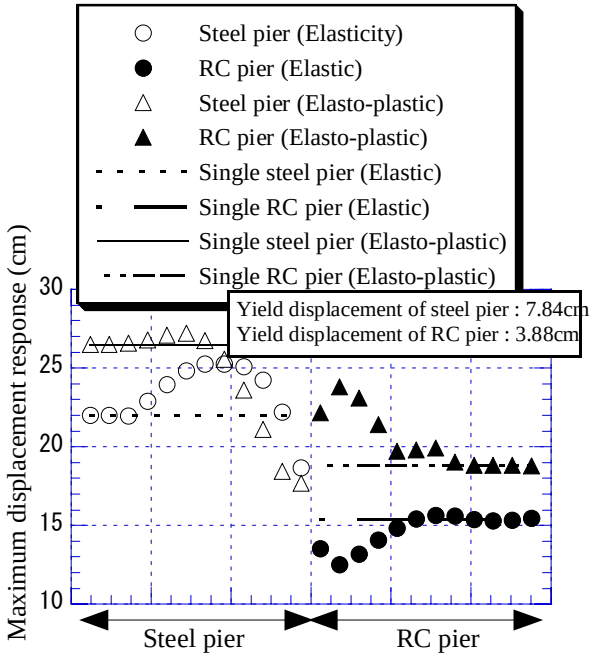

Fig. 2.8 Response characteristics with different restoring force characteristics

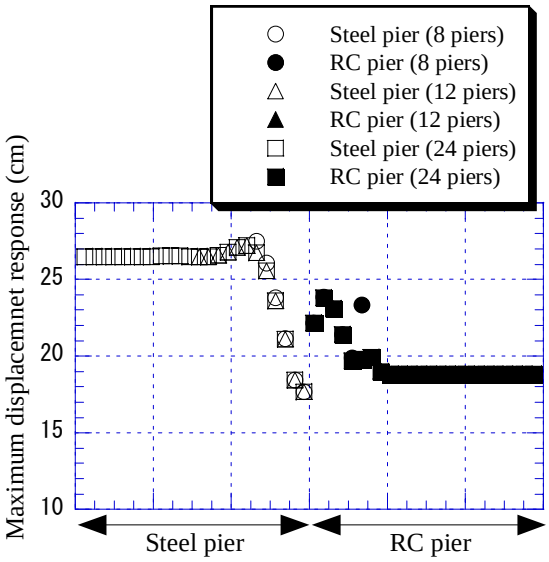

Fig. 2.9 Response behavior (Effect of number of piers)

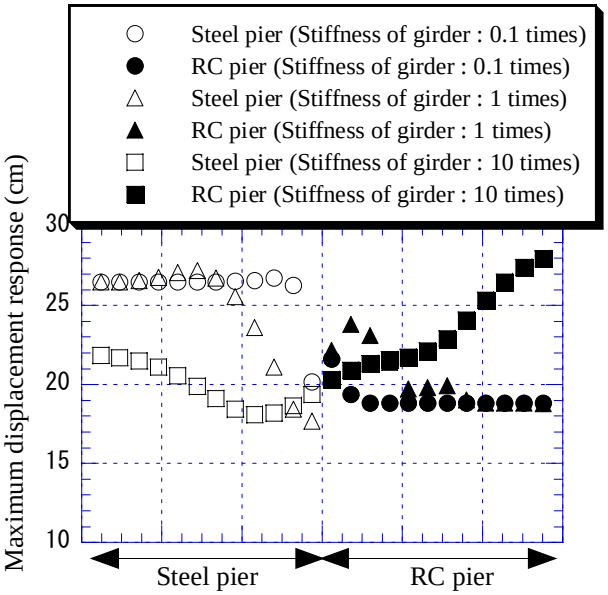

Fig. 2.10 Response behavior (Eeffect of girder stiffness)

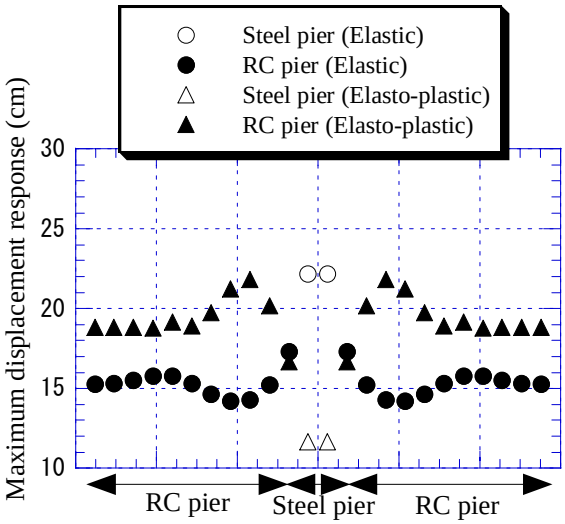

Fig. 2.11 Response behavior (Effect of combination of the pier types)

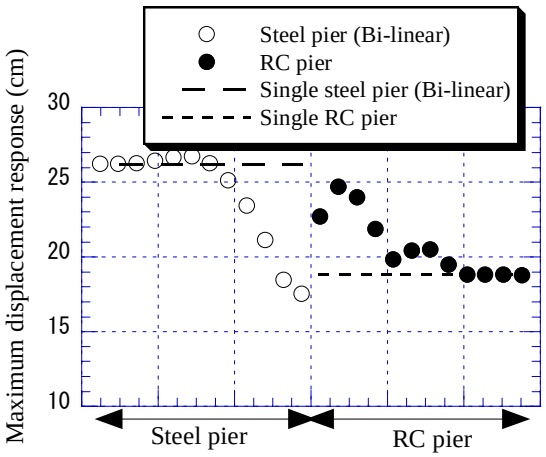

Fig. 2.12 Response behavior (Effect of restoring force model)

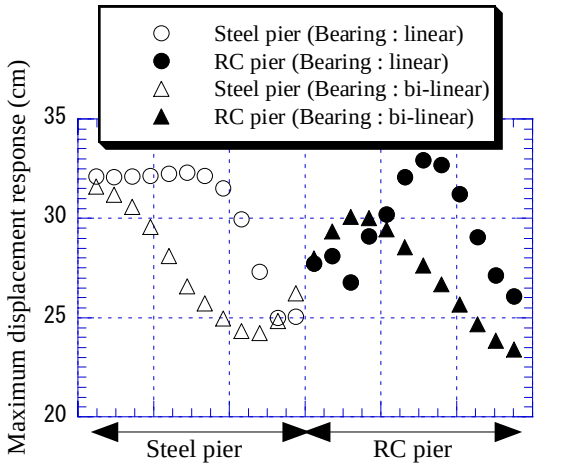

Fig. 2.13 Response behavior (Effect of bearing system)

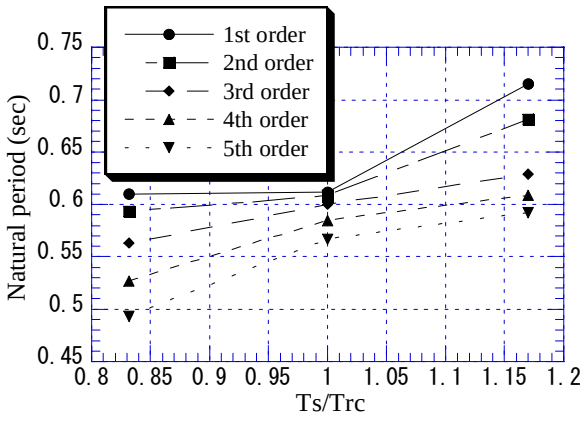

Fig. 2.14 Relationship between natural period of steel pier and natural period of the whole bridge

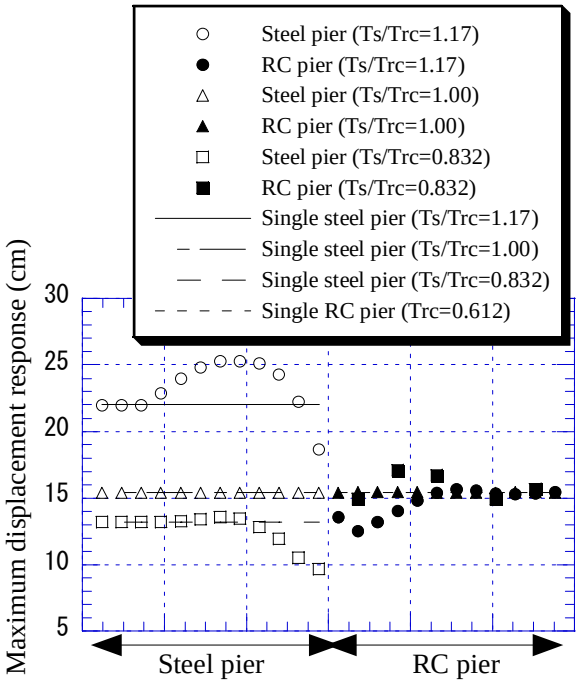

Fig. 2.15 Comparison of elastic response (Effect of pier's stiffness)

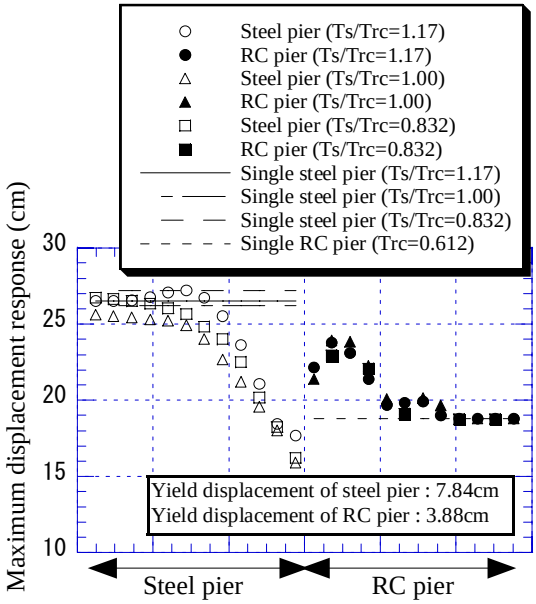

Fig. 2.16 Comparison of elasto-plastic response

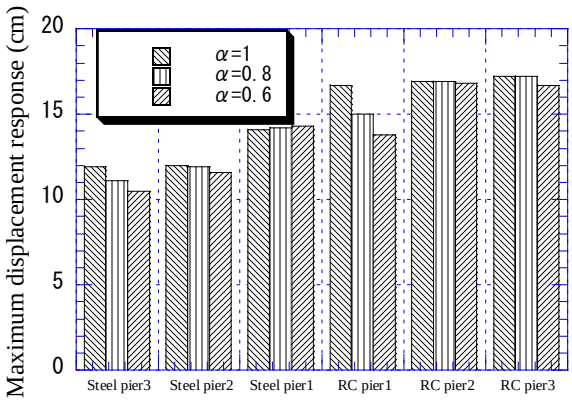

Fig. 2.17 Effect of the plastication of foundation on pier

Chapter 3

Nonlinear Dynamic Interaction of Foundation-Structure Systems

3.1 Introduction

Recently, the necessity to construct structures in severely challenging natural environments such as the ocean, deep ground, great depths and high space has been increasing. Various types of structural analyses and tests have been performed to solve the technical problems posed by the structure-foundation, structure-fluid, and structure-wind interactions. In particular, as the scale of the structure increases, the variation in the function of each structural element also grows and the structural system may be severely affected by interaction with the severe conditions in the surrounding environments. Accordingly, it is important to understand the ultimate state of a structural system under dynamic forces such as the wave force, wind force and seismic force in order to clarify the dynamic interaction among structural elements and ensure the safety of the entire structural system.

Various studies on the dynamic interaction behavior have been carried out by Toki et al. (Toki, 1981). However, there has been no method of structural design that accounts for these interaction behaviors. It seems to be caused by complication of the phenomenon, so that such an interaction is not fully understood to be implemented in the design specification.

The Hyogoken-Nanbu Earthquake, which was classified as a near field earthquake, caused great damage to many civil engineering structures. Even though it was not one of the largest earthquakes occurred in Japan's history, it was associated with enormous destruction, possibly due to the various dynamic interactions between the foundations and structures. Therefore, an improved understanding of such interaction behavior is crucial for the field of civil engineering.

In this study, a nonlinear dynamic response analysis for a simply idealized bridge-foundation structural system subjected to strong ground motions was carried out to examine the effect of the restoring force characteristics of the foundation and the structure on the response, as well as the dynamic interaction from the viewpoint of the vibration energy equilibrium and the ductility.

3.2 Analytical Method and Analytical Models

3.2.1 Analytical Method

The structural system considered herein consists of a foundation and superstructure, as shown in Fig. 3.1. This structural system is a three-degrees-of-freedom system that can take into account the influence of the dynamic interaction between superstructure and foundation. This structural model assumes the horizontal motion of the superstructure in the direction perpendicular to bridge axis as well as the sway and rocking motion of the foundation. The dynamic characteristics for each degree-of-freedom are modeled by a spring-and-dashpot model. The equation of motion for this structural system can be derived for the elastic state and given by Eq.(3.1), where the deformations shown in Fig. 3.2 are assumed (Shibata, 1986; Tanabe et. Al., 1990). A systematic index should be used for understanding the limit state of each degree-of-freedom, since the system in this study has multiple degrees-of-freedom. The absorbed energy, which is a scalar quantity, is also used for this index. This energy is composed of kinetic energy, hysteretic energy and damping energy. It is obtained from the equation of the energy equilibrium given in Eq.(3.2),

$$[M]\{\ddot{Y}\}+[C]\{\dot{Y}\}+[K]\{Y\}=-[M]\{f\}\ddot{Z} \tag{3.1}$$

$$[M]=\begin{bmatrix} m_1 & 0 & 0 \\ 0 & m_0 & 0 \\ 0 & 0 & I \end{bmatrix}$$

$$[C]=\begin{bmatrix} c & -c & -cH \\ -c & c+c_H & cH \\ -cH & cH & cH^2+c_R \end{bmatrix}$$

$$[K]=\begin{bmatrix} k & -k & -kH \\ -k & k+k_H & kH \\ -kH & kH & kH^2+k_R \end{bmatrix}$$

$$\{Y\}=\begin{Bmatrix} y_1 \\ y_0 \\ \theta \end{Bmatrix} \quad , \quad \{f\}=\begin{Bmatrix} 1 \\ 1 \\ 0 \end{Bmatrix}$$

$$\int \{\dot{Y}\}^T[M]\{\ddot{Y}\}dt+\int \{\dot{Y}\}^T[C]\{\dot{Y}\}dt + \int \{\dot{Y}\}^T[K]\{Y\}dt=-\int \{\dot{Y}\}^T[M]\{f\}\ddot{Z}dt \tag{3.2}$$

which is derived by multiplying both sides of Eq.(3.1) by $\{\dot{Y}\}dt$, and integrating with respect to time (Hirao, 1986):

where k, k_H and k_R are the elastic stiffness of the pier and the sway and rocking of the foundation. The restoring force, $[K]\{Y\}$, is modeled by a bilinear relation using the kinematic hardening law, as shown in Fig. 3.3 in the plastic state (Murata, 1993). Although the yield strength of each degree of freedom is related to each other in the design, they are assumed to be independent in this study because the effect of the yield strength ratio on the response is assessed.

Newmark's β method (β=1/6), which is one of the most general techniques for response analysis, was used in this study. When the value of β is 1/6, it expresses a linear acceleration method. First, an elastic response analysis was carried out to elucidate the vibration characteristics of the structural system while considering the foundation in terms of the natural period and the vibration modes. Secondly, a nonlinear dynamic response analysis was conducted for both the one-degree-of-freedom system under assumption of a fixed foundation and a structural system in which the sway and rocking motion of the foundation were considered in order to examine their dynamic interaction. In this latter system, the effects of the vibration of the foundation could be considered, along with the absorbed energy. In addition, a parametric analysis could be carried out to consider parameters such as the type of soil profile (type I/type III), the level of seismic force (level 1 for elastic response analysis; level 2 for checking the horizontal dynamic load-carrying capacity; Kobe_NS wave along the north-south direction of the Hyogoken-Nanbu Earthquake observed at the Kobe marine meteorological observatory), and the restoring force at the yielding and plastic stiffness of the restoring force curve for each degree-of-freedom.

3.2.2 Analytical Models

The analytical model in this study can be referred to the prototype which consists of a steel bridge pier of 1,500 cm height constructed on a footing foundation of which size is 700 cm (bridge axial direction), 900 cm (the bridge axis cross direction) and 200 cm (depth direction) and a superstructure with a span length of 30 m and effective width of 10 m. This model is assumed to be constructed on either type I ground or type III ground. The geometrical dimensions of the superstructure and the foundation are summarized in Table 3.1 and Table 3.2, respectively. Type I soil (rock mass) and type III soil (soft ground), assumed to have the N-value are approximately 40 and 10, respectively. The properties of these soils are summarized in Table 3.3. The reaction force coefficients of type I soil and type III soil summarized in Table 3.4 (Kawashima et. al., 1992) can be calculated according to Part V (entitled Seismic Design) of the Japanese specifications for Highway Bridges (Japan Road Association, 1990). Accordingly, spring constants and damping constants of these soils are obtained as shown in Table 3.5. It is difficult to assume the damping constants of these soils

determinably because these values depend on the soil condition, the type of the foundation, and so on. Consequently, the spring constant is assumed in order that the natural period of the bridge pier becomes about 0.75 seconds, which is the standard value for a steel bridge pier (Management Technology Center of Hanshin Expressway Public Corporation and Japanese Society of Steel Construction, 1994).

Since the shortest natural period obtained from the Eigen frequency analysis is 0.064 sec (see Chapter 3.4.1 and Table 3.6), the time interval used in the time integration scheme is set to 0.001 sec considering the accuracy of the analysis. The plastic stiffness of the bilinear restoring force model is assumed to be 10% of the elastic stiffness.

3.3 Analytical Results and Discussion

3.3.1 Eigen Frequency Analysis

The Eigen frequency analysis is carried out for the foundation-structure system at first. The natural periods obtained from the analysis are tabulated in Table 3.6. Generally speaking, the influence of the damping on the natural period is considered to be small, so that the Eigen frequency analyses are conducted without considering the damping force.

It is found that the first natural period of the foundation-structure system is a little longer than the period of the superstructure only. The second natural period of the foundation-structure system is also slightly longer than that of the foundation only. Therefore, it is considered that the natural period of the actual bridge pier will be a little longer than that of the one mass system in which the foundation is assumed to be fixed.

The influence of the type of soil on the natural period of the foundation-structure system is also assessed. It is found that the natural period of the system on type III soil is longer than that on type I soil. It is confirmed that the natural period tends to be longer as the soil becomes softer. Fig. 3.4 shows the vibration modes for each natural period. From this figure, it is understood that the higher vibration modes represent the opposite phase of vibration in the structure and foundation as the mode becomes higher. But there was no difference in vibration mode even though the soil type is changed.

3.3.2 Elasto-Plastic Response Analysis

Nonlinear dynamic response analyses for a 1 DOF system in which a fixed foundation is assumed and a 3 DOF system for the foundation-structure system were carried out to examine the dynamic interaction with a focus on the influence of the foundation on the superstructure. Results of the response analysis in the case of the acceleration (level 2) on the type I soil are shown in Fig. 3.5 to Fig. 3.8. Fig. 3.5

and Fig. 3.6 show the results of the displacement response of the superstructures in which a rigid foundation and flexible foundation are assumed, respectively. Fig. 3.7 shows the displacement response of the foundation in the sway mode and Fig. 3.8 shows the rotation response of the foundation in the rocking motion. The time history of displacement is shown in Fig.3.5 (a) – Fig. 3.8 (a), and the hysteresis of the load-displacement relation is shown in Fig. 3.5 (b) – Fig. 3.8 (b). In addition, the input energy and the absorbed energy in the system are compared in Fig. 3.5 (c) – Fig. 3.8 (c). The input energy and absorbed energy are normalized by the elastic limit strain energy (W_e=1/2 $P_y \cdot \delta_y$, where, P_y and δ_y are the yield restoring force and yield displacement, respectively). The yield restoring force in the case of the flexible foundation is assumed to be equal to the maximum restoring force obtained from the elastic response analysis subjected to level 1 acceleration input. The yield restoring force of the superstructure is kept constant regardless of the fixture condition of the foundation.

From Fig. 3.5 (a) and Fig. 3.6 (a), it is can be seen that the absolute horizontal displacement of the superstructure reaches a maximum at about 2 sec for both the rigid and flexible foundation, and that the horizontal displacement of the superstructure in the case of the flexible foundation is about 3.4 cm and larger than that in the case of the rigid foundation. This is because there is an increase in the horizontal displacement of the superstructure due to the reduction of the elastic stiffness of the system. That is, the stiffness of the structure-foundation system is reduced to 22.8 tonf/cm, which is 87.7% of the elastic stiffness of the structure only. However, it is also found that this additional displacement consists of the displacement due to the sway of the foundation (about 0.5 cm), the displacement due to the rocking of the foundation (about 2.7 cm) and the displacement of the superstructure (0.2 cm). Thus the increase in displacement response is caused mainly by the rocking of the foundation.

Next, the effect of the dynamic interaction on the response of each degree of freedom of the foundation-structure system is investigated from the viewpoint of the absorbed energy. The energy input is only the ground excitation, and the energy is input into the superstructure and the foundation (Fig. 3.6(c) and Fig. 3.7(c)). In addition, the energy is also input to superstructures by the reaction of the damping force and the restoring force due to the sway and rocking of the foundation in addition to the energy input by ground excitation (Fig. 3.7(c) and Fig. 3.8(c)). Then, the energy is converted to kinetic energy, hysteretic energy, and damping energy (from Fig. 3.5 to Fig. 3.8(d)). On the other hand, the rocking motion of the foundation is being excited by the vibration of the superstructure, although it is not generated by the horizontal ground motion. If the distributed spring and dashpot along the foundation axis for the sway and rocking are attached, the rocking of the foundation may be excited.

The maximum value of the absolute displacement response of the superstructure is tabulated in Table 3.7. From this table, the ratio of the displacement response to that of the rigid foundation is small for

both the case of type I soil and the case of type III soil. On the other hand, the response magnification of level 2 compared to the level 1 for type III soil is smaller than that for type I soil. This means that the natural period of the foundation-structure system exists in the dominant period band of the earthquake of the level 2 (type I soil).

The maximum relative displacement and the ductility factor subjected to the acceleration of level 2 on type I and type III soil are summarized in Table 3.8. The ductility factor is defined by normalizing the maximum displacement divided by the yield displacement. It can be seen that the ductility factor in the sway direction of the foundation is larger than that in the other motions. It is understood from the fact that the energy in the sway direction of the foundation is almost 3 times the energy in the rocking direction of the foundation as well as the structure. Therefore, the yield restoring force should increase in order to have enough elastic strain energy absorption or to have enough plastic energy absorption by deformability. Moreover it is also found that the ductility factor of type I soil is larger than that of type III soil, as shown in Table 3.7.

3.3.3 Effect of the Restoring Force Characteristics

The factors that affect the elasto-plastic response in terms of the restoring force characteristics of the foundation-structure system are the yield strength ratio and plastic stiffness. The yield strength ratio is the ratio of the elasto-plastic response to the largest elastic response of the structure. On the other hand, the plasticity secondary gradient depends on the strain hardening of the material, and it is related to the degree of statically indeterminant of the structure.

In this study, the effect of these two parameters on the response of the foundation-structure is investigated in detail. Moreover, the effect of the input acceleration on the behavior of the foundation-structure system after yielding is examined by using the acceleration record (level 1 and level 2) for type I soil specified in JSHB as well as the Kobe_NS acceleration record observed in Hyogoken-Nanbu Earthquake.

(1) The Influence of the Yield Strength Ratio (Level 1 Acceleration Input)

Analytical results for different yield restoring forces are shown in Fig. 3.9. This figure shows the maximum displacement normalized by the yield displacement, namely, the ductility ratio for level 1 acceleration of type I soil varying the restoring force. However, the other standard values are used without reducing the yield restoring force. Fig. 3.9 (a), (b) and (c) show the response result of the superstructure, the sway of the foundation and the rocking of the foundation, respectively.

As a result, it is found that the maximum plastic deformation of the degree of freedom in which

the yielding restoring force is reduced becomes large, and that the displacement in the other degree of freedom is still within elastic range. In particular, in the case that the yield restoring force was reduced to 40% of its value, the displacement response of the corresponding degree of freedom is about 2-5 times the yield displacement. In the case of the sway of foundation, the response becomes 5.3 times and 3.9 times the value for rocking of the foundation and 1.8 times the value for the superstructure.

Therefore, it is proven that the magnification of the response in the sway of the foundation is larger than that in the rocking of the foundation and horizontal motion of the structure in the case that the yield restoring force of the sway of the foundation is varied. It is also concluded that the elastic response of the sway and rocking of the foundation may reduce the yield restoring force of the superstructure.

(2) The Influence of the Yield Strength Ratio (Kobe_NS Acceleration Input)

The results for Kobe_NS acceleration input are shown in Fig. 3.11. Fig. 3.11 (a), (b) and (c) show the response of the horizontal displacement of the superstructure, the sway of the foundation and the rocking of the foundation, respectively, in cases that the corresponding yield restoring force is reduced. These results are similar to the results for level 1 acceleration input. However, the plastic deformation in the sway and rocking motion of the foundation have occurred, which exceeds the deformation when the foundation yielded ((b) and (c)) subjected to level 1 acceleration input.

(3) The Influence of the Plastic Stiffness

The analytical results for the different plastic stiffness values are shown in Fig. 3.10 (a), (b) and (c). The plastic stiffness values vary within 0% to 20% of the original plastic stiffness, respectively. In these figures, the ductility factor is defined as the absolute value of the maximum displacement divided by the yield displacement. The response analysis is carried out by the level 2 acceleration input after determination of the yield level based on the maximum response by the level 1 acceleration input. The ductility factor for the superstructure and for the foundation are shown in Fig. 3.10 (a), (b) and (c), respectively.

From these figures, it is found that the displacement response of the superstructure decreases and the displacement response of the rocking of the foundation increases as the plastic stiffness of the superstructure becomes large. But it is also recognized that the displacement response of the rocking motion of the foundation decreases and the displacement response of the superstructure increases as the plastic stiffness gradient of the rocking motion of the foundation becomes smaller. The change in the sway response of the foundation is very small compared with other displacements by varying the plastic stiffness gradient. In addition, it is found that the displacement response of the sway of the foundation can be reduced, and that the displacement response of the superstructure and the rocking displacement of the

foundation are not changed even though the plastic stiffness of the sway of foundation is increased. Accordingly, it is understood that there is an interaction between the horizontal motion of the superstructure and the rocking motion of the foundation. It is also understood that the interaction between the sway motion of the foundation and the horizontal motion of the superstructure as well as the interaction between the sway motion of the foundation and the rocking motion of the foundation are small enough to be neglected. In other words, the rocking motion of the foundation is caused not by the sway motion of the foundation, but by the horizontal motion of the superstructure. This is because the sway spring and the rocking spring of the foundation are installed at the center of gravity of the foundation.

The analytical results subjected to Kobe_NS acceleration input while varying the plastic stiffness are shown in Fig. 3.12. Fig. 3.12 (a), (b) and (c) show the ductility factor of the superstructure, sway of the foundation and rocking of the foundation, respectively. These results are similar to those for the acceleration input specified in JSHB for type I soil qualitatively.

However, in the case using the Kobe_NS acceleration input, the response of the superstructure decreases by increasing the plastic stiffness, and the response increases a little when the plastic stiffness is 20% of the elastic stiffness.

The relationship of the plastic stiffness to the ductility factor of the superstructure is assessed in detail in Fig. 3.13. From this figure, it is confirmed that the response can be reduced by increasing the plastic stiffness gradient in the case of the acceleration input specified in JSHB for type I soil, but the response can not be reduced in the case of the Kobe _NS acceleration input even if the plastic stiffness increases.

3.3.4 Allowable Ductility Factor

The ductility factor is one of the important indexes for evaluating the seismic performance of structural systems. Generally, it can be said that a structural system with a large ductility factor will exhibit superior earthquake resistance. The assessment of the seismic design of the structure-foundation system is made by means of the ductility factor of the structural element.

Fig. 3.14 shows the relation of the plastic stiffness to the yield restoring force in cases that the maximum ductility factor is 2, 4, 6, or 8, respectively, and subjected to level 2 acceleration for type I soil. The horizontal axis and the vertical axis of this figure denote the normalized plastic stiffness divided by the elastic stiffness and the normalized yield restoring force divided by the maximum elastic restoring force by level 1 acceleration of type I soil, respectively.

From this figure, it is found that it is possible to reduce the yield restoring force significantly by allowing a large ductility factor. Moreover, the yield restoring force can be further reduced by increasing

the plastic stiffness in order to ensure the given ductility factor. In Particular, a significant difference in the required ductility factor exists in the case that the ratio of the plastic stiffness to the elastic stiffness is less than 10%. This tendency is more profound in the case that the allowable ductility factor is larger. Therefore, it can be said that the ductility evaluation should consider not only the yield restoring force but also the plastic stiffness of structures.

3.4 Concluding Remarks

In this study, in order to examine the influence of the dynamic interaction of the foundation-structure system on the structural response, a simple structural system with 3 degrees-of-freedom consisting of a foundation and superstructure was used in the response analysis. The analysis was carried out while varying the soil type, the level of seismic force, the yield restoring force, and the plastic stiffness for each degree of freedom. Based on the response analysis, the following conclusions can be made.

1) By incorporating the sway and rocking motion of the foundation, in addition to the sway of the superstructure, to yield a system with 3-degrees-of-freedom, the influence of the dynamic interaction between the motion of the structure and the foundation can be clarified from the viewpoint of absorbed energy and ductility factor. It is found that the interaction between the horizontal motion of the superstructure and the rocking motion of the foundation is significant.
2) As for the difference between the fixed foundation condition and flexible foundation condition, the difference in the results becomes more significant for type III soil than type I soil. Therefore, a response analysis assuming a rigid foundation may be insufficient for the soft ground, and in such cases a response analysis that accounts for a flexible foundation should be carried out.
3) By deriving the equation of the energy equilibrium in the elasto-plastic response of the foundation-structure system, the response of 3-degrees-of-freedom is evaluated by the scalar quantity of energy focusing on of the energy distribution. In addition, it is understood that the effect of the dynamic interaction can be clarified by the energy equilibrium. Therefore, the use of the scalar quantity of energy as the index for evaluation of the response of multiple degrees-of-freedom systems is found to be very effective.
4) The analysis considering the yield strength ratio and plastic stiffness is carried out on the basis of the index of ductility factor. It is understood that the effect of the yield strength ratio and plastic stiffness on the elasto-plastic response behavior of the foundation-structure system is very significant. It is also concluded that the ductility factor required to assure the safety of the structure depends on the input acceleration. Therefore, the identification of the restoring force characteristics of every structural

element is very important for the seismic design paying attention to the deformability.

5) It is found that the plastic deformation is concentrated in structural element with low strength. It is possible that the plastic deformation of the foundation is effectively reduced by setting a smaller yield ratio strength of the superstructure if the foundation-structure system subjected to very large seismic force undergoes extensive deformation into a plastic state.

References

Hanshin Expressway Management Technology Center, Japanese Society of Steel Construction, (1994), "Experimental report on horizontal dynamic bearing capacity" (in Japanese).

Hirao, K., Sawada, T., Nariyuki, Y. and Sawada, S., (1986), "On the relation between hysteretic energy and elastic response of single degree of freedom systems under strong earthquake motions", Journal of Structural Mechanics and Earthquake Engineering, JSCE, No.368/I-5, pp. 401-410 (in Japanese).

Japan Road Association, (1990), "Specification of highway bridges, Part V, Seismic design", Maruzen Co, Ltd. (in Japanese).

Kawashima, K. et al., (1992), "Calculation examples of seismic design for highway bridges", Sankaido Publishing Co., Ltd. (in Japanese).

Shibata, A., (1986), "The latest seismic analysis for structures", Morikita Shuppan Co., Ltd. (in Japanese).

Murata, M., (1993), "A primer of mechanics of the elasto-plastic materials", The Nikkan Kogyo Shimbun Ltd. (in Japanese).

Tanabe, Y. and Shinada, M., (1990), "Analytical dynamics", Vol. 3, Shokabo Publishing Co., Ltd. (in Japanese).

Toki, K., (1981), "Seismic analysis for structures", The new system of civil engineering, Vol. 11, Gihodo Shuppan Co.,Ltd. (in Japanese).

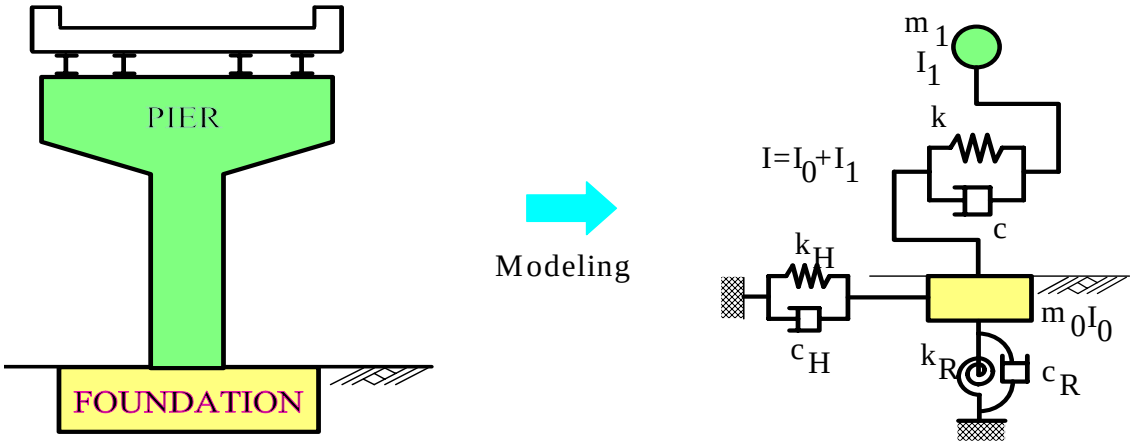

Fig. 3.1 Modeling of structure-foundation system

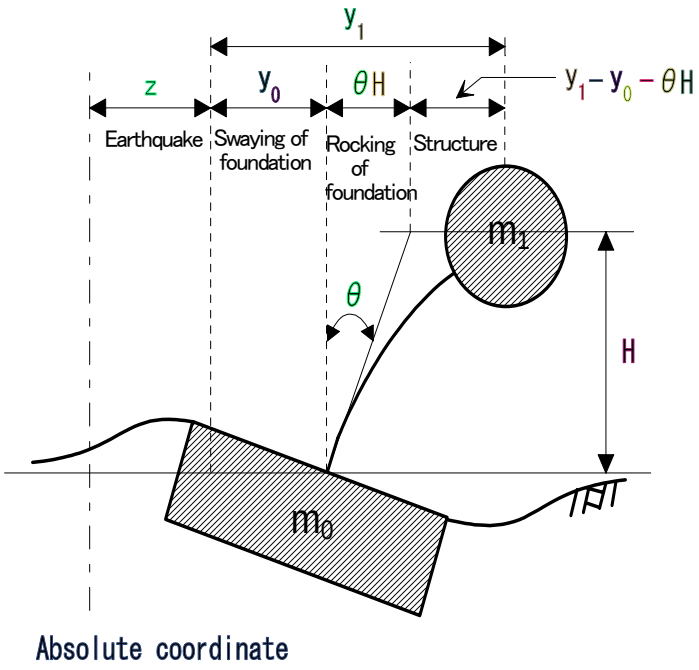

Fig. 3.2 Schematic deformation of structure-foundation system

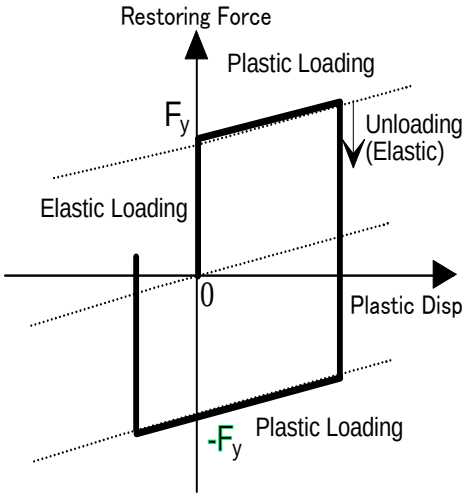

Fig. 3.3 Restoring force model

Table 3.1 Structural parameters of structure

Weight: m_1	360 tonf
Height of pier: H	1500 cm
Rotary inertia: I_1	3.09×10^4 tonf·cm·s^2

Table 3.2 Structural parameters of foundation

Weight: m_0	315 tonf
Length in bridge axis	700 cm
Length in the perpendicular to bridge axis	900 cm
Rotary inertia: I_0	2.28×10^4 tonf·cm·s^2

Table 3.3 Characteristics of ground

Type of soil	Unit weight: γ (tonf/m^3)	Shear wave velocity: V_s (m/s^2)	Dynamic Poisson's ratio: ν
Type Ⅰ soil	2.0	250	0.45
Type Ⅲ soil	1.8	150	0.50

Table 3.4 Coefficient of subgrade reaction

Type of soil	Vertical direction (kgf/cm^3)	Horizontal direction (kgf/cm^3)
Type Ⅰ soil	10.6	3.52
Type Ⅲ soil	3.54	1.18

Table 3.5 Damping factor and spring constant for structure and foundation

Structural component		Damping factor	Spring constant
Structure		0.05	26 tf/cm
Type Ⅰ soil	Swaying of foundation	0.1	2.22×10^{3} tf/cm
	Rocking of foundation	0.1	4.49×10^{8} tf•cm
Type Ⅲ soil	Swaying of foundation	0.1	7.74×10^{2} tf/cm
	Rocking of foundation	0.1	1.51×10^{8} tf•cm

Table 3.6 Eigenfrequency analysis（unit : sec）

	Natural Period	
	Type Ⅰ soil	TypeⅢsoil
1st order mode	0.798	0.893
2nd order mode	0.075	0.128
3rd order mode	0.064	0.099

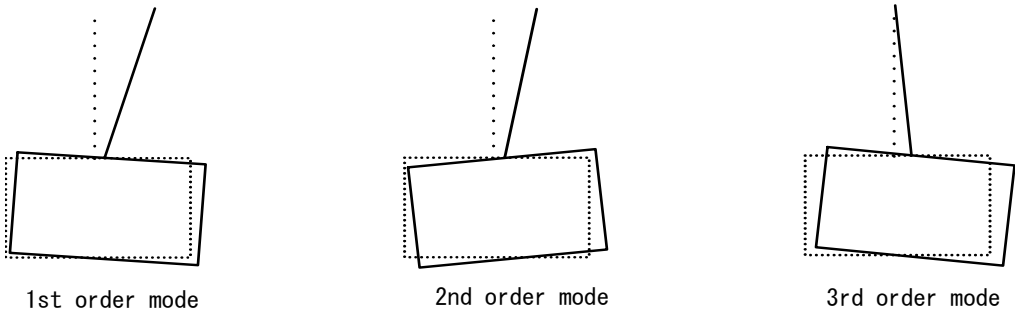

Fig. 3.4 Three vibration modes

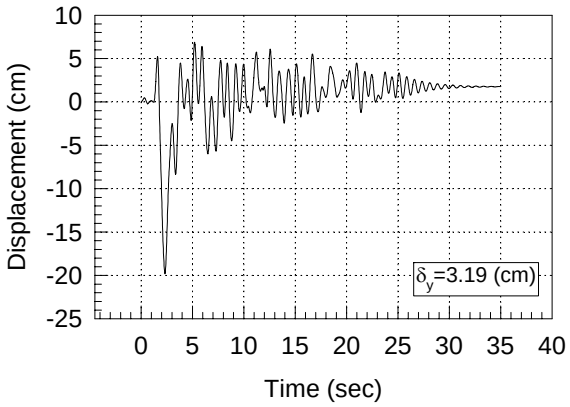

(a) Displacement response

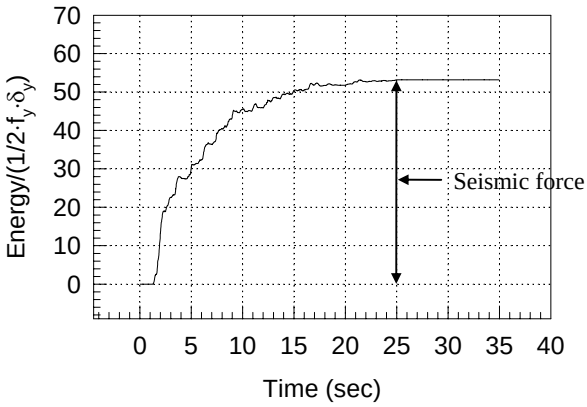

(c) Input energy

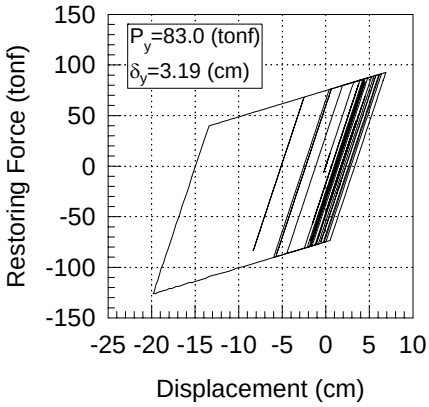

(b) Hysteretic curve

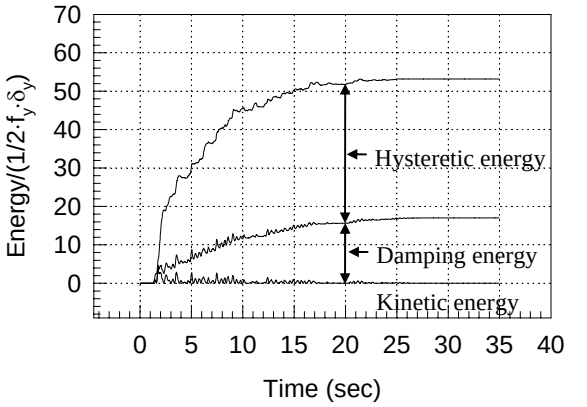

(d) Absorbed energy

Fig. 3.5 Analytical results (Superstructure: Foundation is fixed)

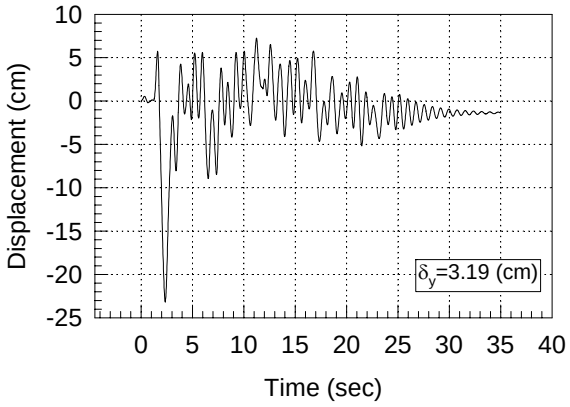

(a) Displacement response

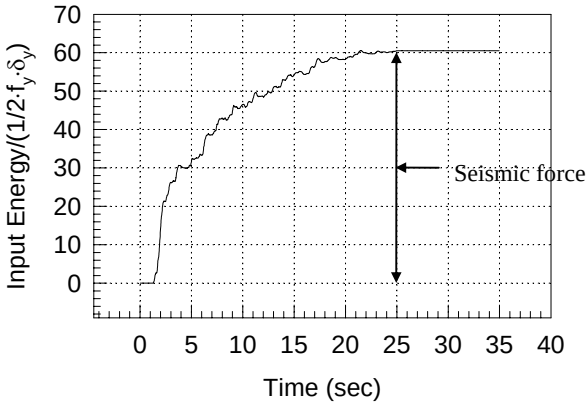

(c) Input energy

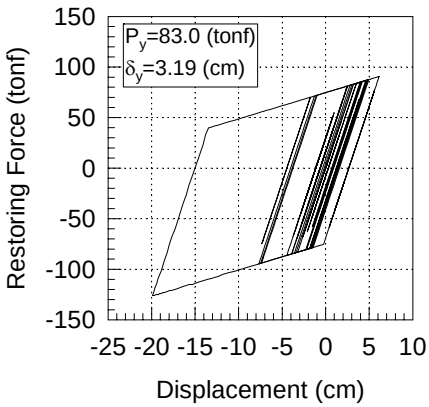

(b) Hysteretic curve

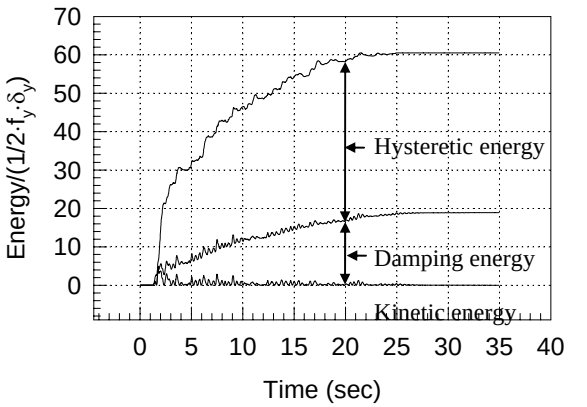

(d) Absorbed energy

Fig.3.6 Analysis results (Superstructure: Foundation is unfixed)

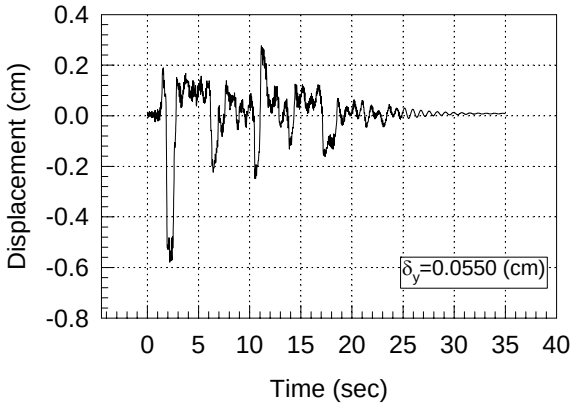

(a) Displacement response

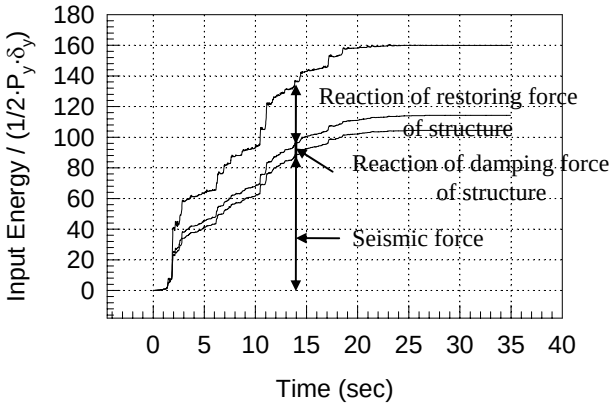

(c) Input energy

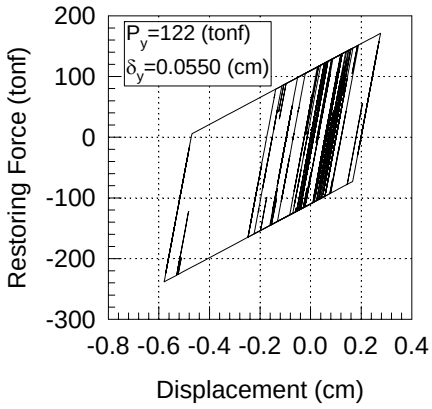

(b) Hysteretic curve

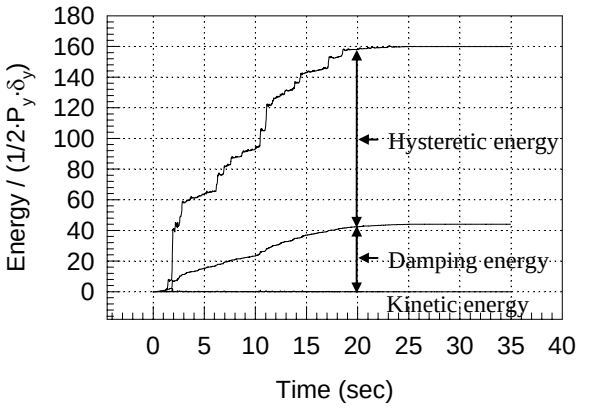

(d) Absorbed energy

Fig. 3.7 Analytical results (Sway of foundation: Foundation is unfixed)

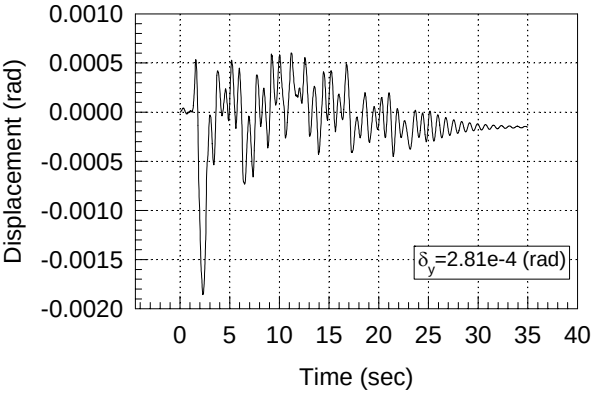

(a) Displacement response

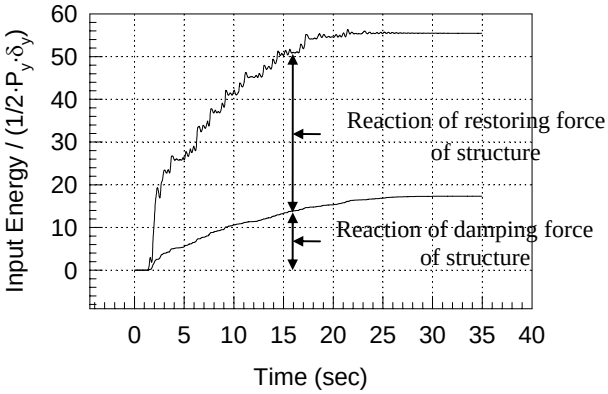

(c) Input energy

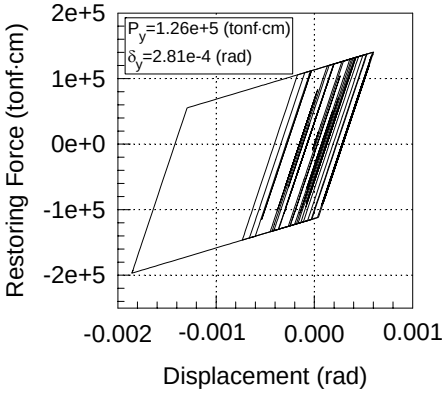

(b) Hysteretic curve

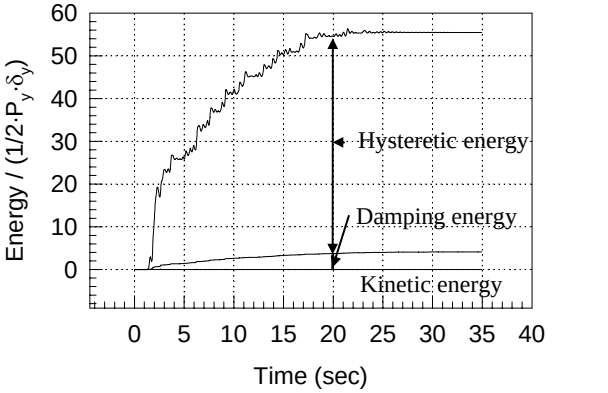

(d) Absorbed energy

Fig. 3.8 Analytical results (Rocking of foundation: Foundation is unfixed)

Table 3.7 Analytical results

Type of soil	Type I soil			Type III soil		
Level of input earthquake	LEVEL 1 (c)	LEVEL 2 (d)	Dynamic magnification factor (d) / (c)	LEVEL 1 (e)	LEVEL 2 (f)	Dynamic magnification factor (f) / (e)
Fixed foundation (a)	2.78(cm)	19.8(cm)	7.12	4.36(cm)	17.0(cm)	3.90
Unfixed foundation (b)	3.65(cm)	23.2(cm)	6.36	7.14(cm)	21.6(cm)	3.03
(b) / (a)	1.31	1.17		1.64	1.27	

Level 1: Elastic response analysis, Level 2: Elasto-plastic response analysis

Table 3.8 Ductility factor

Structural elements	Degree of freedom	Type Ⅰ soil		Type Ⅲ soil	
		Maximum relative displacement	Ductility factor	Maximum relative displacement	Ductility factor
Superstructure	Horizontal direction	19.9(cm)	6.23	14.5(cm)	2.89
Foundation	Sway direction	0.579(cm)	10.54	1.68(cm)	7.79
	Rocking direction	0.00186(rad)	6.61	0.0413(rad)	3.15

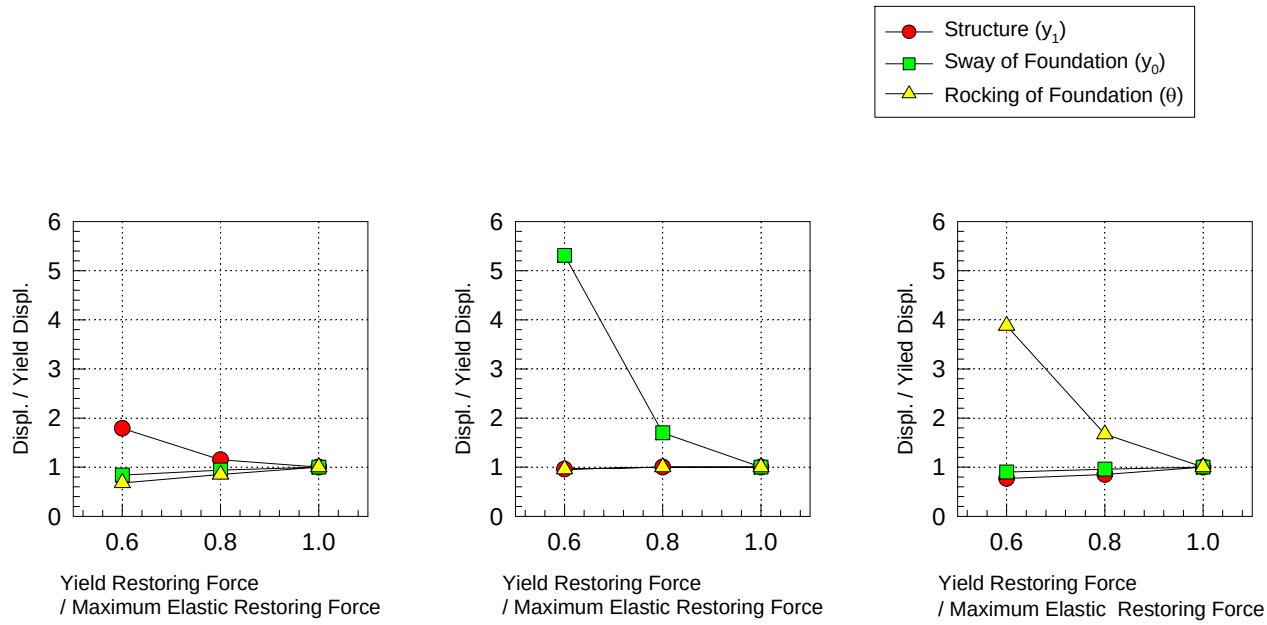

(a) Yield restoring force of structure is changed

(b) Yield restoring force of sway of foundation is changed

(c) Yield restoring force of rocking of foundation is changed

Fig. 3.9 Effect of yield strength ratio (LEVEL 1-1)

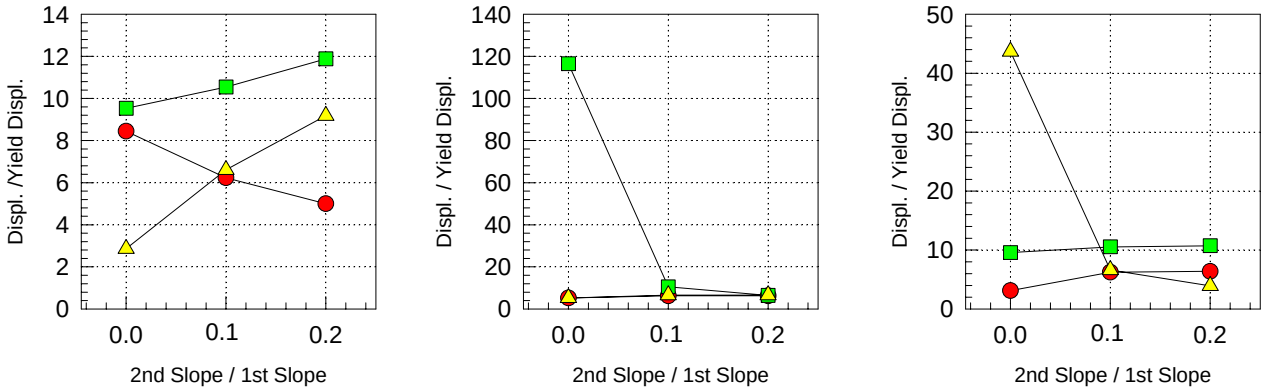

(a) Second slope of structure is changed

(b) Second slope of sway of foundation is changed

(c) Second slope of rocking of foundation is changed

Fig. 3.10 Effect of plastic stiffness (LEVEL 2-1)

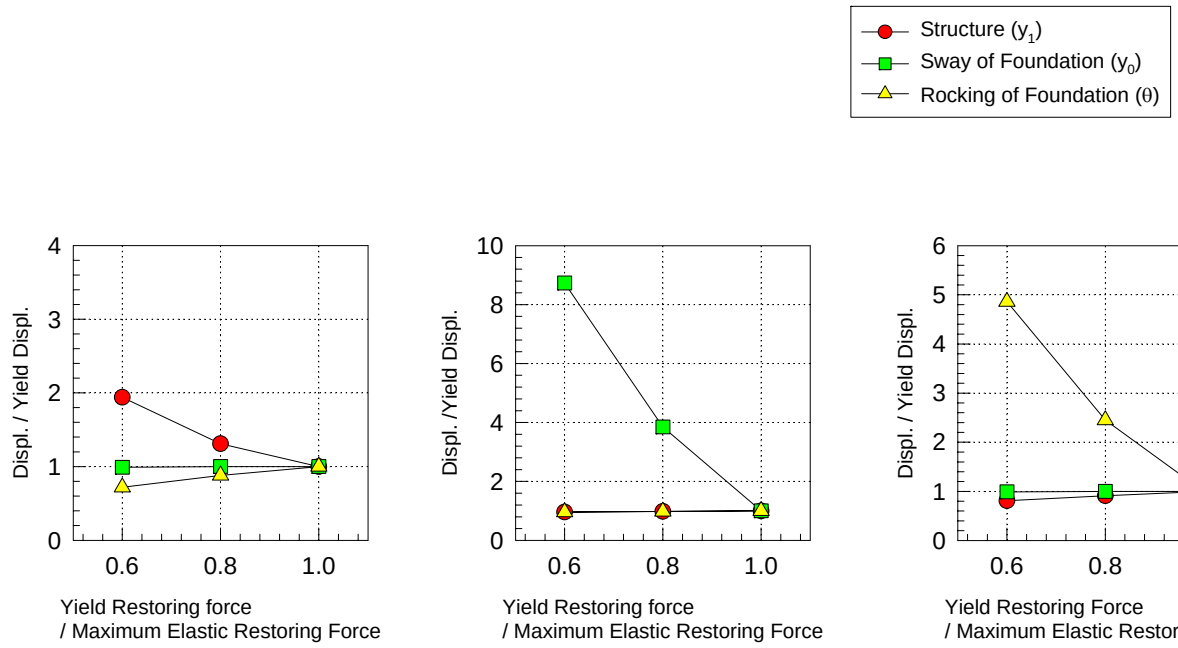

(a) Yield restoring force of structure is changed

(b) Yield restoring force of sway of foundation is changed

(c) Yield restoring force of rocking of foundation is changed

Fig. 3.11 Effect of yield strength ratio (KOBE_NS)

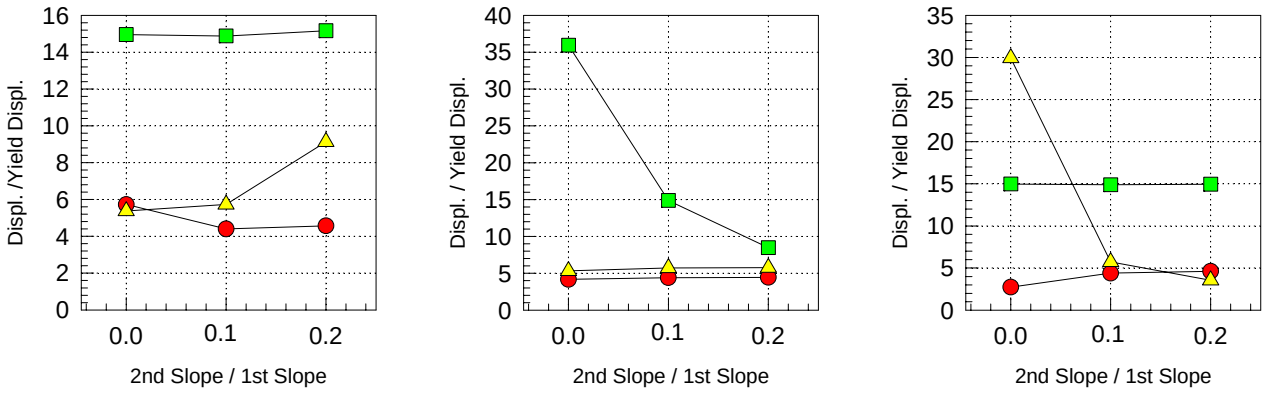

(a) Second slope of structure is changed

(b) Second slope of sway of foundation is changed

(c) Second slope of rocking of foundation is changed

Fig. 3.12 Effect of plastic stiffness (KOBE_NS)

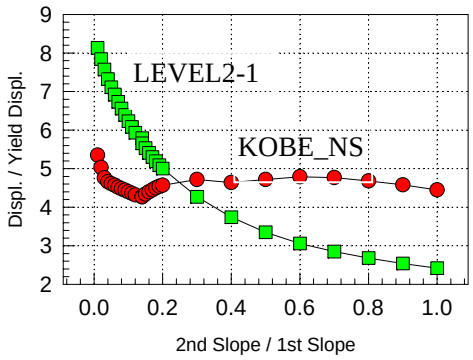

Fig. 3.13 Compared LEVEL2 with KOBE_NS

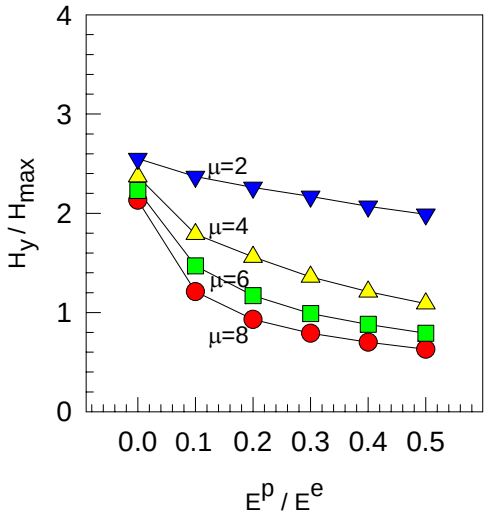

Fig. 3.14 Allowable ductility factor

Chapter 4

Behavior of Steel Rigid-Frame Piers Subjected to In-Plane Horizontal Loads and Their Seismic Performance

4.1 Introduction

Many rigid-frame bridge piers sustained minor to severe damage during the 1995 Hyogoken-Nanbu Earthquake, as shown in Photo 4.1. However, in the current Japanese Specifications for Highway Bridges V, Earthquake Resistant Design (Japan Road Association, 1996), there is no requirement to check the ultimate lateral load-carrying capacity of steel rigid-frame piers that are statically indeterminate and have larger lateral load-carrying capacity and ductility than single-column piers, which are statically determinate structures.

It is well known that the horizontal load-carrying capacity method can be used for the seismic resistant design of structures where the fundamental vibration mode dominates, and that the seismic response and locations of plastic hinges can be easily determined because the energy-equivalent method can be applied for such structures (Usami, T., 1999; Nakajima, A. and Onodera, O., 1998). In the current Japanese Specifications for Highway Bridges, Earthquake Resistant Design, the horizontal load-carrying capacity method is provided only for the RC piers. Although many researches have been conducted to understand the seismic behavior of steel piers since the Hyogoken-Nanbu Earthquake, there are many areas that need further investigation (Aoki et al., 1997; Ida et al., 2000; Ikeda et al., 2000; Miki et al., 1998; Nakai et al., 1987; Nara et al., 1999; Subcommittee on New Technology for Steel Structures of Japan Society of Civil Engineers, 1996; Sugimoto et al., 2000; Takahashi et al., 1998; Usami et al., 1994).

To gain a better understanding of the in-plane behavior of steel rigid-frame piers under in-plane horizontal loading, it is necessary to perform a loading test on the entire pier system with both horizontal and vertical loads applied, and to investigate its load carrying capacity and ductility. Therefore, in this study, monotonic and cyclic loading tests were performed on test specimens in the transverse direction of the bridge. Moreover, an elasto-plastic finite displacement analysis was performed using the general-purpose finite element analysis program, ABAQUS. In the analysis, all structural components were modeled with shell elements to accurately predict the local buckling of thin steel plates.

4.2 Experimental Program

4.2.1 Test Specimen

Test specimens in this study were fabricated based on the geometry of Kishi P34, which is one of the standard steel rigid-frame piers of the Hanshin Expressway Route 5 Line (Wangan Line). Due to the spatial restrictions of the experimental facility at Kyoto University, the size of the specimen was scaled down to the 1/17 of the actual size of Kishi P34. The geometry of the specimen is shown in Fig. 4.1. Since it was not practical to scale down every dimension by a factor of 1/17, columns and beams were designed to have a uniform cross section. Section properties of the column and beam were designed based on the column base section and the beam middle section of the prototype, respectively. To achieve a force-displacement relationship similar to that of the prototype, structural parameters including the width-to-thickness ratio and longitudinal stiffener's relative stiffness were designed to be as close as possible to those of the prototype. Table 4.2 and Table 4.3 provide a comparison of the buckling parameters of Kishi P34 and the specimen.

To prevent weld fractures at the corners from controlling the ultimate load-carrying capacity during the loading test, the beam-column connection parts indicated in Fig. 4.1 were strengthened by increasing the plate thickness from 1.6 mm to 2.3 mm. A steel grade of SS400 was used in the specimen rather than the grade SM490Y steel used in Kishi P34. Table 4.1 shows the mechanical properties of SS400 obtained from the material testing. The specimens were carefully fabricated to limit the initial imperfections to within 1/200 of the sectional dimensions.

4.2.2 Loading Method

Fig. 4.2 shows the loading apparatus used in this study. The vertical load is applied to the top of each pier by using two actuators. During the test, the axial load ratio, σ_c/σ_y (σ_c : axial compressive stress due to dead load of the superstructure; σ_y : yield stress of steel), was set at 4.15% and kept constant, where 4.15% is the actual value in the design of Kishi P34. The horizontal load was applied by one actuator to the tops of columns that were linked by rigid links that can distribute the load to two columns equally without restraining the deformation of the beam. The displacement control was used in the horizontal loading. An overview of the test setup is shown in Photo 4.2. In this study, horizontal load values were obtained from the actuator, and horizontal displacements were taken as an average of the displacement measurements at the displacement transducers LVDT-1 and LVDT-2, as shown in Fig. 4.2.

4.3 Elasto-Plastic Finite Displacement Analysis

4.3.1 Analytical Model

The general purpose finite element analysis program, ABAQUS (Hibbit, Karlsson Sorensen, Inc. 1999), was used to perform the elasto-plastic finite displacement analysis of the test specimen. To be able to model local buckling, all components of the specimen were modeled by shell elements, SR4 (4-node reduced integration element).

Fig. 4.3 shows the analytical model used in this study. The total number of nodes and elements in this model are 18,754 and 18,658, respectively. Element sizes were determined to accurately predict local buckling. Web and flange plates of columns between longitudinal stiffeners were divided into 6 elements, longitudinal stiffeners in the columns were divided into 4 elements in their depth direction, and 56 elements were used in the column axis direction. Flange plates of the beam were divided into 10 elements between longitudinal stiffeners, while web plates of the beam were divided into 16 elements. Longitudinal stiffeners had 4 elements in their depth direction, and 40 elements were provided in the beam axis direction. All the shell elements consisted of 16 layers through plate thickness. To reduce the computational effort, one half of the specimen was analyzed by making use of a symmetry about the x-z plane. The model was completely fixed at the bottom of the columns.

The von Mises yield function, the associated flow rule, and a mixed isotropic/kinematic hardening model were used to model the plasticization of steel. Uniaxial stress-strain data from the material testing were used as input.

Initial imperfections of the specimen were not measured; therefore, residual stresses and initial deflections available in the literature (Komatsu et al., 1977) were used in the elasto-plastic finite element analysis. The distributions of residual stresses and initial deflections used in the analysis are shown in Fig. 4.5 and Fig. 4.6, respectively.

4.3.2 Loading Conditions

Loading is applied to the model by a pantograph structure as shown in Fig. 4.4. The loading configuration is slightly different from that used in the experiment, but the difference will not affect the results significantly.

The total horizontal load to the model is obtained by multiplying the sum of the horizontal load at loading points C and D (see Fig. 4.4) by two, and the horizontal displacement of the model is obtained as the average value of horizontal displacements at points A and B (see Fig. 4.4). Yield load is defined as the load at which stress in any element reaches the value of the von Mises equivalent yield stress, and the displacement value at the yield load is defined as the yield displacement.

4.4 Results and Discussion

4.4.1 Monotonic Loading

The horizontal load-displacement curve and collapse process obtained from the monotonic loading test are shown in Fig. 4.7. The occurrence of local buckling was judged by a visual inspection during the experiment, whereas it was determined at the point where the strain on one surface of plate started diverging from the strain on the other surface. The load-carrying capacity, ductility, and collapse process are discussed in the following.

(1) Load-Carrying Capacity and Ductility

In Fig. 4.7, the following four characteristic points are indicated: (1) the yield point; (2) the maximum horizontal displacement point; (3) the maximum horizontal load point; and (4) the 95% H_{max} (5% degradation) point. The horizontal load kept increasing after the yield point, and became 2.3 times the yield horizontal load, H_y, at the maximum load, H_{max}. The ductility ratio, δ/δ_y, at H_{max} was approximately 10 in the finite element analysis (FEA) and 9 in the experiment. Since these ductility ratios are much higher than those reported for steel single-column piers (Watanabe et al., 1994), it can be concluded that rigid-frame piers have superior ductility.

The results from the FEA and the experiment are in very good agreement up to the yield point. However, after the yield point, the load-displacement curve from the FEA does not show as much stiffness reduction as the curve from the experiment. This slight difference may have been caused by a difference in initial imperfections. The maximum loads and horizontal load degradation (softening) rates after the maximum load are in good agreement between the FEA and the experiment.

(2) Collapse Process

Damage was observed at the base of columns as well as in the beam in both the FEA and the experiment. Local buckling became very visible near the maximum load point. It was found that local buckling at the base of columns together with local buckling at the beam would reduce the load-carrying capacity of the pier.

In the experiment, local buckling of the web plate of the beam due to shear stress was observed near the maximum load point. After the maximum load point, local buckling was observed at the right flange plates of right and left column bases and the upper and lower flange plates of the beam at the left and right corners. Then, near the failure point (95% H_{max}), local buckling was also observed at web plates of the left and right side column bases.

Fig. 4.8 and Fig. 4.9 show the strain distributions obtained at the left column and the beam during the loading test, respectively. At the horizontal displacement of 10 mm, where the stiffness reduction was significant, the strain values at both column bases and the beam were higher than the yield strain (ε_y=801$\times$ 10^{-6} (mm/mm)). Several locations were experiencing plastic deformation at the same time, which led to a further reduction in stiffness. As can be seen in the figures, strains were significantly high at the column bases and corners of the beam, where significant local buckling was observed.

In the FEA, local buckling of the flange plate of the beam occurred at 10 mm horizontal displacement. Then, near the maximum load point, local buckling due to shear stress occurred at the flange plate of the beam, followed by local buckling at the flange plates of both column bases.

The FEA accurately predicted the collapse process and damage locations obtained from the experiment, except that local buckling of the beam flange plate occurred at 10 mm horizontal displacement in the FEA. Fig. 4.10 shows local buckling shapes at various locations from the FEA and the experiment, and again indicates that the FEA adequately predicted the buckling shapes. In conclusion, the results from the FEA and the monotonic loading test were in very good agreement.

4.4.2 Cyclic Loading

The horizontal load-displacement curve, envelope curve, and collapse process obtained from the cyclic loading test are shown in Fig. 4.11 and Fig. 4.12. The occurrence of local buckling was judged in the same manner as in the monotonic loading test. The load-carrying capacity, ductility, and collapse process are discussed in the following.

(1) Load-Carrying Capacity and Ductility

The horizontal load kept increasing after the yield point, and became 2.4 times the H_y at H_{max}. The ductility ratio at H_{max} was 7 in the experiment and 5 in the FEA. These results indicate that steel rigid-frame piers have superior horizontal load-carrying capacity and ductility.

The envelope curves show good agreement between the FEA and the experiment, and the horizontal load degradation (softening) behaviors past the maximum load point are also in good agreement between the FEA and the experiment.

(2) Collapse Process

During the cyclic loading test, the first local buckling was observed at the right flange plate of the right column base at $+6\delta_y$. After the first local buckling, the horizontal load slightly increased, and at $+7\delta_y$, where the maximum load was obtained in the positive direction, local buckling was observed at several

locations: the flange plate of the left column base; the upper and lower flange plates of the left and right corners of the beam; and the web plates of the beam. Then, the horizontal load decreased as the displacement increased. Finally, local buckling was also observed at the web plates of column bases, and the pier reached a failure state.

The principal strain obtained on the web plate of the beam at midsection is shown in Fig. 4.13. The measurement location is designated as point A in Fig. 4.1. The minimum principal strain in the beam web plate increased significantly between the cycles of $+8\delta_y$ and $+9\delta_y$ because shear buckling occurred at the beam web plate during the $+7\delta_y$ cycle. The maximum strain value of $\varepsilon=42{,}394\times10^{-6}$ mm/mm is as much as 50 times the yield strain ($\varepsilon_y=801\times10^{-6}$ mm/mm), which shows severe damage at the beam web plates.

Axial strains obtained on the flange plate of the beam at points B and C (see Fig. 4.1) are shown in Fig. 4.14. It can be seen in the figure that the strain increased significantly between the cycles of $-8\delta_y$ and $-9\delta_y$ due to a the progression of local buckling at the upper flange plate of the right corner of the beam. The maximum strain shown in Fig. 4.15 was $\varepsilon=43{,}090\times10^{-6}$ mm/mm, which is twice the maximum strain ($\varepsilon=20{,}960\times10^{-6}$ mm/mm) obtained at the left column base (points D and E in Fig. 4.1). Therefore, the beam underwent severe damage during the cycling loading test.

The FEA was able to accurately predict the progression of the damage at the beam and column bases, except that local buckling of the beam flange plate occurred during the $+5\delta_y$ cycle. The buckling shapes and locations of local buckling were also in good agreement between the FEA and the experiment. In general, the FEA results matched the experimental results well.

Fig. 4.16 shows the bending moment-curvature relationships at the column base from the FEA and the experiment. The bending moment at the column bases reached the yield moment during approximately the $\pm3\delta_y$ cycle in both the FEA and the experiment. The maximum bending moment from the experiment was 1.14 times that from the FEA on the positive side and 1.41 times that from the FEA on the negative side. This discrepancy can be explained by the calculation method of bending moment during the experiment. To obtain the bending moment in the experiment, the curvature was first calculated based on axial strain values obtained at the middle of the column, where the bending moment always be low the yield bending moment. These strains were still in the elastic range. Then, the bending moment distribution was estimated linearly based on bending moments at two sections that were calculated from curvatures.

In the experiment, the curvature at the left column base changed significantly between the cycles of $+8\delta_y$ and $+9\delta_y$, and the bending moment decreased, because the out-of-plane deformation of the flange plate that started at the $+7\delta_y$ cycle became larger, which is in good agreement with the observed collapse process.

In the FEA, due to the progress of local buckling at the left column base, the bending moment decreased abruptly between the cycles of $+8\delta_y$ and $+9\delta_y$. The maximum bending moment in the beam was about 95% of the yield bending moment. Also, due to the progress of local buckling at the lower flange plate of the left corner of the beam that started at the $+5\delta_y$ cycle, the curvature increased during the cycles of $+5\delta_y$ and $+6\delta_y$. The curvature at sections with a plate thickness of 2.3 mm was about 60% smaller than that at sections with a plate thickness of 1.6 mm, because the deformation due to local buckling was smaller at the sections with thicker plates than at the sections with thinner plates.

4.5 Pseudo-Dynamic Testing

4.5.1 Introduction

It is well known that the horizontal load-carrying capacity method can be used for the seismic resistance design of structures in cases where the fundamental vibration mode will dominate the seismic response and the locations of plastic hinges can be easily determined, because the energy-equivalent method can be applied for such structures (Usami, 1998; Nakashima and Onodera, 1998). In the current Japanese Specifications for Highway Bridges V, Earthquake Resistant Design (Japan Road Association 1996), the horizontal load-carrying capacity method is provided only for RC rigid-frame piers, but not for steel rigid-frame piers, and not even for steel single-column piers.

Although many researches have been conducted since the Hyogoken-Nanbu Earthquake to clarify the seismic behavior of steel rigid-frame piers, there are many research areas that need further investigation. To improve our understanding of the in-plane behavior of steel rigid-frame piers under in-plane horizontal loading, it is necessary to understand the structural behavior of the entire pier system, including the columns, beam, and corners, with both horizontal and vertical loads applied, and to investigate its load-carrying capacity and ductility.

Hanshin Highway Public Corporation and Kyoto University have been conducting a collaborative research on the in-plane behavior of steel rigid-frame piers. In this study, the pseudo-dynamic testing was performed on a scale model of an existing steel rigid-frame pier, and the in-plane seismic response and elasto-plastic behavior of such piers were examined. Moreover, the validity of a one degree-of-freedom model of the steel rigid-frame pier for a simplified analysis was also investigated.

4.5.2 Experimental Program

(1) Test Specimen and Loading Method

The test specimens in this study were fabricated based on the geometry of Kishi P34, which is one of the

standard steel rigid-frame piers of the Hanshin Expressway Route 5 Line, as described in 4.2.1. The elasto-plastic finite displacement analysis of this pier has been performed by using the general purpose finite element analysis program ABAQUS. According to the results of the analysis, the maximum load-carrying capacity of this pier is about three times the yield load (7.20 MN), and the ductility ratio (yield displacement: 4.53 cm) at the maximum load is about 12. The yield load is defined as the load at which any element reaches the von Mises equivalent yield stress. The maximum load-carrying capacity of the Kishi P34 turned out to be higher than the seismic load, $K_{he} \cdot W$, in which K_{he} and W are the seismic coefficient factor and weight of the superstructure, which takes into account a reduction of the seismic load by the energy equivalent method.

(2) Pseudo-Dynamic Testing

To accurately predict the seismic responses of a steel rigid-frame pier in which the axial force in the columns and the shear force in the beam vary and several plastic hinges are developed under seismic excitations, it is extremely important to accurately represent the restoring force-displacement relationship. The pseudo-dynamic testing is a very useful tool for such this purpose.

The superstructure of Kishi P34 consists of 3-span continuous steel box girders with steel deck plate. In this study, the steel rigid-frame pier was modeled by a one degree-of-freedom system with the equivalent mass and the horizontal load-displacement relationship obtained from the loading test. The equation of motion for the one degree-of-freedom system was solved by the Newmark's β method with a time increment of 0.01 sec. The equivalent mass, damping ratio, and stiffness of the system were 1,590 tons, 2%, and 1.6 MN/cm, respectively. The equivalent natural period of the system turned out to be 0.63 sec.

The ground acceleration record shown in Fig. 4.17 was used as the input ground motion in this study; this record was modified from the acceleration time history recorded at the Higashi Kobe Bridge to meet the response spectrum specified in the Japanese Specifications for Highway Bridges, particularly for the soil profile III. By increasing the amplitude of the input acceleration, three input ground motions were prepared for the pseudo-dynamic test: Input 1 used the acceleration time history shown in Fig. 4.17; in Input 2, the amplitude of the acceleration time history shown in Fig. 4.17 was doubled; and in Input 3 the amplitude was tripled. The seismic response characteristics of the steel rigid-frame pier at different damage levels were investigated using the three different levels of ground accelerations.

4.5.3 Results and Discussion

Fig.s 4.18 to 4.23 show the displacement response time histories and force-displacement curve obtained from the pseudo-dynamic test. The results shown in these figures were converted values for the prototype

pier. As indicated in the figures, the yield load and displacement were 7.20 MN and 4.53 cm, and the allowable residual displacement was 19.3 cm. In the test, the ground acceleration was used for 50 sec, and free vibration was measured for the following 10 sec. However, only results from the first 30 sec are shown in the figures because the system would become stable within only the first 30 seconds of the ground acceleration. Photos 4.3 to 4.5 show the damage locations of the specimen.

With Input 1, the maximum displacement of $3.3\delta_y$ was obtained at 6.8 sec, and the residual displacement was close to zero. The maximum load reached 2.2 H_y, which is smaller than the maximum load-carrying capacity, H_{max}, that was obtained by the cyclic loading test. It is reasonable to assume that part of a section started yielding at several locations because the slope of the load-displacement curve near the maximum load was not as steep as the initial slope. However, there was no visible damage in the specimen.

With Input 2, the maximum displacement reached $9.0\delta_y$ at 7.0 sec, and the residual displacement of 6.5 cm was still smaller than the allowable residual displacement (L/100; L: height of pier). The maximum load reached the maximum load-carrying capacity ($2.8H_y$), and a slight reduction of the load-carrying capacity was observed. At several locations, at least the flanges should be yielding at this stage.

With Input 3, the maximum displacement reached as high as $16\delta_y$ at 7.1 sec, and the load-carrying capacity gradually decreased as the local buckling at the column base progressed, as shown in Photo 4.4. As the load-carrying capacity decreased further, the displacement increased and finally exceeded the measurable range of the control displacement transducer. Then, the testing was terminated. The termination point is indicated in the figure by X. The degraded load carrying capacity was 72% of H_y, and cracking and local buckling were observed at the corners at the end of the test, as shown in Photo 4.5.

The elasto-plastic seismic response analysis of the steel rigid-frame pier was carried out by using a one degree-of-freedom system with a bilinear restoring force model. The structural parameters for the one degree-of-freedom system are those used in the pseudo-dynamic test. Since the restoring force-displacement relationship was modeled as a bilinear relationship, the negative slope after the maximum load-carrying capacity was not considered in this study. Input 2 ground acceleration time history was used in the analysis. By changing the second slope of the bilinear model, seismic responses from the one degree-of-freedom system was compared with results from the pseudo-dynamic testing. The yield point was defined as the maximum load point from the pseudo-dynamic testing with Input 1 ground acceleration.

The maximum displacement, the maximum load, and the residual displacement obtained from the time history analysis are shown in Table 4.6. When the second slope of the restoring force-displacement relationship is 10% of the initial slope, the results are closest to the response values from the

pseudo-dynamic testing among other cases with different second slopes. However, the differences are not small. It is recommended that a proper restoring force-displacement relationship be developed for a steel rigid-frame pier modeled by the single degree-of-freedom system.

4.6 Conclusions

In this study, the in-plane behavior and collapse process of steel rigid-frame piers under in-plane horizontal loading were investigated through a loading test and elasto-plastic finite displacement analysis. A pseudo-dynamic test of a steel rigid-frame pier under in-plane horizontal loading was also carried out, and the seismic response characteristics and elasto-plastic behaviors of such a pier were closely examined.

1) The steel rigid-frame pier investigated in this study has a maximum horizontal load-carrying capacity of 2.3 times the yield horizontal load, and it has a superior load carrying capacity and ductility ratio compared to a single-column pier.
2) The FEA can accurately predict the in-plane behavior and collapse process of a steel rigid-frame pier under in-plane horizontal loading. The load-displacement behaviors up to the yield point are found to be in good agreement between the FEA and the experiment. Although there is a slight difference in the stiffness reduction rate after the yield point is reached, the maximum horizontal load and horizontal load degradation behavior are accurately predicted by the FEA.
3) The severe local buckling appears at a load close to the maximum. The local buckling at the column bases as well as the beam reduces the horizontal load-carrying capacity of the steel rigid-frame pier. It is found that the steel rigid-frame pier develops plastic hinges at several locations before it reaches a failure state, and that it has a high ductility ratio.
4) It is necessary to develop a well-balanced earthquake-resistant design for the steel rigid-frame pier by investigating correlations among parameters, including the strength ratio between the beam and column, the ratio of the yield load to the maximum load, and the ductility ratio, because in the steel rigid-frame pier one plastic hinge will not cause a collapse of the entire structural system.
5) The steel rigid-frame pier investigated in this study experienced a maximum displacement of only $3.3\delta_y$ and no significant damage when subjected to ground acceleration as large as that recorded in the Hyogoken-Nanbu Earthquake, which indicates its good seismic performance.
6) The steel rigid-frame pier investigated in this study had a large reserve strength of $2.8\ H_y$ ($=H_{max}- H_y$). The displacement at the maximum load-carrying capacity was as large as $9\ \delta_y$. Thus the pier has superior strength and ductility.
7) The seismic responses obtained from the single degree-of-freedom system with a bilinear restoring force-displacement relationship did not match well with those from the pseudo-dynamic testing. It is

necessary to develop a proper restoring force-displacement model for the single degree-of-freedom system that can accurately represent the collapse process of the steel rigid-frame pier.

References

Aoki, T., Hasegawa, K. and Yamada, M., (1997), "An experimental study on load-deflection behavior of steel box section beam-to-column connections under static repeated loading", Journal of Structural Engineering, JSCE, Vol. 43A, pp.177-186 (in Japanese).

Hibbit, Karlsson Sorensen Inc., (1999), "ABAQUS /Standard user's manual", Ver.5.8.

Ida, Y., Nakamura, S. and Takahashi, K., (2000), "Study on applicability of equal-energy principle to steel portal frame bridge piers", Journal of Constructional Steel, Japanese Society of Steel Construction, Vol. 8, pp.277-284 (in Japanese).

Ikeda, M., Yamada, M., Ichikawa, A., Yasunari, H. and Tominaga, T., (2000), "A study on seismic design method of steel rigid frame piers for railway", Proceedings of the Third Symposium on Nonlinear Numerical Analysis and its Application to Seismic Design of Steel Structures, pp. 17-24 (in Japanese).

Japan Road Association, (1996), "Specification of highway bridges, Part V, Seismic design", Maruzen (in Japanese).

Komatsu, S., Ushio, M. and Kitada, T., (1977), "An experimental study on residual stresses and initial deformations of stiffened plates", Journal of Structural Mechanics and Earthquake Engineering, JSCE, No.265, pp. 25-35 (in Japanese).

Miki, C., Aizawa, T. and Anami, K., (1998), "Brittle fracture at beam-to-column connection during earthquake", Journal of Structural Mechanics and Earthquake Engineering, JSCE, No.591/I-43, pp. 273-281 (in Japanese).

Nakai, H., Miki, T. and Ohgaki, K., (1987), "An approximate method for calculating critical strength of thin-walled steel frames", Journal of Structural Mechanics and Earthquake Engineering, JSCE, No.380/I-7, pp. 263-272 (in Japanese).

Nakajima, A. and Onodera, O., (1998), "A Study on Elasto-plastic behavior of steel portal frames under sever earthquake and applicability of equal energy assumption to its seismic design", Proceedings of the Second Symposium on Nonlinear Numerical Analysis and its Application to Seismic Design of Steel Structures, pp.135-142 (in Japanese).

Nara, S., Murakami, S. and Ikejiri, T., (1999), "Elasto-plastic dynamic behaviors of steel rigid frame piers under seismic load", Journal of Constructional Steel, Vo. 7, Japanese Society of Steel Construction, pp.117-124 (in Japanese).

Subcommittee on New Technology for Steel Structures of Japan Society of Civil Engineers, (1996), “Final report on researches on seismic design” (in Japanese).

Sugimoto, H., Murabe, T., Watanabe, T., Takaku, T. and Furukawa, K., (2000), “On seismic design of steel-framed bridge piers reinforced by mild steel members”, Journal of Constructional Steel, Japanese Society of Steel Construction, Vol. 8, pp.285-292 (in Japanese).

Takahashi, M., Murakoshi, J., Nishikawa, K. and Matsuda, H., (1998), “Elasto-plastic finite displacement analysis on displacement ductility of steel piers strengthened by corner plates”, Proceedings of the Second Symposium on Nonlinear Numerical Analysis and its Application to Seismic Design of Steel Structures, JSCE, pp. 77-84 (in Japanese).

Usami, T., Totani, K., Suzuki, M. and Koretsu F., (1994), “Pilot test on the strength and ductility capacity of steel rigid frame structures under cyclic loading”, Journal of Structural Engineering, JSCE, Vol. 41A, pp.289-300 (in Japanese).

Usami, T., Zheng, Y. and Ge, H., (1999), “A Seismic performance evaluation procedure for steel framed bridge piers through a pushover analysis and an equivalent SDOF model”, Journal of Structural Mechanics and Earthquake Engineering, JSCE, No.626/I-48, pp. 213-240 (in Japanese).

Watanabe, E., Sugiura, K., Utsunomiya, T., Kitane, Y. and Nanjo A., (1994), “Effective box section for steel bridge piers considering strength and ductility”, Proceedings of the Ninth Japan Earthquake Engineering Symposium, Vol. 2, pp. 1471-1476 (in Japanese).

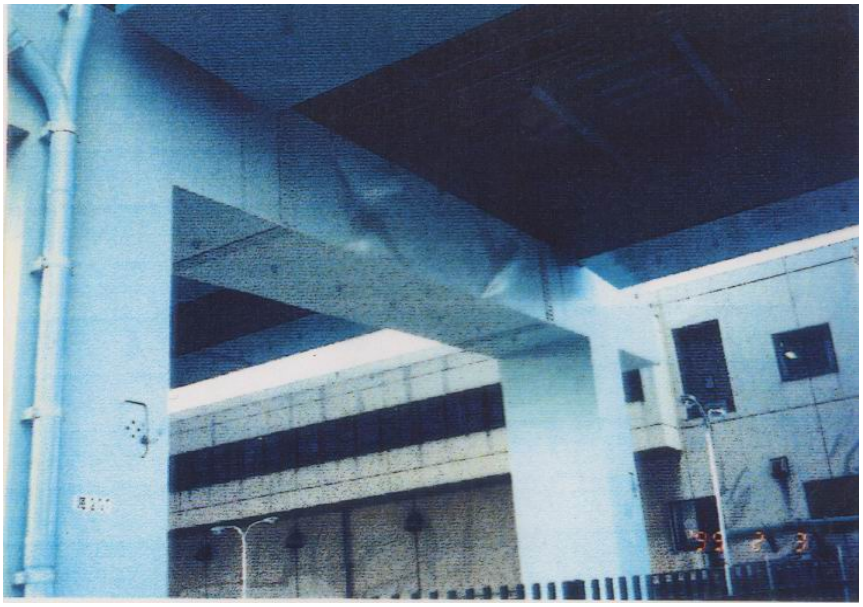

Photo 4.1 Example of damage

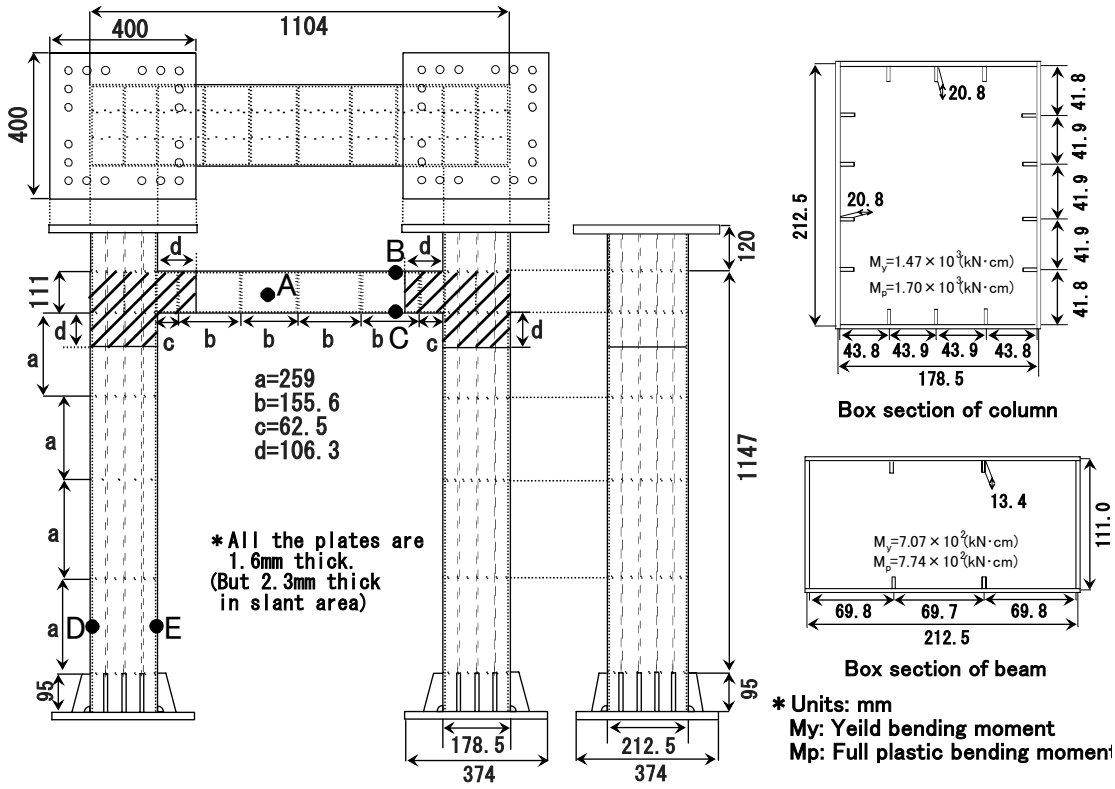

Fig. 4.1 Appearance of the specimen and stiffened box section

Table 4.1 Steel material properties

Thickness (mm)	Young's Modulus (GPa)	Poisson's ratio	Yield stress (MPa)	Tensile strength (MPa)	Elongation (%)
1.6	191	0.336	153	281	61.6
2.3	211	0.281	278	350	65.8

Table 4.2 Comparison of buckling parameters of stiffened box（Flange）

	Column		Beam	
	Prototype	Specimen	Prototype	Specimen
R_r	0.469	0.398	0.781	0.663
R_f	0.398	0.330	0.424	0.436

Table 4.3 Comparison of buckling parameters of stiffened box（Web）

	Column		Beam	
	Prototype	Specimen	Prototype	Specimen
R_r	0.491	0.417	—	—
R_f	0.401	0.333	1.220	1.030
γ/γ^*	1.57	0.333	—	—

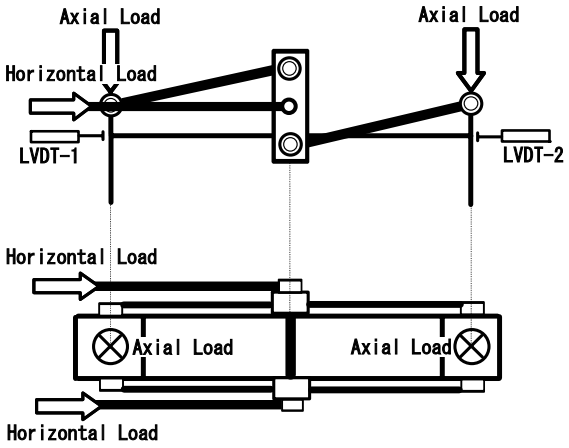

Fig. 4.2 Loading apparatus

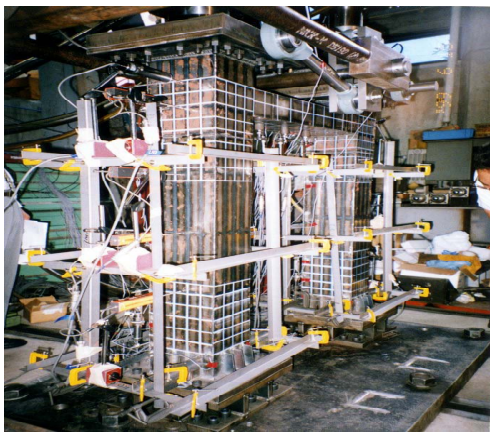

Photo 4.2 Overview of loading test

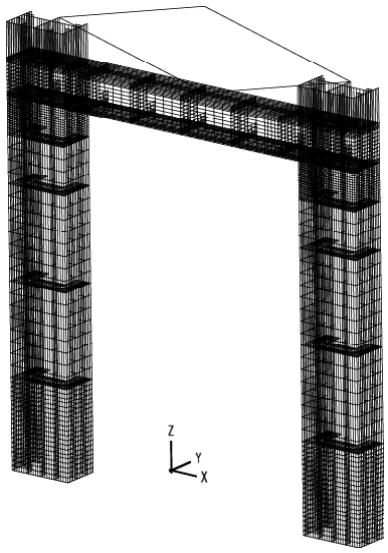

Fig. 4.3 Analysis model

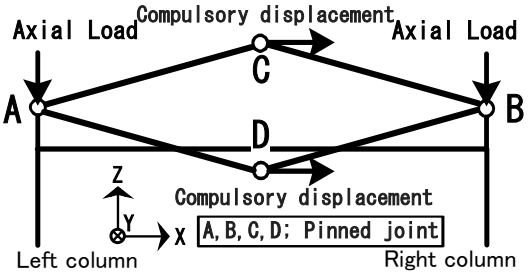

Fig. 4.4 Loading method for the analysis

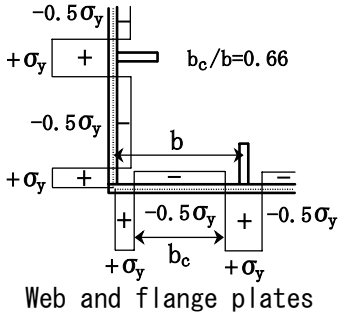

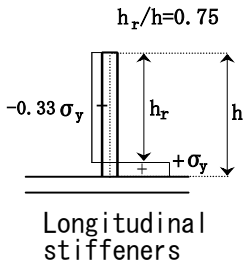

Fig. 4.5 Distribution of residual stresses

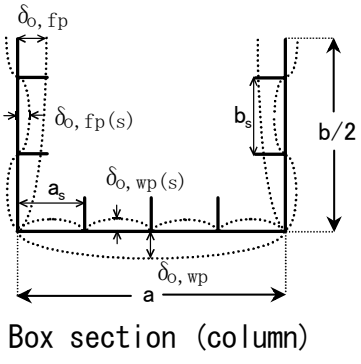

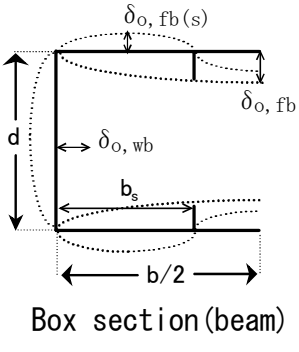

Fig. 4.6 Shape of initial deflections

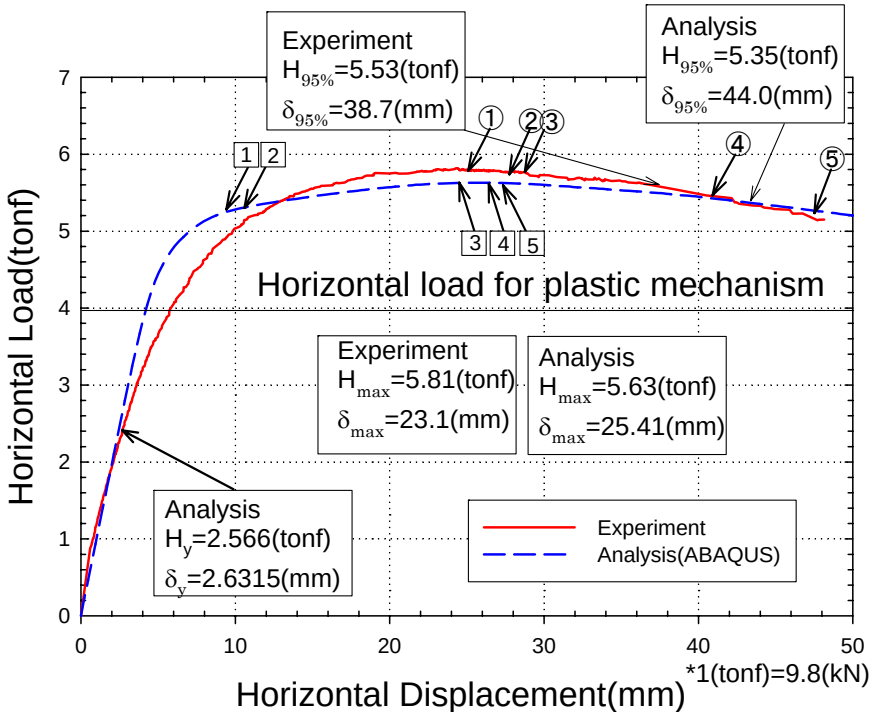

Fig. 4.7 Results of monotonic loading

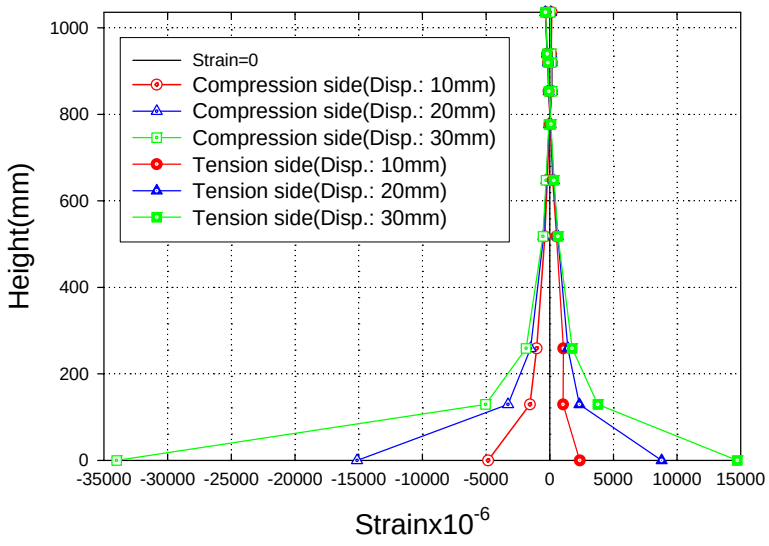

Fig. 4.8 Distribution of strain (left column)

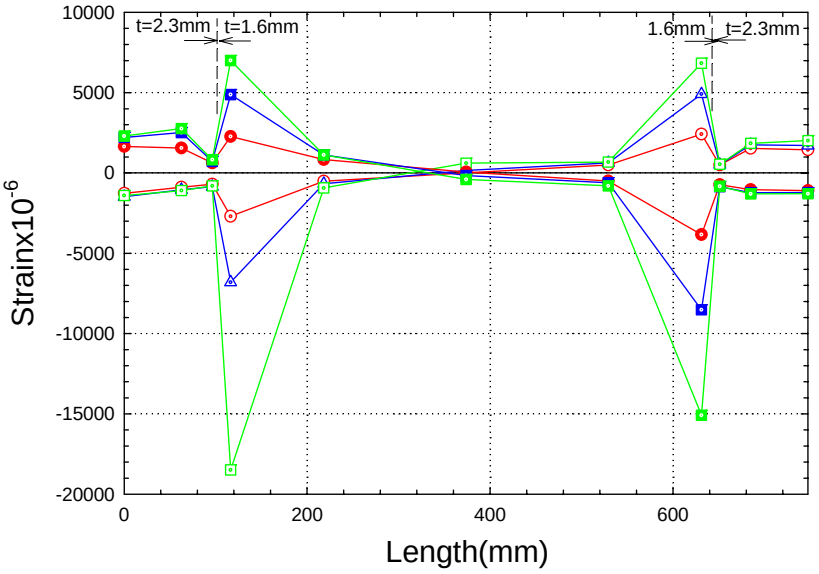

Fig. 4.9 Distribution of strain (beam)

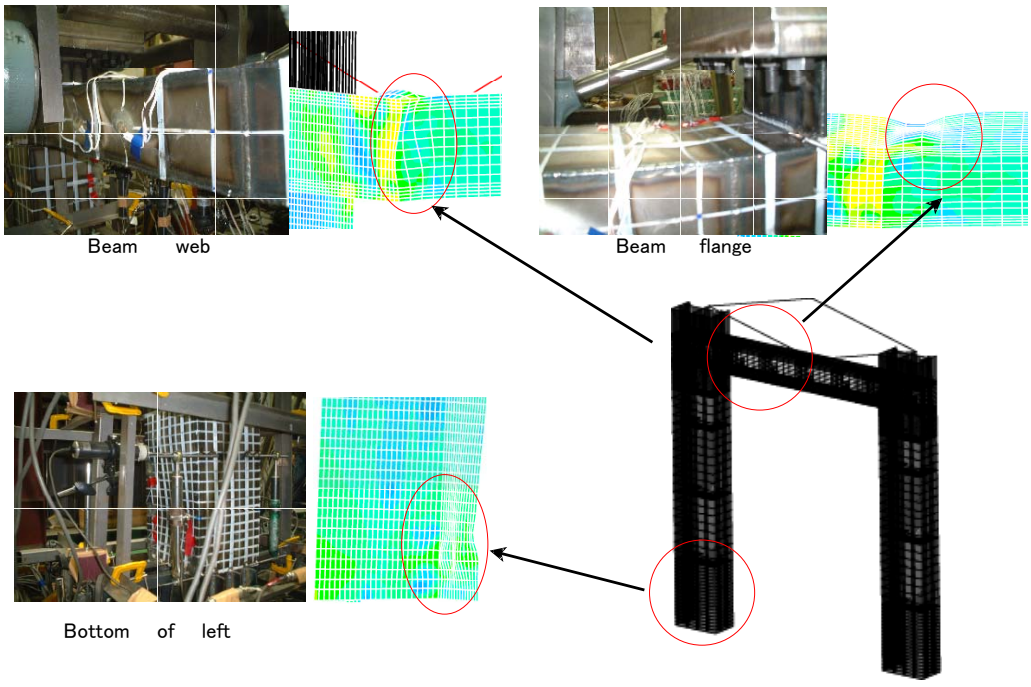

Fig. 4.10 Damage of pier after monotonic loading

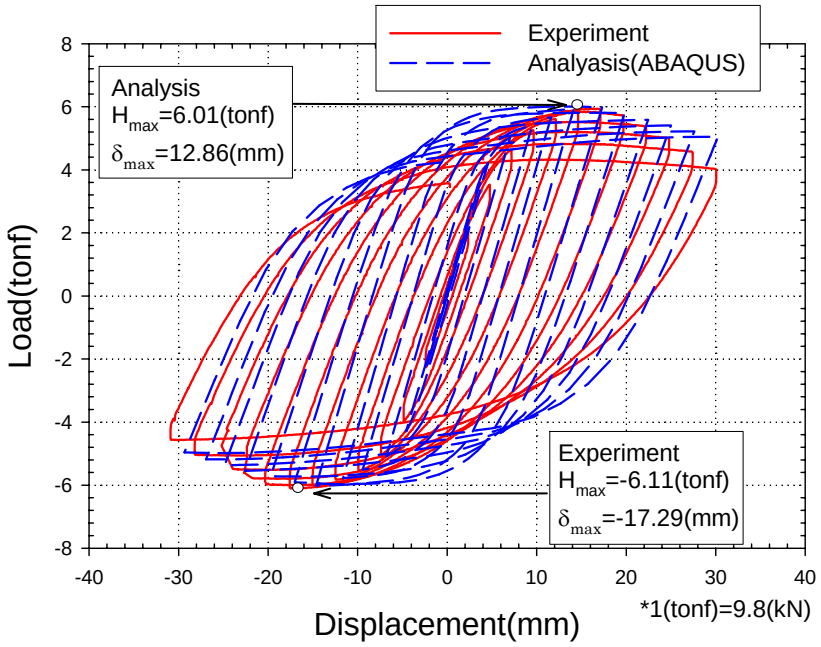

Fig. 4.11 Hysteresis of cyclic loading

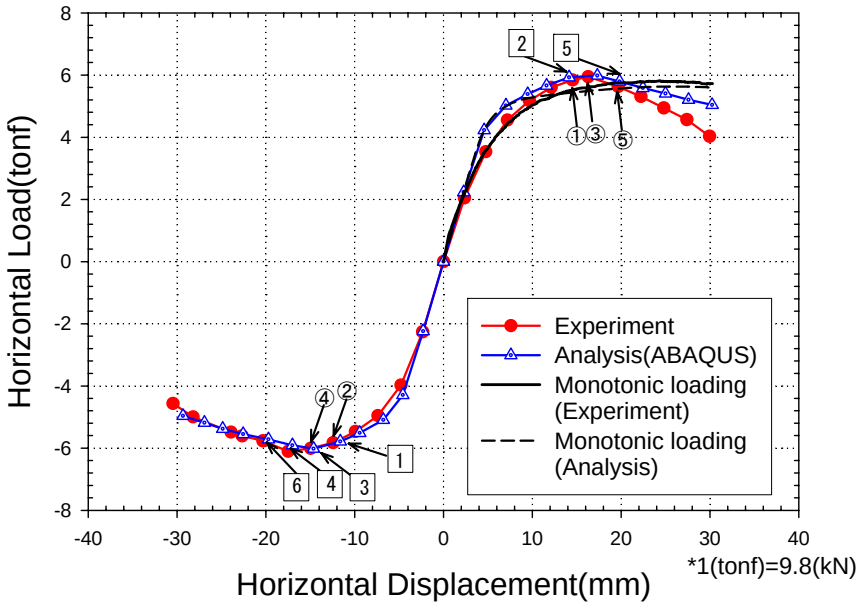

Fig. 4.12 Collapse processes of cyclic loading

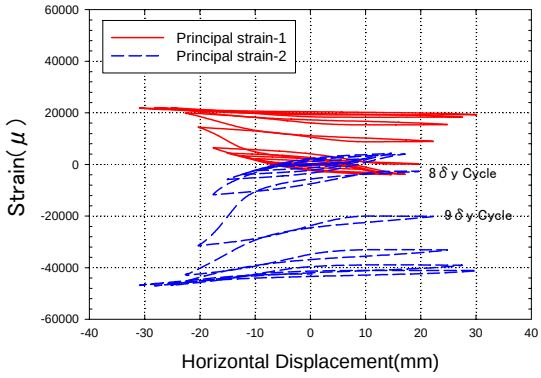

Fig. 4.13 Principal strain (Web plate in center of beam)

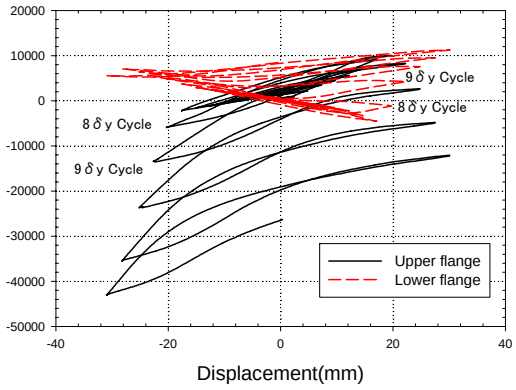

Fig. 4.14 Axial strain (Flange plate in right beam)

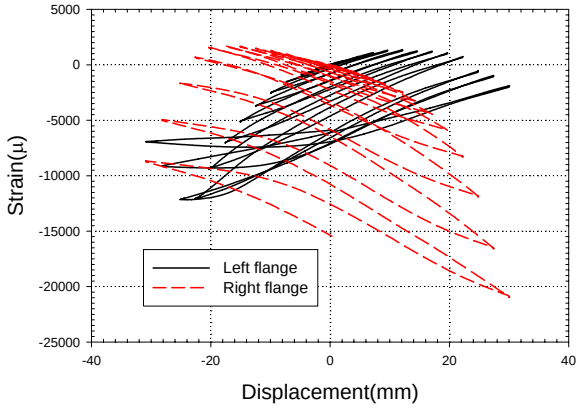

Fig. 4.15 Axial strain (Flange plate in left column)

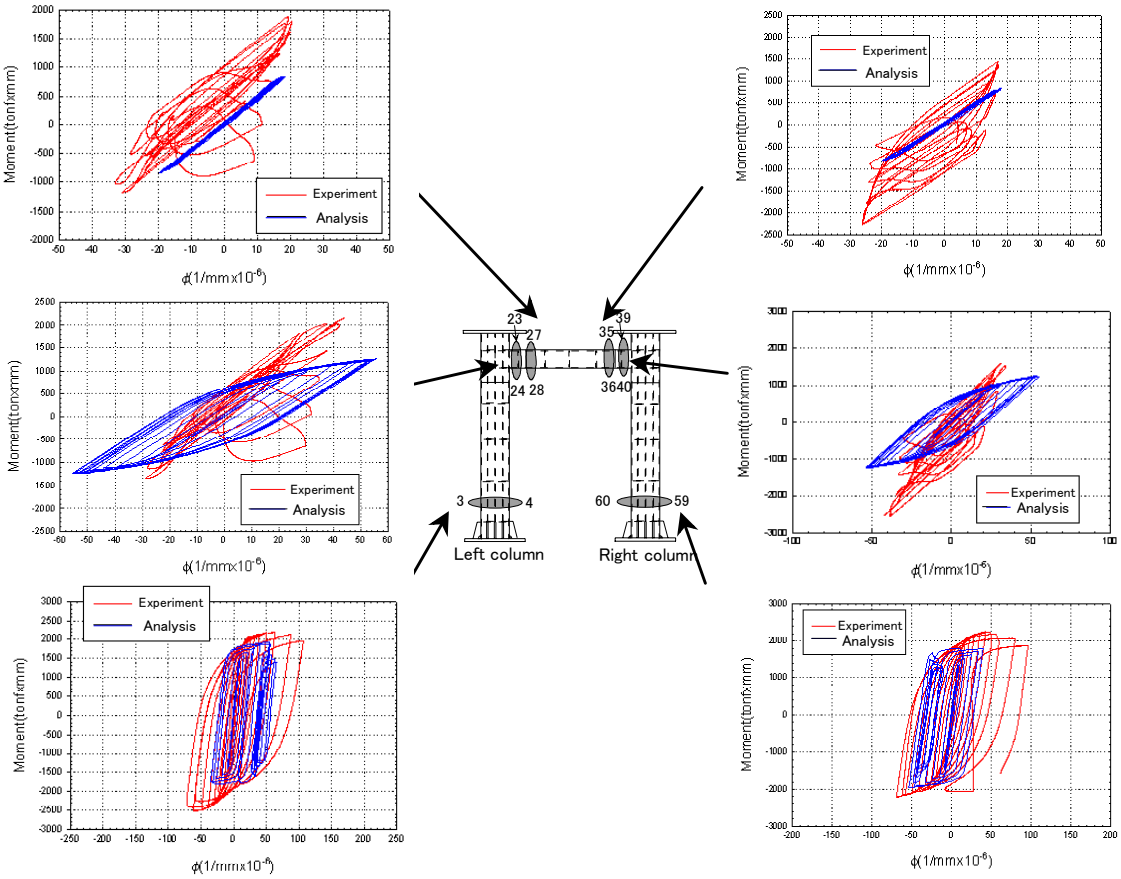

Fig. 4.16 Relationship between bending moment and curvature

Table 4.4 Steel material properties

Thickness (mm)	Young's modulus (GPa)	Poisson's ratio	Yield stress (MPa)	Tensile strength (MPa)	Elongation (%)
1.6	205.0	0.33	194.0	308.6	60.8
2.3	204.0	0.34	174.0	320.7	66.0

Table 4.5 Buckling parameters of stiffened box

	Bottom of column		Centre of beam	
	Prototype	Specimen	Prototype	Specimen
R_r	0.500	0.438	0.781	0.731
γ / γ^*	1.810	1.470	3.990	2.460
σ_c / σ_y	4.15(%)	4.15(%)		

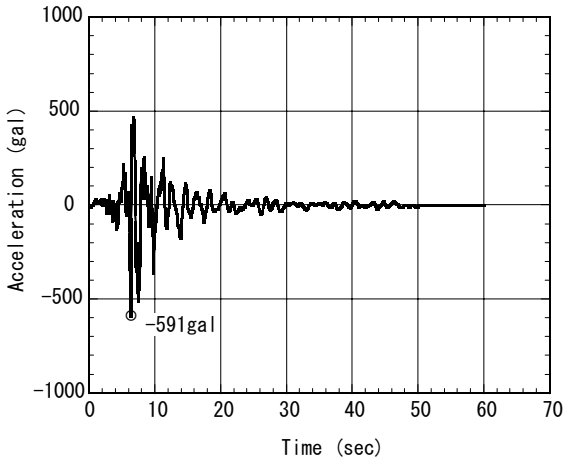

Fig. 4.17 Input acceleration

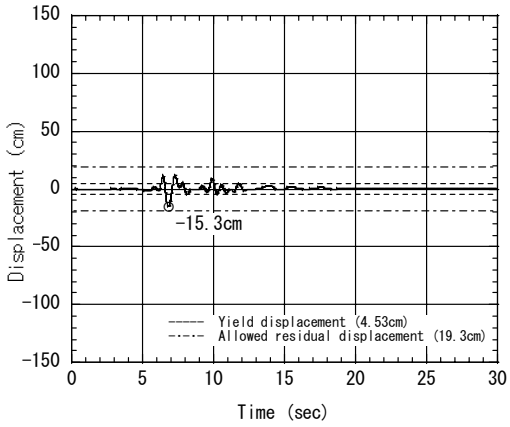

Fig. 4.18　Displacement response（Input acceleration 1: 1 time）

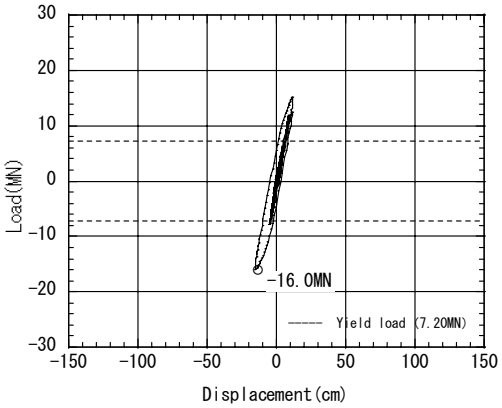

Fig. 4.19 Hysteretic response (Input acceleration 1: 1 time)

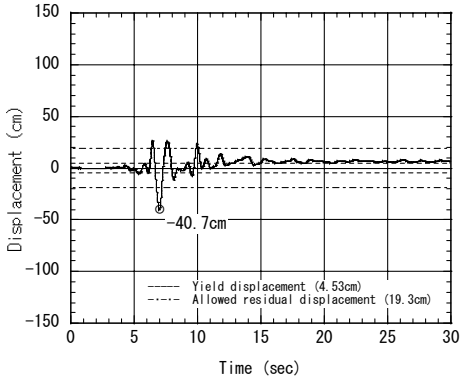

Fig. 4.20 Displacement response (Input acceleration 2: 2 times)

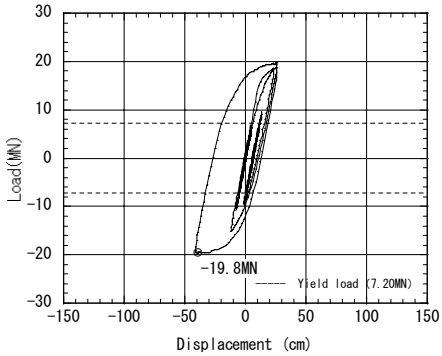

Fig. 4.21 Hysteretic response (Input acceleration 2: 2 times)

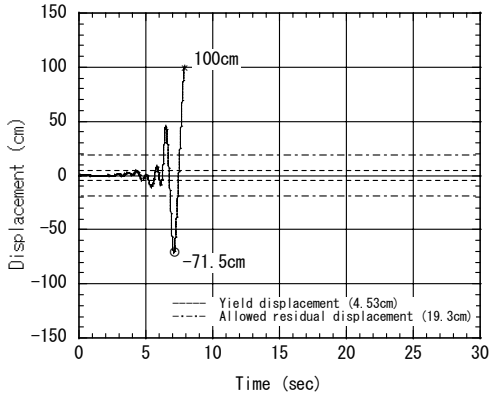

Fig. 4.22 Displacement response (Input acceleration 3: 3 times)

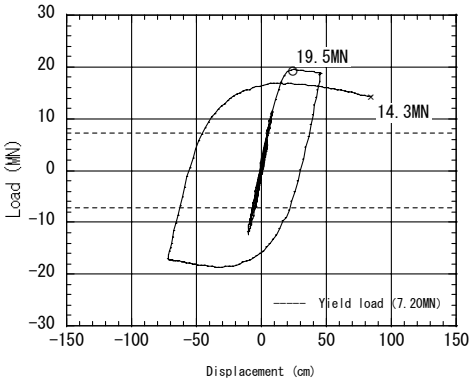

Fig. 4.23 Hysteretic response (Input acceleration 3: 3 times)

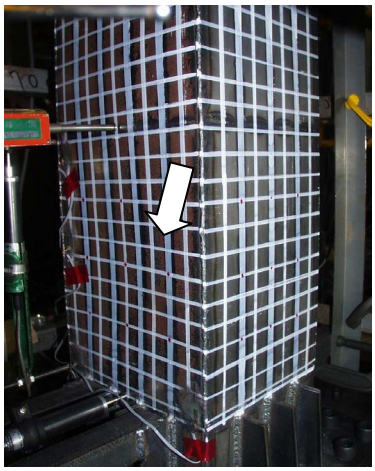

Photo 4.3 Damage (No. 1)

(Input acceleration 2: 2 times)

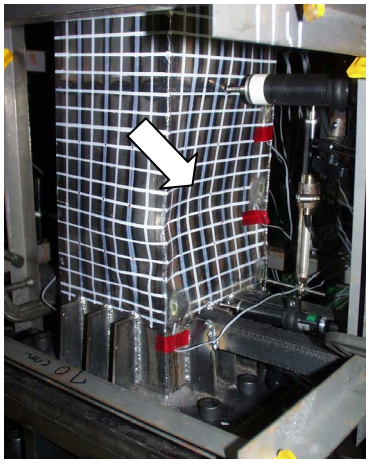

Photo 4.4 Damage (No. 2)
(Input acceleration 3: 3 times)

Photo 4.5 Damage (No. 3)
(Input acceleration 3: 3 times)

Table 4.6 Comparison to the analyses

Plastic secondary slope (%)	0	10	30	50	100	Experiment
Maximum displacement response (cm)	52.6	51.6	57.2	55.8	52.2	40.7
Maximum load (MN)	16.0	19.9	29.5	37.7	55.6	19.8
Residual displacement (cm)	18.9	13.7	1.51	0.585	0.0	6.5

Chapter 5

Seismic Performance of Steel Bridge Piers subjected to Bidirectional Horizontal Ground Motions

5.1 Introduction

The 1995 Hyogoken-Nanbu Earthquake caused severe damage to civil infrastructures, including buildings, roadways, railways, subways, port facilities and so on. The ground motions observed during the Hyogoken-Nanbu Earthquake were very strong and its intensity of ground acceleration was very large in all three components that are the North-South, East-West and Up-Down components, so that the complex spatial response of structures has been reported. Particularly the difference in the locations of gravity center and stiffness center of structures even make their response complicated (JCCA, 1995). Therefore, it is strongly recommended that the development of the reliable seismic design methodology should be made based on the full understandings of the spatial behavior of structures subjected to 3D ground motions.

According to the current Japanese Specifications for Highway Bridges, the design earthquake load is assumed to be decomposed into two arbitrary and orthogonal directions, and it is specified that these components of the earthquake load can be applied to the structures independently (JRA, 2002). In general, the safety of bridges against strong earthquakes is currently assessed in both the direction of the bridge axis and the direction perpendicular to the bridge axis. The building structures are also assessed by applying the design earthquake loads independently to two directions orthogonal to each other. After the Hyogoken-Nanbu Earthquake, the Architectural Institute of Japan began to investigate the spatial response of building structures, including the torsional response caused by the inconsistency of gravity center and stiffness center, such as in buildings with irregularly located columns (AIJ, 1998). On the other hand, in regard to the seismic design specifications in other countries, the CQC (Complete Quadratic Combination), the 30 percent rule, or the 40 percent rule are often applied (AASHTO, 1996). However, these rules were developed based on the elastic response of structures, such as random vibration theory. Because it is well known that the inelastic behavior of structures is path-dependent, it is expected that the three components of input acceleration to structures as well as the design safety factor for earthquake loads should be determined according to the inelastic response of structures in consideration of the interaction of strength in biaxial loading as well as the dependency of strength and ductility on the loading directions (JSSC and

JSCE, 2000).

As for steel bridge piers, numerous studies had been performed in an attempt to improve their strength and ductility even before the Hyogoken-Nanbu Earthquake (e.g., Subcommittee on Stability Design, JSCE, 1987). Since the Hyogoken-Nanbu Earthquake caused substantial damage to steel bridges, there have been further developments in the seismic design procedures, which have been emerged and has been made under the comprehensive guide of the Ministry of Construction of Japan, currently the Ministry of Land and Transportation. However, there is very limited number of research work on the response of bridge piers subjected to bidirectional horizontal ground motions, particularly the experimental and analytical work on the interaction of ductility of bridges piers for complicated loading path in orthogonal and horizontal two directions (Watanabe et al., 2000). The Japanese Specifications for Highway Bridges only specify the restoring force characteristics of partially concrete-filled steel bridge piers with box sections. They also require the design engineers to evaluate the restoring force characteristics either by the static loading test or by elasto-plastic finite displacement analysis. On the other hand, as for the in-pane response of the frame-type steel bridge piers, no comprehensive guideline exists because of the ambiguous understanding such that an indeterminate structure may always have high ductility. For the response in the direction of the bridge axis, it is generally designed such as single bridge piers which is statically determinate structure and considered to be less ductile.

In this chapter, in order to assess the dependency of the loading directions on the strength and the ductility, the a T-shaped single-column steel bridge pier with a thin-walled rectangular cross section and frame-type steel bridge piers subjected to two-directional horizontal ground motions were taken into consideration. In particular, the behavior of the frame-type steel bridge piers can be characterized by that of the single-column piers in the direction of the bridge axis. On the other hand, it behaves as the moment resisting frame in the direction perpendicular to the bridge axis. First, the hysteretic behavior of the a T-shaped single-column steel bridge pier with thin-walled rectangular cross sections was assessed experimentally through a monotonic and cyclic loading test by utilizing the three-dimensional structures testing system specially developed at Kyoto University jointly with Shimadzu Corporation (Kyoto Univ., 1997). Secondly, a pseudo-dynamic test was carried out in order to quantify the inelastic response of structures subjected to the bidirectional horizontal ground motions. The pseudo-dynamic test method was developed by Hakuno in 1969, and numerous researchers have since made further adjustments to assure the reliability of the test results (Hakuno, 1969). Now this test method is authorized as one of the preferred methods for evaluating the seismic response of structures. More details on the method can be found in Chapter 6, as well as in Hakuno et al. (1990) and Saizuka et al. (1995). Furthermore, in order to determine the strength and ductility of the model structures in the two orthogonal directions, an elasto-plastic finite

displacement analysis was carried out using the general purpose finite element analysis codes known as ABAQUS (HKS, Inc., 1998). Then, a simple model consisting of a mass, spring and dashpot with two degrees of freedom was proposed and assessed, with special emphasis placed on the dependency of the inelastic response on the strength interaction curve. The simple proposed model was then assessed by comparing the responses obtained the pseudo-dynamic testing. Finally, the frame-type steel bridge piers were investigated analytically, because the loading apparatus used to apply the bidirectional horizontal loads by the proper combination of actuators is very complicated. The frame-type steel bridge piers were modeled by ABAQUS, and the effects of their strength and ductility on the loading directions were assessed in detail.

5.2 Assessment for T-Shaped Single-Column Steel Bridge Piers

5.2.1 Outline of the Loading Test

(1) Testing System and Specimens

As a typical steel bridge pier, the T-shaped single-column steel bridge pier with rectangular thin-walled hollow sections (Photo 5.1) is assessed. In order to evaluate the seismic performance of such piers, a scaled model structure is fabricated for the loading test. As shown in Fig. 5.1, this bridge pier model has a rectangular cross section with a width of B=150 mm, a height of D=100 mm, and a thickness of t=4.21 mm. In addition, the total height of this bridge pier model is L=874.8 mm, but the height of the tested section is set at h=853.2 mm. Diaphragms of a plate thickness of t=6.38 mm are welded to the outside of the hollow section. The definitions of the X and Y coordinates are given in Fig. 5.1(b); namely, the X direction denotes the strong axis and the Y direction the weak axis. The material properties of the steel plates used to fabricate the specimens are tabulated in Table 5.1. Based on the strength of steel used, the yield horizontal force and displacement in the X and Y directions are given by:

$$(\delta_{y0})_X = 6.15(mm) \tag{5.1a}$$

$$(H_{y0})_X = 39.9(kN) \tag{5.1b}$$

$$(\delta_{y0})_Y = 9.22(mm) \tag{5.1c}$$

$$(H_{y0})_Y = 31.9(kN) \tag{5.1d}$$

These values are calculated for the cantilever column of one fixed end and free end in the other subjected to the horizontal force at the free end of the column by using the simple beam theory. Therefore, the yield of the cantilever column can be defined at the base of the column. For the pseudo-dynamic test, the model

bridge pier used herein is assumed to have a scale factor of one tenth of the prototype of steel bridge piers.

The testing system utilized in this research is shown in Photo 5.2 and schematically illustrated in Fig. 5.2. This system, which was developed jointly by Kyoto University and the Shimadzu Corporation, which has nine electrically controlled hydraulic actuators to test the six degrees of freedom of the structures; that is, the displacements in the X, Y, and Z directions of 100 mm and the rotations along the X, Y, and Z axis of 10.3 degrees. The capacity of corresponding loading are 100 kN in the X and Y directions, 500 kN in the Z direction 300 kN (in tension); 100 kN-m for all bending forces. All actuators are synchronized with each other and digitally controlled so as to have an accurate trace of the displacement or force path prescribed in the computer program. The loading frame is also stiff enough to have accurate displacement control.

As shown in Fig. 5.2, the specimens were set upside down, and the two actuators laid in the horizontal plane were mainly controlled to give the horizontal forces to the structures due to bidirectional ground motions (these were referred to as FX and FY). In addition, in order to execute an accurate trace of the displacement history, external displacement transducers are attached and used to control the actuators through the digital control unit. Furthermore, the compressive force is assumed to be zero even though the compressive force of the column due to the weight of the superstructures is estimated to be about 5-15% of the yield force. This is because this research mainly focuses on the interaction of strength and ductility of bridge piers under biaxial loading conditions.

(2) Procedure of Pseudo-Dynamic Test

Fig. 5.3 shows the test system used to evaluate the seismic response by the pseudo-dynamic test. The test setup was the same as described in the previous section for the cyclic loading test. In addition to the computer for load control, another computer was utilized in order to carry the response analysis and data communication over the Internet. The comprehensive data flow between these computers and test systems is also illustrated in Fig. 5.3, where the execution of response analysis is made step-by-step following the measurement of restoring forces in the loading execution for a given prescribed displacement computed in the response analysis. The communication between the computers is basically accomplished by the disc sharing in the computer for response analysis. Details of this procedure, which was developed at Kyoto University, are given in Chapter 6.

In order to evaluate the seismic response in the X-and Y direction of the steel bridge pier model, the equation of motion given by Equation 5.2 is used, which is based on the mass-spring-dashpot model, where a single mass, but two springs and two dashpots are considered:.

$$M\ddot{X} + C\dot{X} + F = -M\ddot{Z} \tag{5.2}$$

in which,

$$M = \begin{pmatrix} m & 0 \\ 0 & m \end{pmatrix}, \quad C = \begin{pmatrix} c_x & 0 \\ 0 & c_y \end{pmatrix}, \quad F = \begin{pmatrix} f_x \\ f_y \end{pmatrix}$$

$$\ddot{X} = \begin{pmatrix} \ddot{x} \\ \ddot{y} \end{pmatrix}, \qquad \dot{X} = \begin{pmatrix} \dot{x} \\ \dot{y} \end{pmatrix}, \qquad \ddot{Z} = \begin{pmatrix} \ddot{z}_x \\ \ddot{z}_y \end{pmatrix}$$

$\ddot{X}$, $\dot{X}$ are the relative acceleration and velocity vectors at mass location to the ground; and M , C , and F are the Mass Matrix, Damping Matrix and Restoring force vector, respectively. The subscript of x and y indicates the component of the physical quantity in the X and Y directions. The response analysis is carried out by the central difference method, and the time increment is set to be 0.02 sec according to the natural period of structures of 0.855 sec and 1.17 sec in the X and Y directions, respectively. Table 5.2 summarizes the primary structural parameters of the model structure.

In the pseudo-dynamic test, the restoring forces of f_x and f_y are measured through the loading test and the response analysis is carried out for the prototype of structures by scaling the restoring forces and target displacements (Saizuka et al., 1995). The damping matrix is calculated and used for both the pseudo-dynamic test and numerical analysis by assuming that the responses in the X and Y directions are independent in Equation 5.3, and the following relation is used:

$$c = 2h\sqrt{MK} \tag{5.3}$$

Here, h, M, and K are the damping factor of 0.05, the mass and the initial stiffness, respectively. The time history of ground acceleration used in the pseudo-dynamic test is the first 15 sec of acceleration recorded at the Kobe Meteorological Observatory during the Hyogoken-Nanbu Earthquake, because the main ground motion to cause the large response is up to first 15 sec. The acceleration and its trajectory in the X-Y horizontal plane are shown in Figs. 5.4 and 5.5. As a reference, a dashed line is drawn to indicate the dominant direction of ground acceleration. However, it is understood that the inertia force applied to the structures always changes its direction as well as its intensity. For the pseudo-dynamic test, the cases listed in Table 5.3 are investigated in order to evaluate the response characteristics of steel bridge piers in the horizontal X and Y directions.

5.2.2 General Description of Elasto-Plastic Finite Displacement Analysis

In order to perform the parametric analysis, the test results are compared with those obtained by the elasto-plastic finite displacement analysis using a general-purpose FEM code called ABAQUS (1998). The discretization of a steel bridge pier model is shown in Fig. 5.7. In order to evaluate the local buckling of a thin-walled section, special care must be taken regarding the size of the shell elements; namely, finer at the base of the bridge pier column. The shell elements SR4 with 4 nodes are used with reduced numerical integration. The rectangular hollow cross section is divided into 15 elements in the X direction and 10 elements in the Y direction, the column is divided into 20 elements in the lower two blocks separated by diaphragms, and the others are divided into 10 elements. The loading block is modeled by the rigid elements to prevent local crushing near the loading points. All the displacements along the cross section at the column base are fixed, and the horizontal displacement at the top of the column in the X and Y directions is pre-specified just as in the loading test, but the force resultant in the Z direction is kept at zero. The material properties are input according to the material test results given in Table 5.1, and the constitutive relation of steel is assumed to be modeled by the associated flow rule in conjunction with the von-Mises yield criterion and kinematic hardening rule. The initial imperfections, such as the initial out-of-plane deflection of the thin plate and residual stress in the thin plates, are not considered.

5.2.3 Results and Discussion

(1) Cyclic Loading Test Results

The displacement history shown in Fig. 5.6 was used, where the maximum displacement was up to five times of the yield displacement in each of the X and Y directions. The relation of the horizontal load to the displacement and their envelope curves in the X and Y directions is shown in Figs. 5.8 and 5.9, respectively. It is understood from these curves that the horizontal loads in the X and Y directions increase slightly even after the initial yielding, and that after the maximum loads of 54.1 kN in the X direction and 39.4 kN in the Y direction, the loads decrease gradually. These maximum loads are $1.36(H_{y0})_X$ and $1.24(H_{y0})_Y$. The numerical results are also shown in the figures. The good agreement between the experimental and numerical results indicate that the modeling of steel bridge piers by ABAQUS is adequate for evaluating the hysteretic behavior of steel bridge piers, and that the loading test setup and measuring system are also sufficiently accurate.

The local bucklings of the rectangular hollow section at the base of the column are shown in Photos 5.3 and 5.4, and are compared with those obtained by the finite element analysis as shown in Figs. 5.10 and 5.11. In the cyclic loading test of the X direction, the local buckling of the flange plate occurs outward, resulting in the inward buckling of the web plate when the horizontal displacement amplitude reaches $+3\,\delta_{y0}$, and then the horizontal load decreases gradually to less than 90% of its maximum value

when the horizontal displacement amplitude is $\pm 5\,\delta_{y0}$. In the finite element analysis, the local buckling is observed when the horizontal displacement amplitude is $+3\,\delta_{y0}$, but the direction of the out-of-plane deflection of the thin flange plate is opposite; namely, inward. On the other hand, in the cyclic loading test of the Y direction, the local buckling of the flange plate occurs outward, resulting in the inward buckling of the web plate when the horizontal displacement amplitude is $+2\,\delta_{y0}$, and then the horizontal load decreases rapidly to less than 90% of its maximum value even before the horizontal displacement amplitude reaches $\pm 5\,\delta_{y0}$. The degradation in the Y direction is found to be more significant than that in the X direction. In the finite element analysis, the local buckling is observed when the horizontal displacement amplitude is $+2\,\delta_{y0}$, but the direction of the out-of-plane deflection of the thin flange plate is also opposite. These differences may be caused by the initial displacement of the thin plates, which is outward in all of hollow-section plates during the manufacturing process.

(2) Seismic Response as Evaluated by the Pseudo-Dynamic Test

In order to evaluate the elasto-plastic response of the T-shaped single-column steel bridge pier subjected to strong ground motions in the arbitrary horizontal directions, the three cases listed in Table 5.3 are assessed by the pseudo-dynamic test. As a comparison, a response analysis without the strength interaction of the cantilever column in the biaxial loading condition is also carried out, in which the bilinear restoring force characteristics with plastic stiffness of 10% of the initial stiffness are assumed. The hysteresis is also predicted by ABAQUS, by tracing the displacement history in the X and Y directions obtained by the pseudo-dynamic test.

a) Case 1 (Response in the X Direction only)

The time histories of the horizontal displacement response by the pseudo-dynamic test and the response analysis for the Mass-Spring-Dashpot model, and the hysteresis obtained by both analyses are shown in Fig. 5.12.

Even though there exists little difference in the hysteresis of the horizontal load and the horizontal displacement, as shown in Fig. 5.12(b), a good agreement is observed for the time history of the displacement response, as shown Fig. 5.12(a). In addition, the hysteresis obtained by ABAQUS agrees well with that by the pseudo-dynamic test, as shown in Fig. 5.12(c). Therefore, the procedure of the pseudo-dynamic test method used herein is sufficiently accurate for evaluating the seismic response of steel bridge piers.

At t=5.70 sec, 285 steps, the displacement and restoring force are 6.92 cm and 4,165 kN, respectively, and exceed the yield values of the prototype, which are obtained by multiplying the scale

factor of 10 in Equations 5.1a and 5.1b. Then, at t=6.38 sec, the maximum restoring force of -5,047 kN is obtained in the negative X direction and the maximum displacement response in the negative X direction of -18.7 cm is obtained at t=6.44 sec. In the positive X direction, the maximum restoring force of 5,214 kN at t=6.88 sec and the maximum displacement response of 18.0 cm at t=8.60 sec are obtained.

Photo 5.5 and Fig. 5.13 show the damage at the base of the cantilever column observed during the test. At about t=5.86 sec, the flange plate at the height of 4.0 cm buckles outward, but this can only be observed by manual examination, not by the naked eye. Even though the peak in the load-displacement curves is obtained, and the local buckling of thin steel plates occurs, the amplitude of the out-of-plane deflection of the buckled plates is not significant enough to be clearly visible by the naked eye.

b) Case 2 (Response in the Y Direction only)

The time histories of the horizontal displacement response by the pseudo-dynamic test and the response analysis for the Mass-Spring-Dashpot model, and the hysteresis obtained by both analyses are shown in Fig. 5.14.

Similar to Case 1, even though there exists little difference in the hysteresis of the horizontal loads and the horizontal displacement, a good agreement is observed for the time history of the displacement response. It can be also concluded that the procedure of the pseudo-dynamic testing method used in this research is sound. On the other hand, the hysteresis obtained by ABAQUS agrees well with that by the pseudo-dynamic test, as shown in Fig. 5.14(c).

At t=5.80 sec, 290 steps, the displacement and restoring force are -10.1 cm and -3,156 kN, respectively and exceed the yield values of the prototype. Then, at t=5.86 to 5.90 sec, the maximum restoring force of -3,616 kN is obtained in the negative X direction and the maximum displacement response in the negative X direction of 17.8 cm is obtained at t=5.96 sec. In the positive X direction, the maximum restoring force of 3,753 kN at t=6.36 sec and the maximum displacement response of 11.8 cm at t=6.40 sec are obtained.

Photo 5.6 and Fig. 5.15 show the damage at the base of the cantilever column observed during the test. At about t=5.96 sec, the compressive side of the flange plate also buckled outward, and only observed by hand touching, not by eye observation like Case 1. Even though the peak in the load-displacement curves is obtained, and the local buckling of thin steel plates occurs, the amplitude of the out-of-plane deflection of the plates is again not significant enough to be clearly visible by the naked eye.

c) Case 3 (Responses in X and Y Directions)

The time histories of the horizontal displacement response by the pseudo-dynamic test and the response

analysis for the Mass-Spring-Dashpot model, and the hysteresis obtained by both analyses are shown in Figs. 5.16 and 5.18, respectively. In these figures, the hysteresis obtained by the finite element analysis is also compared.

Unlike in Case 1 and Case 2, a large discrepancy in the hysteresis of the horizontal load and the horizontal displacement, and the time history of the horizontal displacement response between the experimental results and the results by the response analysis is observed. However, the hysteresis obtained by the finite element analysis of ABAQUS is in good agreement with the experimental results. Therefore, it is understood that the modeling of the restoring force is a very critical issue in terms of evaluating the response in the X and Y directions. Namely, the significant interaction of responses in the X and Y directions exists, and, in particular, a complex change of stiffness in the Y direction is observed. This change can be predicted by the finite element analysis, but not by the Mass-Spring-Dashpot model without the strength interaction.

At t=6.42 sec, 321 steps, the restoring force becomes the largest in the negative X direction, -4,753 kN, and then the horizontal displacement of -12.1 cm is obtained at t=6.44 sec. Furthermore, at t=6.86 sec, a maximum restoring force of 4,675 kN is obtained in the positive X direction and the maximum displacement response in the positive X direction of 24.4 cm is obtained at t=6.88 sec. At t=5.52 sec, the displacement and restoring force in the Y direction are 8.12 cm and 2,313 kN, respectively. Then, at t=5.70 sec, the sudden change of stiffness in the X direction is observed and followed by the change of stiffness in the Y direction. The maximum restoring force of -2,911kN in the negative Y direction is obtained at t=5.98 sec and the maximum displacement response in the negative Y direction of -20.3 cm is obtained at t=6.00 sec.

Photos 5.7, 5.8 and Figs. 5.17, 5.19 show the damage of flanges at the base of the cantilever column in the loading to the X and Y directions observed during the test. At about t=5.76 sec, the positive side of the flange plate in the X direction buckled outward, and the negative side of the flange plate in the Y direction buckled inward. Furthermore, these local bucklings were not only observed by manual examination, but also by the naked eye. As the response becomes large, the buckling of the flange plates becomes significant. At t=8.58 to 8.88 sec, the amplitude of the out-of-plane deflection of the buckled plates becomes the largest. Fig. 5.20 shows the trajectory of the horizontal restoring forces in the X and Y directions. For purposes of comparison, the assumed yield surface is also drawn in this figure. It is understood the complex history of restoring forces is observed and it is concluded that the sudden change of stiffness when the restoring force point is located beyond an assumed yield surface.

5.2.4 Response Analysis by a Simple Mass-Spring-Dashpot Model

(1) Outline of Response Analysis

If the interaction in the strength of the structures in the biaxial loading directions, e.g., the X and Y directions in this study, is not considered, the non-diagonal elements of the stiffness matrix vanish to zero. Namely, the equation of motion for the X and Y directions can be independent. This is the case for the elastic response. However, the strength of structures under the biaxial loading condition strongly affect each other; in particular, the elasto-plastic stiffness of the structures depends on the sectional forces and loading directions. Therefore, the non-diagonal elements of the stiffness matrix in the elasto-plastic state are properly modeled and the response analysis is carried out by solving the simultaneous equation of motions in the X and Y directions for the spatial behavior of structures. The derivation of the stiffness matrix, namely, the elasto-plastic spring constants, is made by means of the analogy of the theory of plasticity.

In Equation 5.4, the restoring force vector can be rewritten as:

$$\Delta F = \begin{Bmatrix} \Delta F_x \\ \Delta F_y \end{Bmatrix} = K \cdot \Delta X = K \cdot \begin{Bmatrix} \Delta x \\ \Delta y \end{Bmatrix} \tag{5.4}$$

where K is the stiffness matrix, and Δx, Δy are displacement increments in the X and Y directions, respectively. As mentioned before, the non-diagonal elements of the stiffness matrix are zero for the elastic response and can be written as follows.

$$K = \begin{bmatrix} K_x & 0 \\ 0 & K_y \end{bmatrix} \tag{5.5}$$

The subscripts indicate the directions, such as the X and Y directions. However, the non-diagonal elements of the stiffness matrix are no longer zero for the elasto-plastic response because the interaction of plastification in the X and Y directions becomes significant. By means of the fundamentals of the theory of plasticity, the yield surface G of restoring forces is assumed by Equation 5.6. By applying the normality rule to define the plastic displacement increment on this yield surface, the elasto-plastic stiffness matrix can be derived as in Equation 5.6.

$$G = \left(\frac{F_x}{F_{x0}} \right)^{\gamma} + \left(\frac{F_y}{F_{y0}} \right)^{\gamma} - \phi \tag{5.6}$$

$$\begin{Bmatrix} \Delta F_x \\ \Delta F_y \end{Bmatrix} = \frac{K_x \cdot K_y}{n_x{}^2 \cdot K_x - n_y{}^2 \cdot K_y} \begin{bmatrix} n_y{}^2 & -n_x \cdot n_y \\ -n_x \cdot n_y & n_x{}^2 \end{bmatrix} \begin{Bmatrix} \Delta x \\ \Delta y \end{Bmatrix} \tag{5.7}$$

where F_{x0} and F_{y0} are the yield horizontal forces in the X and Y directions, respectively, and the components of normal vector on the yield surface are given by:

$$n_x = \frac{\partial G}{\partial F_x}, \quad n_y = \frac{\partial G}{\partial F_y} \tag{5.8}$$

In this analysis, the case of γ=2 and ϕ=1 is considered for simplicity; that is, the yield surface is ellipsoid and the restoring force characteristics are elastic-perfectly plastic. Finally, the elasto-plastic stiffness matrix can be rewritten as following.

$$\begin{Bmatrix} \Delta F_x \\ \Delta F_y \end{Bmatrix} = [K]_p \begin{Bmatrix} \Delta x \\ \Delta y \end{Bmatrix}$$

$$= \frac{K_x \cdot K_y}{\left(\frac{2F_x}{F_{x0}{}^2} \right)^2 \cdot K_x - \left(\frac{2F_y}{F_{y0}{}^2} \right)^2 \cdot K_y} \begin{bmatrix} \left(\frac{2F_y}{F_{y0}{}^2} \right)^2 & -\left(\frac{2F_x}{F_{x0}{}^2} \right) \cdot \left(\frac{2F_y}{F_{y0}{}^2} \right) \\ -\left(\frac{2F_x}{F_{x0}{}^2} \right) \cdot \left(\frac{2F_y}{F_{y0}{}^2} \right) & \left(\frac{2F_x}{F_{x0}{}^2} \right)^2 \end{bmatrix} \begin{Bmatrix} \Delta x \\ \Delta y \end{Bmatrix} \tag{5.9}$$

(2) Results and Discussion

The time history of the displacement response and he hysteresis curves in the X directions are shown in Fig. 5.21; the time history of the displacement response and the hysteresis curves and the Y directions are also shown in Fig. 5.22. In these figures, the results obtained by the pseudo-dynamic test are also shown for comparison. It is understood that fairly good agreement is observed. In particular, the complex behavior, such as the sudden change of stiffness, is well predicted. However, because the elastic-perfectly plastic

relation is assumed, the maximum displacement response by numerical analysis is a little larger than that obtained by pseudo-dynamic testing. It is concluded that the interaction of the plastic response in the X and Y directions must be considered in order to evaluate the real response of structures subjected to horizontal ground motions in the arbitrary direction. The parameters of γ and ϕ in Equation 5.5 must be further investigated.

5.3 Assessment for Frame-Type Steel Bridge Piers

5.3.1 Outline of Elasto-Plastic Finite Displacement Analysis

(1) FE Modeling

In Chapter 4, the in-plane collapse behaviors of the frame-type of steel bridge piers were investigated, and a typical bridge pier model was designed according to the actual dimensions of Pier 34 in the Wangan line of the Hanshin Expressway as shown in Photo 5.9. The experiments were performed on this scaled model, which was about one-seventeenth the original, as shown in Fig. 5.23. In this modeling, the plate thickness parameter and rigidity of longitudinal stiffeners of the stiffened box section are kept constant for the scaled model and the prototype. In addition, the half model with symmetry of structure and loading was analyzed by an elasto-plastic finite displacement analysis usingABAQUS, and the good agreement in the in–plane elasto-plastic behavior under monotonic and cyclic loading confirms the validity of FE modeling, as discussed in Chapter 4. By improving the memory allocation and hard disk availability of the Engineering Workstation, a full model of the frame-type of steel bridge piers is modeled by shell elements, as shown Fig. 5.24. This can also be used to assess the accuracy of the half model to evaluate the seismic performance for the complex structures.

In this full model, finer meshing is adopted in order to predict the local buckling behavior more accurately. For example, for the column member, the flange and web plates are divided into 6 elements between longitudinal stiffeners. The longitudinal stiffeners are consist of 4 elements. The stiffened plates are divided into 56 elements between diaphragms. On the other hand, for the beam member, the flange and web plates are divided into 10 and 16 elements, respectively, between longitudinal stiffeners. The longitudinal stiffeners also consist of 4 elements. Then, the stiffened plates are divided into 40 elements over the length of the beam member. The number of layers for all the shell elements is 16 in this analysis. Furthermore, at the top of both column members the rigid elements are attached to prevent local deformation near the loading points.

Both column bases are fixed; that is, all displacements are fixed. The material properties tabulated in Table 5.4 are used in this analysis. The coordinate system shown in Fig. 5.24 is adopted. In

order to assess the fundamental behavior of the frame-type steel bridge piers, all the initial imperfections are eliminated for simplicity.

(2) Loading and Definition of Initial Yielding

The loading paths adopted in this analysis were the 5 cases shown in Fig. 5.25. In all 5 cases, at first the vertical load due to the weight of the superstructures was applied to the top of both columns through the rigid elements, and then the prescribed horizontal displacements were given to the top of columns as well. For Case 1, the loads were applied into the in-pane of the frame. Then, the loading direction was shifted to 30 degree from the in-plane of the frame for Case 2, to 60 degree for Case 3, and to 75 degree for Case 4. For Case 5, the loading direction is the direction to the bridge axis.

For all 5 cases, the yield horizontal force and yield horizontal displacement are defined when the von Mises equivalent stress in any elements reaches the yield stress. When this condition is satisfied, the yield horizontal force and yield horizontal displacement are characterized by δ_y and H_y, respectively. The loading is also monotonically applied and continued until the horizontal loads decrease to 95% of the maximum value.

5.3.2 Numerical Results and Discussion

In order to compare the results by the finite element analysis to the results by the loading test, the following values are defined and compared for the horizontal load and horizontal displacement in each case.

a) Experiment: The horizontal load is the sum of the measured loads of load cells of two actuators attached to column tops. The horizontal displacement is the average of the displacements measured by two external transducers attached to column tops.

b) Analysis: The horizontal load is the sum of the load resultants at the column tops. In the case that bidirectional loading is considered, the horizontal load is defined by the square root of the components of load resultants.

On the other hand, the local buckling is assessed by the naked eye observation in the experiments and the Post function of ABAQUS to check the difference of axial strain at both surfaces of the thin steel plate. In addition, the column at the left side in Fig. 5.25 is named to be “LEFT Column” and the other is called “RIGHT Column”

Table 5.5 summarizes the yield horizontal displacement, the yield horizontal load, the maximum

horizontal load, displacement at the maximum horizontal load obtained, ductility and maximum horizontal load nondimensionalized by the yield horizontal load for all 5 cases. In addition, the trajectory of horizontal load and horizontal displacement in the X –Y space (horizontal plane) for all 5 cases are shown in Fig. 5.26.

The relation of the horizontal load to the horizontal displacement for all 5 cases is shown in Figs. 5.27, 5.28, 5.29, 5.30, and 5.31, respectively. Furthermore, the relation of the dimensionless horizontal load to the dimensionless horizontal displacement is shown in Fig. 5.32.

For Case 1, that is, the in-plane behavior of the frame-type steel bridge piers, there exists little difference in damage location and damage process; however, the maximum horizontal load and the degradation process are in good agreement with the previous analytical and experimental results. Therefore, the full FE modeling constructed in this analysis is shown to be accurate for evaluating the behavior.

On the contrary, for Case 5, that is, the out-of-plane behavior of the frame-type steel bridge pier, the degradation process seems to be similar to that of the single-column bridge pier. Therefore, extracting a column member out of the frame, the elasto-plastic finite displacement analysis is also carried out, in which the horizontal load is multiplied by two on order to make it comparable to that of the frame. The results of this comparison showed that both numerical results were in good agreement, and thus the beam did not make any contribution to the strength or ductility.

It can be understood from the results in Figs. 5.27 to 5.31 that the maximum horizontal load decreased and the member failed at first is changed to the column member of the frame from the beam member of the frame as the loading direction is changed to out-of-plane from in-plane of the frame. In addition, Table 5.5 shows that the ductility is very large, more than 11, except in Case 5, which is same as that of the single-column bridge piers. On the other hand, the maximum horizontal load of Case 5 is almost 60% that of the other cases, Case 1, Case 2, Case 3, and Case 4. Consequently, it is concluded that for Case 1, Case 2, and Case 3, several locations, such as the flange and web plates at the column member base and the beam member ends with plate thickness change, web plate in the middle of the beam member have severe buckling damages; but for Case 4 and Case 5, damages occur only at the column member bases. This observation demonstrates that the behavior of the frame-type bridge piers depends on the collapse mechanism of the beam member. It is required to have the plastic hinge formation at the beam member necessary with other multiple plastic hinge formations, so as to cause the in-plane collapse of the frame. On the other hand, a single plastic hinge formation is enough to make the frame-type bridge piers collapse in the out-of-plane direction. As shown Table 5.5, the load-carrying capacity of the frame-type bridge piers is the largest in the case of loading to the in-plane direction, up to $1.5H_y$. Then, the maximum load gradually decreases as the loading direction shifts to the out-of-plane direction. It is also understood that the initial

yielding can be expressed by the equation.

$$\frac{Fx}{Fx)_1} + \frac{Fy}{Fy)_5} = 1 \tag{5.9}$$

where F_x and F_y are the horizontal loads in the X and Y directions, respectively. As the loading direction shifts to the X direction, an increase in the linearity of the load path beyond the elastic limit specified by Equation 5.9 can be obtained, with the result that a larger maximum horizontal load is achieved. Again, it should also be mentioned that the degradation becomes significant as the loading direction shifts to the Y direction as well. Special attention should be paid to the degradation of bridge piers dependent on the loading directions, which may affect the seismic safety against strong ground motions with uncertainty in acceleration orientation.

According to the allowable stress design based on initial yielding, the proportion of the rectangular cross section of frame-type steel bridge piers is such that the longer edge coincides with the direction of the bridge axis, and the shorter edge with the direction perpendicular to the bridge axis. This is because of the indeterminacy of the structural configuration. Therefore, there exists a wide variation of load-carrying capacity and deformability dependent on the loading direction. This fact strongly suggests that the seismic design of frame-type steel bridge piers should be made considering the inelastic spatial response under horizontal ground motions in arbitrary directions.

5.4 Concluding Remarks

In order to evaluate the inelastic response of the T-shaped single-column steel bridge piers subjected to earthquake loads with variable loading direction, a static loading test, a pseudo-dynamic test, and an elasto-plastic finite displacement analysis, as well as a response analysis using a simple mass-spring-dashpot model were carried out. Furthermore, as for the frame-type steel bridge piers, the detailed structural models were analyzed by the elasto-plastic finite displacement analysis of ABAQUS, paying attention to the effect of the loading direction on the strength and ductility. The results obtained through the current work can be summarized as follows:

1) A significant strength degradation due to bidirectional and nonproportional load was identified, compared to the hysteretic response under unidirectional loading. The dynamic response subjected to bidirectional ground motions was also larger compared to that in unidirectional acceleration input; in particular, the increase of the response in the weak axis was more significant.

2) The response obtained by the pseudo-dynamic test was simulated by the elasto-plastic finite displacement analysis. The hysteretic behavior could be predicted well by the elasto-plastic finite displacement analysis. Even for the response of structures subjected to bidirectional ground motions, the complex change in stiffness was simulated quantitatively.
3) A simple mass-spring-dashpot model for evaluating the response of structures subjected to bidirectional ground motions was proposed, wherein the elasto-plastic stiffness was defined based on the strength interaction curve in conjunction with basic principles of the theory of plasticity. The proposed simple model was shown to be capable of accurately predicting the bidirectional response of structures.
4) The rectangular cross section can cause a variation in strength and ductility dependent on the loading direction; in addition, the structural indeterminacy makes this variation even larger. Therefore, the frame-type bridge piers should be carefully designed by considering these differences of strength and ductility for the proper load combinations.
5) As the loading direction shifts from in-plane to out-of-plane of the frame, the collapse process may change; that is, only the cantilever column base collapses for out-of-plane loading, but for in-plane loading the beam collapses first, and then the cantilever column base collapses. In this study, up to the loading angle from in-plane of the frame of 60 degree, the beam collapse occurs first and the structure can have larger deformability.
6) The degradation of bridge piers depends on the loading directions, and degradation in each component affects the degradation in every other component. Therefore, it is necessary to investigate the collapse process under nonproportional loading in the direction of the bridge axis and its perpendicular direction, and the seismic design methodology should be based on this complex response.

In addition, the future research needs can be summarized as follows:

1) In this study, only bridge piers with rectangular cross sections with specific plate slenderness were assessed. Any combinations of plate slenderness to form the box cross section should be examined under bidirectional loading, in conjunction with the loading direction as well as acceleration intensity.
2) The inelastic response of structures considering the interaction of strength and ductility in two directions was evaluated, only limited assumption such as elastic-perfectly plastic restoring force characteristics. The more realistic restoring force characteristics, such as the bilinear type, should be incorporated to assess the inelastic response.
3) The current research defines the scalar quantity of loads by the square root of the load components. This definition should be further investigated in order to make a unified prediction for all the loading

combinations.

4) The current research only picked up the particular steel bridge. By considering the plate slenderness, column slenderness, and ratio of the vertical load, the seismic design specifications should be provided.

References

American Association of State Highway and Transportation Officials, (1996), “Standard specification for highway bridges”, 16th Edition.

Architectural Institute of Japan, (1998), “Structural performances under multi-dimensional earthquake ground motions” (in Japanese).

Department of Civil Engineering and Civil Engineering Systems, (1997), “Multi-phase dynamics experimental system”, Kyoto University (in Japanese).

Hakuno, M., Okada, T., Takanashi, K., Toki, K., Ikeda, S., Iemura, H. and Katada, T., (1990), “Application manual of pseudo-dynamic testing” (in Japanese).

Hibbit, Karlsson&Sorensen Inc., (1998),“ABAQUS/Standard user's manual”, Ver.5.8

Japan Civil Engineering Consultants Association, (1995), “Report on damage investigation of Great Hanshin-Awaji Earthquake” (in Japanese).

Japan Road Association, (2002), “Specifications for highway bridges Part V, Seismic design”, Maruzen Co., Ltd. (in Japanese).

Saizuka, K., Itoh, Y., Kiso, E. and Usami, T., (1995), “A consideration on procedures of hybrid earthquake response test taking account of the scale factor”, Journal of Structural Engineering and Earthquake Engineering, No. 507, pp. 179-190 (in Japanese).

Japanese Society of Steel Construction and Japan Society of Civil Engineers, (2000), “Benchmark for seismic design of steel structures and advanced seismic design method”, p. 330 (in Japanese).

Subcommittee on Stability Design, Committee on Steel Structures, Japan Society of Civil Engineers, (1987), “Guidelines for stability design of steel structures” (in Japanese).

Watanabe, E., Sugiura, K. and Oyawa, W.O., (2000), “Effects of multi-directional displacement paths on the cyclic behavior of rectangular hollow steel columns”, Journal of Structural Engineering and Earthquake Engineering, JSCE, No.647, pp. 79-95.

Photo 5.1 T-shaped single column steel bridge pier

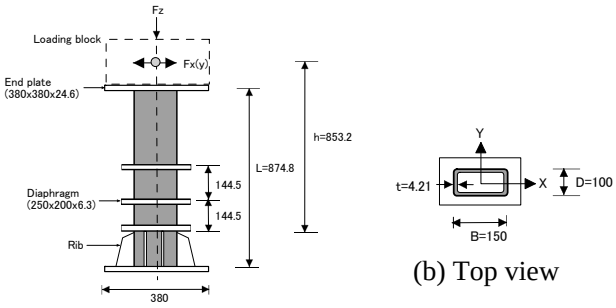

(a) Side view

(b) Top view

Fig. 5.1 Specimen (unit: mm)

Table 5.1 Material properties

Young's Modulus	Poisson’s Ratio	Yield Stress	Tensile Strength
(Gpa)		(Mpa)	(Mpa)
208	0.283	395	492

Photo 5.2 Three-dimensional testing machine

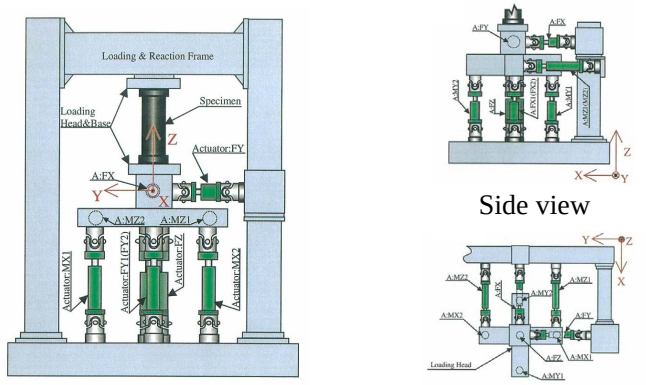

Front view　　Side view　　Top view

Fig. 5.2　Loading apparatus

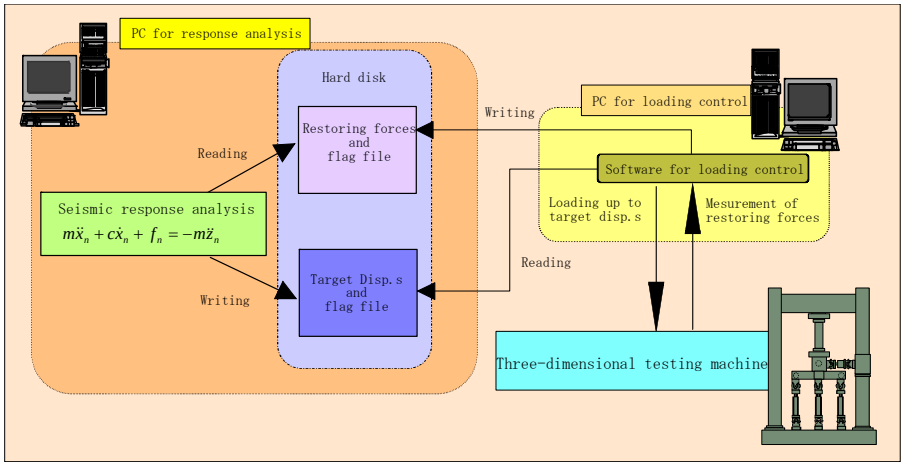

Fig. 5.3　Pseudo-dynamic testing system for seismic response

Table 5.2 Parameters of structural elements

	Unit	X direction	Y direction
Mass	ton	1179	
Damping ratio		0.02	
Stiffness	kN/mm	63.74	33.88

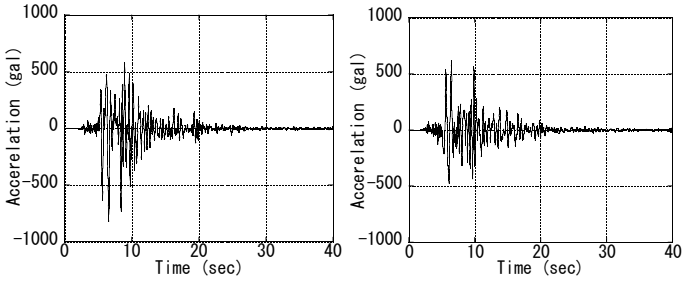

(a)NS component　　(b)EW component

Fig. 5.4 Seismic wave observed at the Kobe marine meteorological observatory

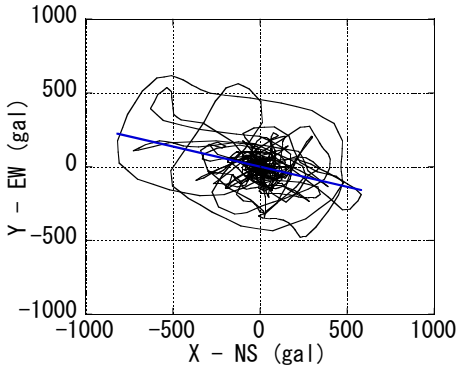

Fig. 5.5 trajectory in X-Y horizontal plane

Table 5.3 Experiment cases

Case-1	X direction
Case-2	Y direction
Case-3	X direction and Y direction

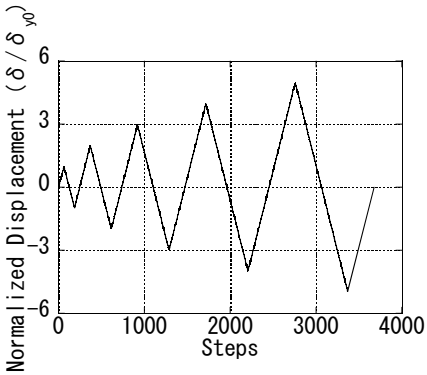

Fig. 5.6 Loading history

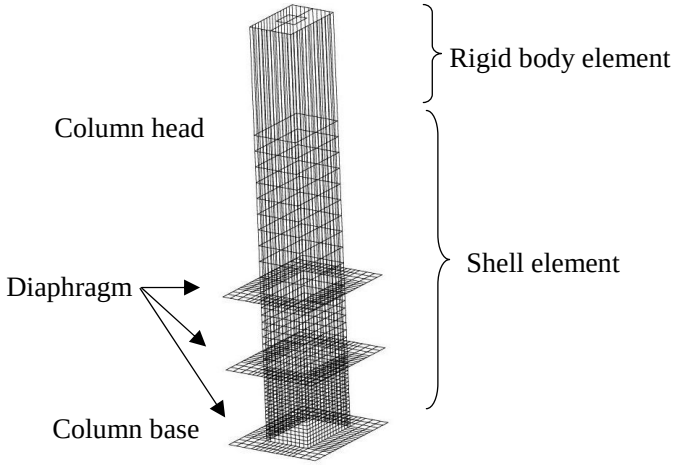

Fig. 5.7 Elasto-plastic finite displacement analytical model

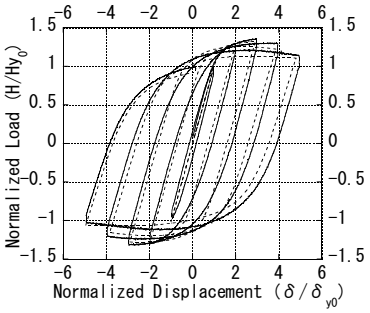

(a) Load-displacement

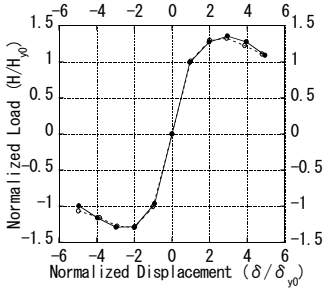

(b) Envelope curve

Fig. 5.8 Cyclic loading test (X component)

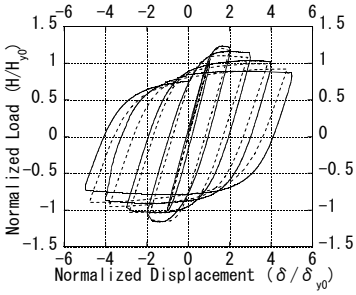

(a) Load-displacement

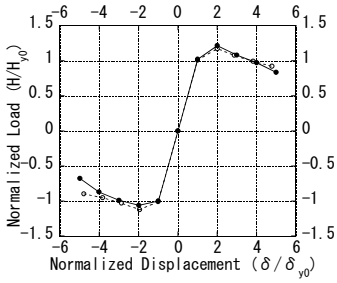

(b) Envelope curve

Fig. 5.9 Cyclic loading test (Y component)

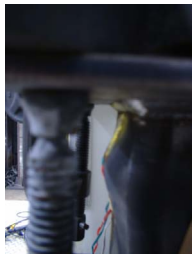

Photo 5.3 Cyclic loading test (X component)

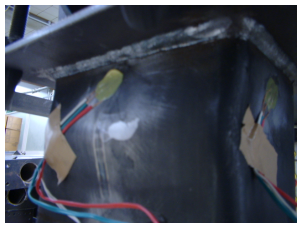

Photo 5.4 Cyclic loading test (Y component)

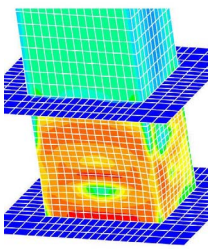

Fig. 5.10 Analytical result (X component)

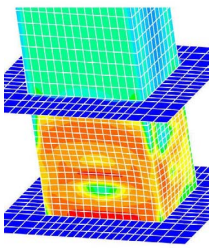

Fig. 5.11 Analytical result (Y component)

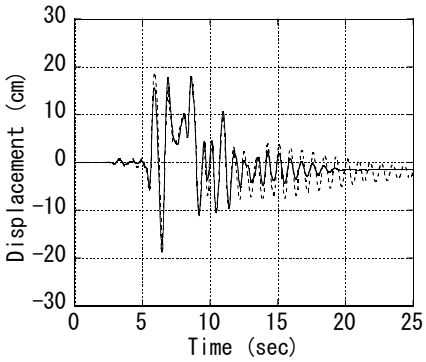

(a) Time history response

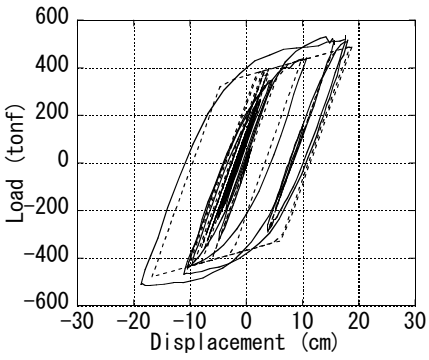

(b) Load-displacement (Analysis of system of particles)

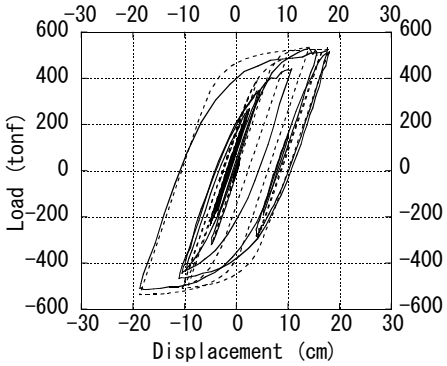

(c) Load-displacement (Elasto-plastic finite displacement analysis)

Fig. 5.12 Case-1 (X component)

Photo 5.5 Damage of base of column (Pseudo-dyna test, X component)

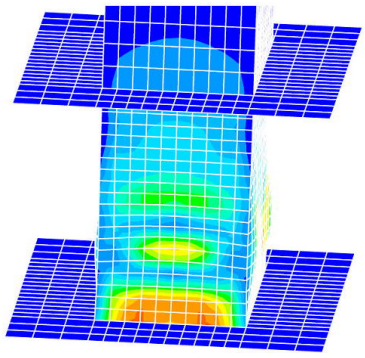

Fig. 5.13 Damage of column (Elasto-plastic finite displacement analysis, X component)

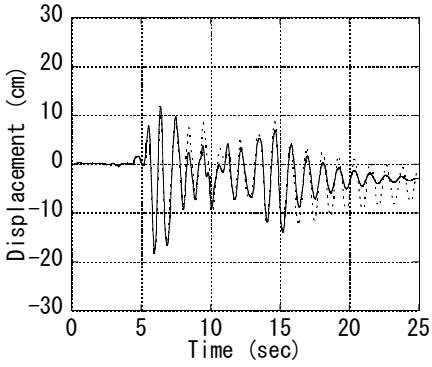

(a) Time history response

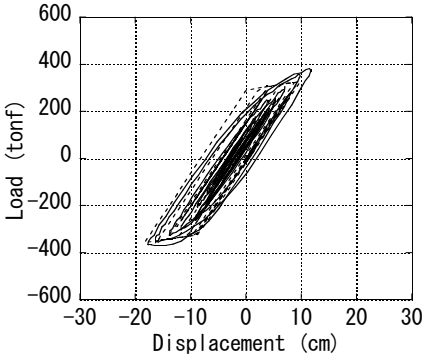

(b)Load-displacement (Analysis of system of particles)

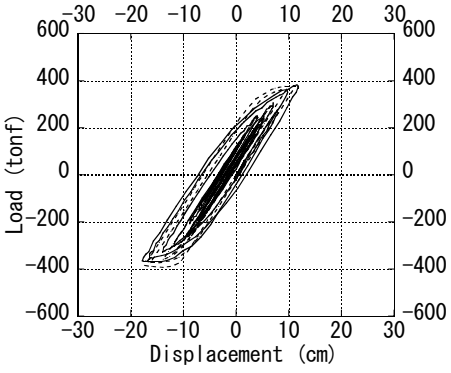

(c) Load-displacement (Elasto-plastic finite displacement analysis)

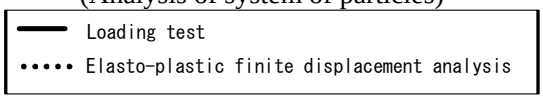

Fig. 5.14 Case-2 (Y component)

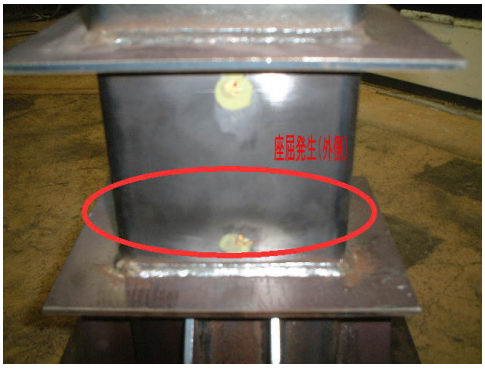

Photo 5.6 Damage of base of column
（Pseudo-dynamic test, Y component）

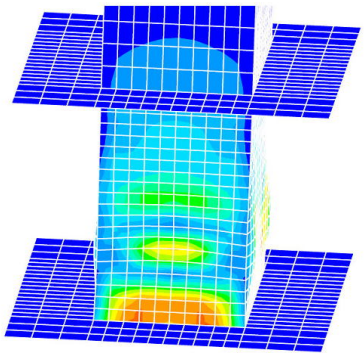

Fig. 5.15 Damage of column（Elasto-plastic finite displacement analysis, Y component）

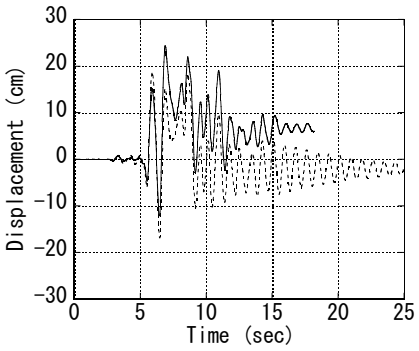

(a) Time history response

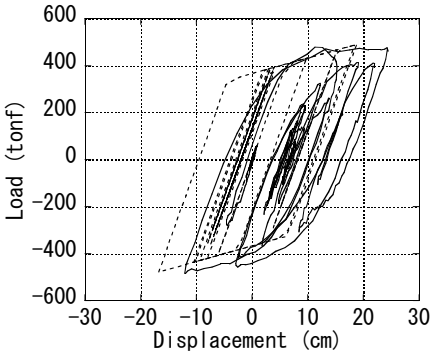

(b) Load-displacement
(Analysis of system of particles)

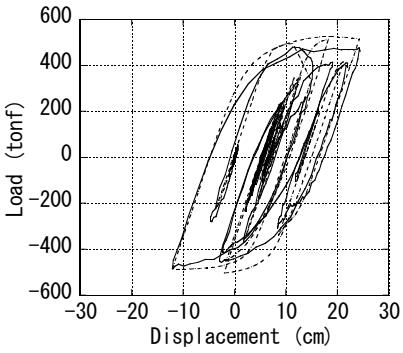

(c) Load-displacement
（Elasto-plastic finite displacement analysis）

Fig. 5.16 Case-3 (X component)

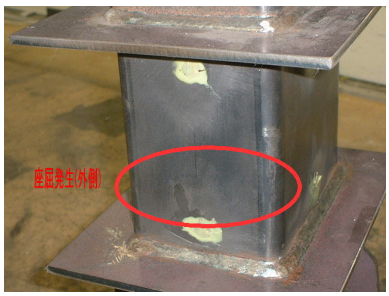

Photo 5.7 Damage of base of column
（Pseudo-dynamic test, X component）

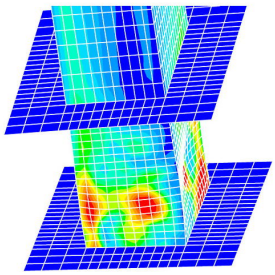

Fig. 5.17 Damage of column（Elasto-plastic finite displacement analysis, X component）

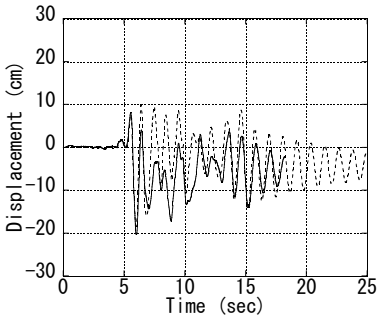

(a) Time history response

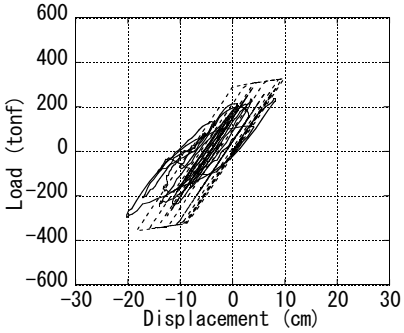

(b) Load-displacement (Analysis of system of particles)

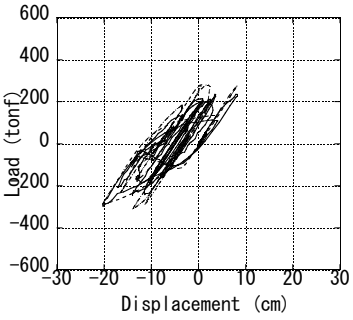

(c)Load-displacement (Elasto-plastic finite displacement analysis)

Fig. 5.18 Case-3 (Y component)

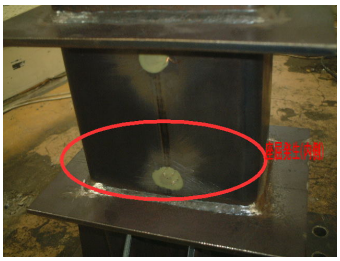

Photo 5.8 Damage of base of column (Pseudo-dynamic test, Y component)

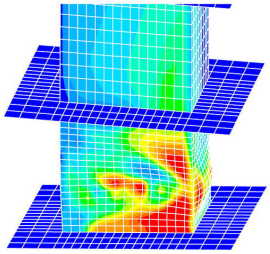

Fig. 5.19 Damage of column (Elasto-plastic finite displacement analysis, Y component)

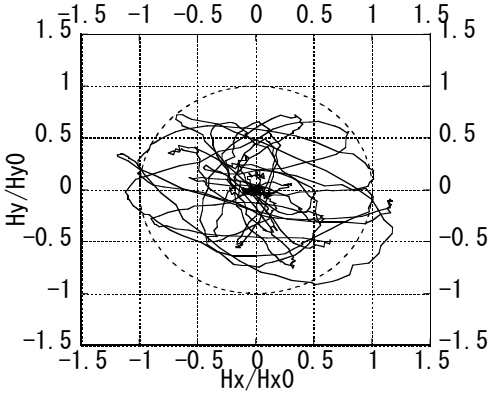

Fig. 5.20 Trajectory of the horizontal restoring forces in X and Y directions

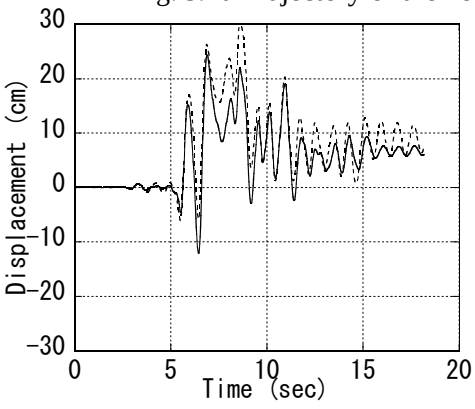

(a) Time history response

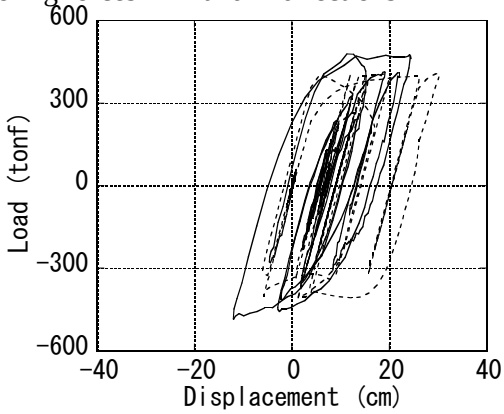

(b) Load-displacement

Fig. 5.21 Response results considering the correlation of 2 directions (X component)

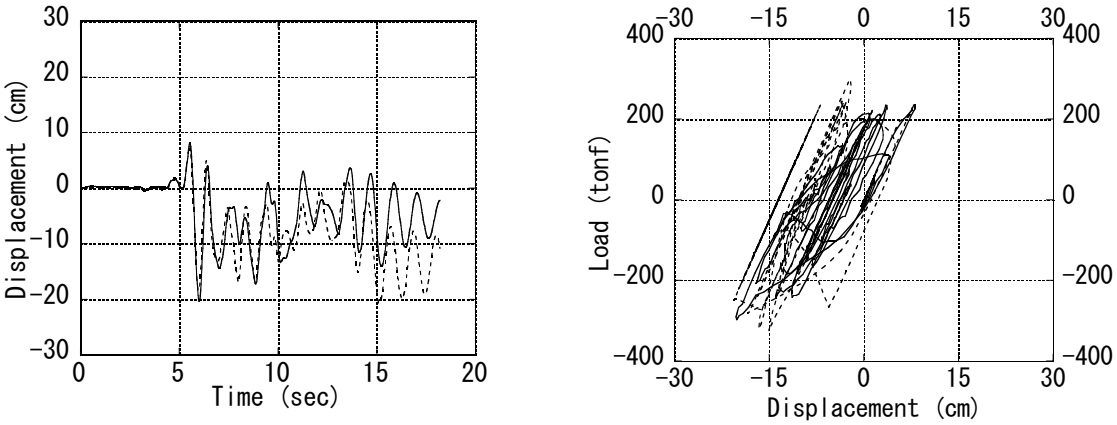

(a) Time history response (b) Load-displacement

Loading test
Elasto-plastic finite displacement analysis

Fig. 5.22 Response results considering the correlation of 2 directions (Y component)

Photo5.9 Frame-type of steel bridge piers

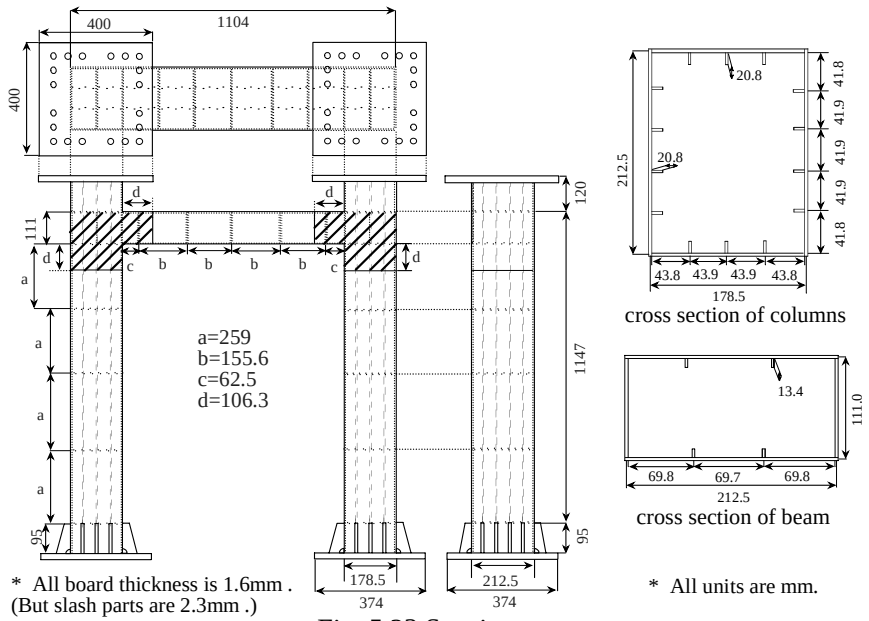

Fig. 5.23 Specimen

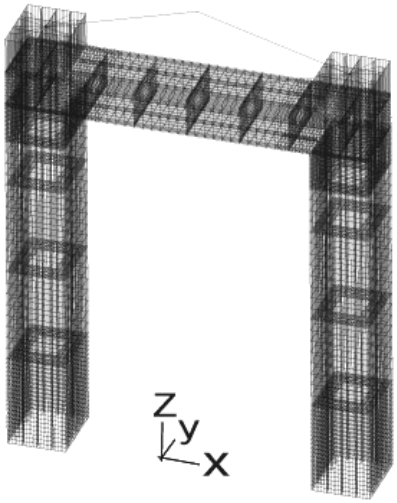

Fig. 5.24 FEM model

Table 5.4 Material properties

Thickness (mm)	Width (mm)	Young's Modulus (Gpa)	Poisson's ratio	Yield stress (Mpa)	Maximum stress (Mpa)	Elongation (%)
1.6mm	25.164	191.2	0.336	153.2	280.7	61.6
2.3mm	25.104	210.7	0.281	277.5	350.4	65.8

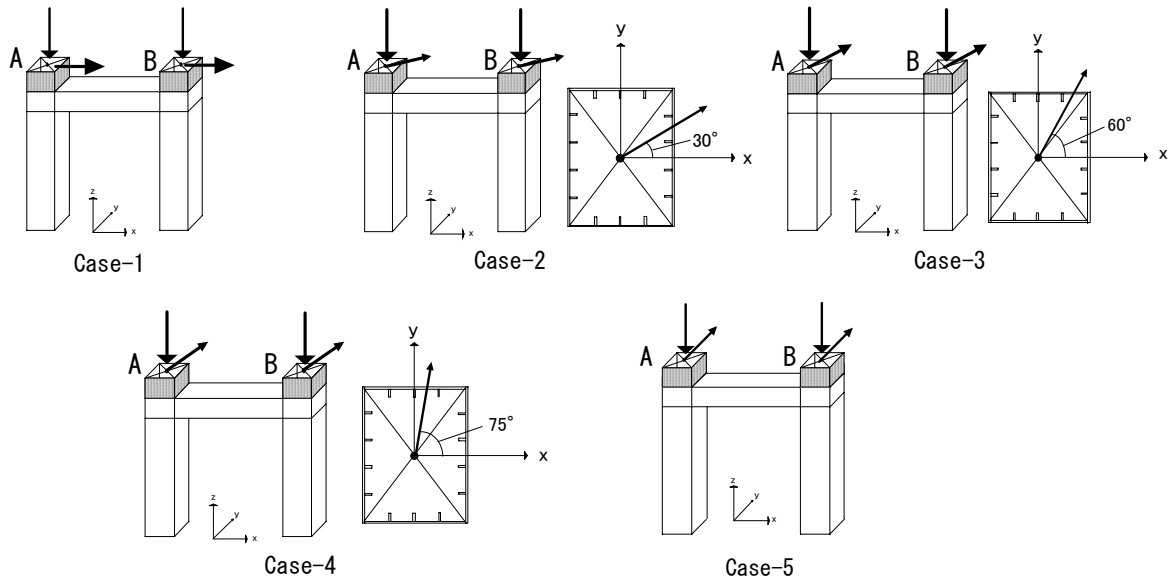

Fig. 5.25 Loading method for FEM model

Table 5.5 Analytical results (Case-1 - Case-5)

	Case-1	Case-2	Case-3	Case-4	Case-5
Yield displacement δ y(mm)	2.503	2.522	2.837	3.109	4.095
Yield load Hy(tonf)	2.511	2.363	2.122	2.074	2.595
Maximum displacement δ max(mm)	27.7	30.32	34.04	38.72	32.21
Maximum load Hmax(tonf)	5.865	5.708	5.106	4.574	3.766
Modification performance δ / δ y	11.07	12.02	11.99	12.45	7.866
Hmax on the bass on the direction of out-plane of the frame	1.557	1.516	1.356	1.215	1

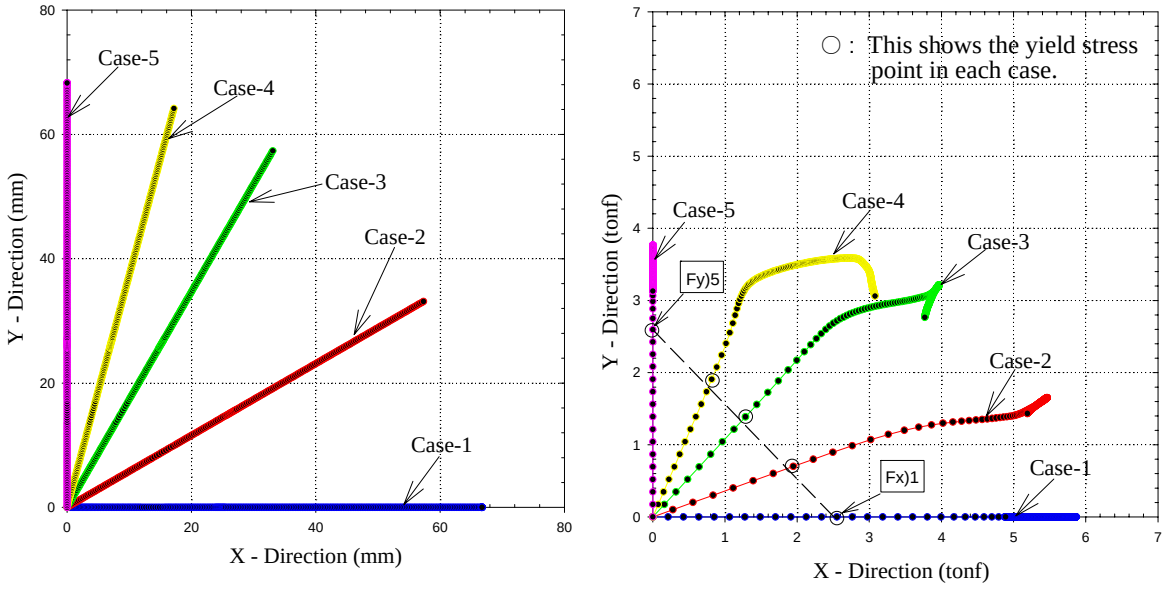

(a) Displacement (b) Load

Fig. 5.26 Displacement curve and load curve indicating the correlation between X-direction and Y-direction

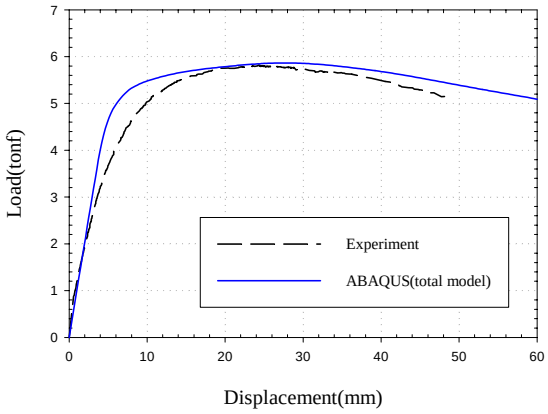

Fig. 5.27 Load-displacement (Case-1)

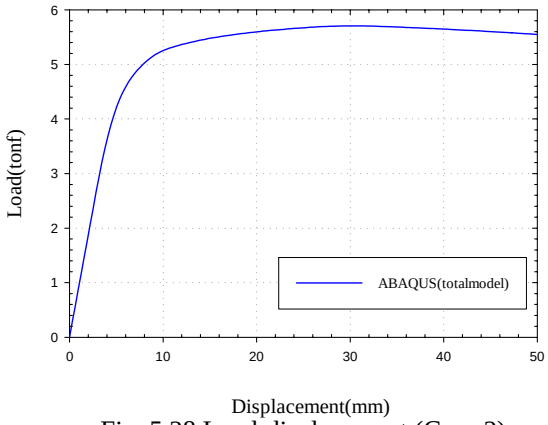

Fig. 5.28 Load-displacement (Case-2)

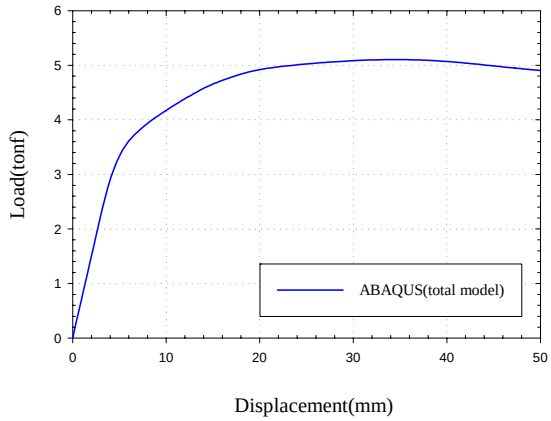

Fig. 5.29 Load-displacement (Case-3)

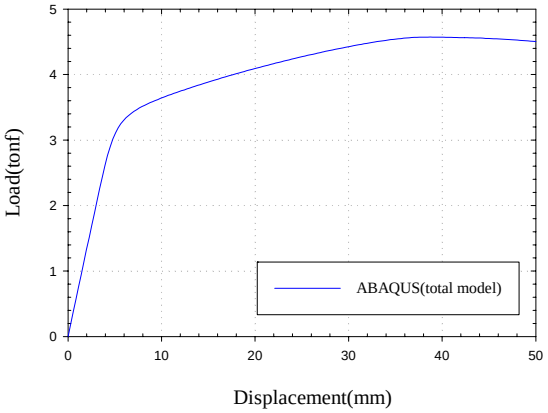

Fig. 5.30 Load-displacement (Case-4)

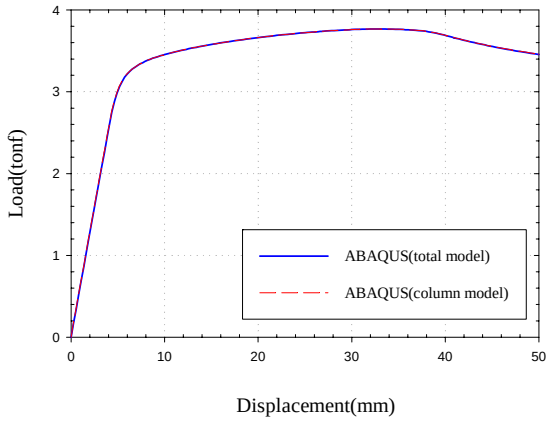

Fig. 5.31 Load-displacement (Case-5)

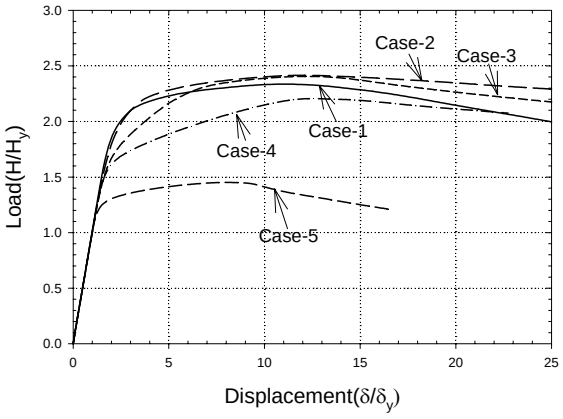

Fig. 5.32 Load-displacement (Non-dimension)

Chapter 6

Response Evaluation by a Pseudo-Dynamic Testing System using the Internet

6.1 Introduction

Structural engineers often must perform complicated analyses to ensure the safety of structures against various types of extreme loading from the surrounding environment. However, because of difficulties in the mathematical modeling of nonlinear structural behavior, experimental evaluation procedures inevitably must be carried out. In fact, a numerical response analysis cannot represent the true behavior of real structures in the nonlinear range unless the constitutive relation of stress to strain, or force to displacement is precisely prescribed. Recently, a semi-analytical method that combines analysis and experiment, so-called hybrid testing, was developed (Hakuno et al., 1990; Nakajima, 1985; Watanabe et al., 1994) besides with dynamic testing using shaking table. It has been utilized specifically to evaluate the nonlinear dynamic response of structures, and is also referred to as pseudo-dynamic testing (Kitada et al., 1998; Research Group on Ductility of Steel Structures of the Kansai Branch of Japan Society of Civil Engineers, 1991; Research Subcommittee on Dynamic Limit State of Steel Structures of Japan Society of Civil Engineers, 1994; Saizuka et al., 1995; Subcommittee on New Technology for Steel Structures of Japan Society of Civil Engineers, 1996; Usami et al., 1995). When pseudo-dynamic tests are performed to assess the response of a structural system consisting of a plural number of structural elements, each of the nonlinear elements must be tested to update its constitutive relation at each time step. Many damages around the joints of structures were reported in the Hyogoken-Nanbu Earthquake (Committee on Roadway Bridge Damage by the Hyogoken-Nanbu Earthquake, 1995; Nagata et al., 1999). Therefore, not only the behavior of each nonlinear element but also the interactions among arbitrary elements and their remaining parts in the structure must be considered interactively (Watanabe et al., 1994). As the number of the nonlinear elements increases, the same number of actuators is generally required to control the displacement of each structural element for the pseudo-dynamic testing. One of the recent developments in the study of seismic responses is the network of an on-line parallel pseudo-dynamic testing system to consider the interactions among the structural elements. But the larger the number of nonlinear elements becomes, due to the difficulty of preparing a sufficiently large structural testing space and facilities.

Although a small scale specimen would seem to an efficient and convenient way to understand the overall response, the behavior of the scaled-model tends to differ from the response of the prototype and thus becomes unrealistic.

Depending on the number of nonlinear elements, a corresponding number of testing stations may be required to perform pseudo-dynamic testing on the total system. Thus, the concept of the on-line parallel pseudo-dynamic testing system was proposed. In order to assess the dynamic interaction of structural system, the proposed evaluation method is considered to be versatile; namely the parallel pseudo-dynamic testing system with the Internet. At first, an error propagation in response evaluation by the proposed system was assessed, where the system has been established by connecting experimental stations located at Osaka City University and Kyoto University through the Internet. Then, the feasibility of using the proposed system to connect international testing and computing facilities was assessed. For this evaluation, a link was established among Korea Advanced Institute of Science and Technology (KAIST) in Korea, the State University of New York at Buffalo in the U.S.A., Monash University in Australia, and Osaka City University and Kyoto University in Japan. Moreover, between KAIST and Kyoto University, a demonstration of international collaborative testing using this proposed method was carried out.

6.2 Development of Parallel Pseudo-Dynamic Testing System using the Internet

Fig. 6.1 presents a schematic of the network for the parallel pseudo-dynamic testing system through the Internet. It is described as referring to the testing system that connected the testing equipments at Kyoto University and Osaka City University through the Internet. Fig. 6.2 shows a flow chart of this testing system. Engineering Workstation 1 (EWS1) at Kyoto University carries out the management of the whole testing, namely, the dynamic response analysis and the data communication control; a personal computer (PC) at each university is assigned tasks for loading management, namely loading tests and data acquisition; and Engineering Workstations 2 and 3 (EWS2 and EWS3) at two universities are used to exchange the information between EWS1 and the PCs. In this system, the technique of the information communication with client-server system was utilized. Here, the client manages the whole system by controlling the communication and the server offers various services. Hence, the client is EWS1 and the servers are EWS2 and EWS3. Thus the system consists of one client and two servers. As a reference, the testing equipment at the two universities is shown in Photos 6.1 and 6.2.

The data flow during the parallel testing between two universities is shown in Fig. 6.2 and summarized as follows: First, a response analysis to determine the target displacements for the next step is carried out on EWS1 by referring to the restoring forces measured independently in the previous step by

each of the testing facilities. The computed target displacements are transferred through the Internet and written on the shared disk units of EWS2 and EWS3, respectively. Once files for the target displacements are found to exist in the disk units, each PC reads the data from the file and starts to control the actuator at each testing site to impose the target displacement. After the loadings are completed, the restoring forces are measured, and the results are written in the specific files on the disk units in EWS2 and EWS3, respectively. Thus the dynamic response analysis proceeds to the next time step. The client computer and the local personal computers controlling the loadings are enabled to read either the restoring forces or the target displacements from the shared disks in the server computers by timing adjustments made through checking the corresponding flag files.

The data communication between the client (EWS1) and the two servers (EWS2 and EWS3) is carried out using the conventional transmission control protocol and Internet protocol (TCP/IP) for their reliability and speed of data communication. On the other hand, the communication between the two server EWSs and the PCs is carried out using a general purpose software package, SAMBA, since the EWSs and PCs use different operating systems (Sharpe, 2000): i.e., the EWSs use the UNIX system and the PCs use the Windows system.

6.3 Verification of the proposed Testing System

6.3.1 Modeling for Verification

As shown in Fig. 6.3, the elastic response characteristics of a single span of elevated bridge were evaluated in order to assess the proposed testing system. The equation of the horizontal motion of the elevated bridge was modeled by a two degrees-of-freedom system as

$$\boldsymbol{M}\cdot\ddot{\boldsymbol{X}}+\boldsymbol{C}\cdot\dot{\boldsymbol{X}}+\boldsymbol{F}=-\boldsymbol{M}\cdot\boldsymbol{U}\cdot\ddot{z} \tag{6.1}$$

in which,

$$\boldsymbol{M}=\begin{pmatrix} m_a & 0 \\ 0 & m_b \end{pmatrix},\quad \boldsymbol{C}=\begin{pmatrix} c_a+c_g & -c_g \\ -c_g & c_g+c_b \end{pmatrix},\quad \boldsymbol{F}=\begin{pmatrix} f_a+k_g\cdot(x_a-x_b) \\ -k_g\cdot(x_a-x_b)+f_b \end{pmatrix}$$

$$\ddot{\boldsymbol{X}}=\begin{pmatrix} \ddot{x}_a \\ \ddot{x}_b \end{pmatrix},\qquad \dot{\boldsymbol{X}}=\begin{pmatrix} \dot{x}_a \\ \dot{x}_b \end{pmatrix},\quad \boldsymbol{X}=\begin{pmatrix} x_a \\ x_b \end{pmatrix}$$

Here, $\boldsymbol{M}$, $\boldsymbol{C}$, $\boldsymbol{F}$, $\ddot{z}$, $\ddot{\boldsymbol{X}}$, $\dot{\boldsymbol{X}}$, $\boldsymbol{X}$ and $\boldsymbol{U}$ designate the mass matrix, damping matrix, restoring force vector, ground acceleration, response acceleration vector, velocity vector, displacement vector of the

superstructure relative to the ground surface, and unit vector, respectively. Subscripts a , b and g indicate variables of Pier-A, Pier-B, and Girder, respectively. Parameters of these structural elements are tabulated in Table 6.1. The stiffness of both bridge piers in this table was based on material testing. The central difference method was utilized for the time integration to solve the equation of motion, Eq. 6.1, with the time increment of 0.01 sec (Shimizu et al., 1980). In this verification, the restoring forces of the two bridge piers were tested by the testing equipment at each university. Namely, the forces for Pier-A and Pier-B were set at Osaka City University and Kyoto University, respectively.

6.3.2 Outline of Verification Procedure

The experiments that focused on the elastic response behavior of the fictitious elevated bridge were carried out by using an H-shaped steel column of SS400, and the model was fabricated carefully so as to have the designed structural performance, i.e., no buckling. In order to check the stiffness of the model pier in different experimental equipment, the heights of these specimens, namely, the distance to the horizontal loading position from the bottom of the column, were kept equal. These specimens were conducted in 1/5 the scale of the fictitious prototype bridge piers, and set to experimental equipment are shown as Photos 6.1 and 6.2.

In pseudo-dynamic testing, it is very important to carry out measurements and to control the loading displacement in order to improve the accuracy in the experiments. So in this verification test, the measurement and control were made by the internal displacement transducer in experimental setup A, and additional measurement and control was made by an external displacement transducer set on each specimen in the experimental setup B.

At first, the loading was carried out to evaluate the stiffness of these specimens within the elastic response. From the experimental results, the obtained stiffness of 9.8 kN/mm for a specimen agreed well with the theoretical stiffness by experimental setup B, but that by experimental setup A was only 60% of the theoretical stiffness. This means that the measurement and control method using an external displacement transducer (experimental setup B) was suitable to eliminate rigid body rotation due to the elastic deformation of fixtures at the base of the bridge column, such as the high strength bolts, and non-tested column section.

Secondly, a dynamic response evaluation was made by using the same model with the structural details shown in Table 6.1. Fig. 6.4 shows the input acceleration record. The acceleration record is in sine wave with its maximum value of 70 gal, and its period of 0.7 sec, and the duration of excitation is 20 sec. These experiments were carried out for only the first 5 sec of the 20 sec acceleration record. In order to compare the experimental results with the analytical results, the responses of the main girders of bridges are

the most important members to assess dynamic interaction of bridge structural system such as girders, piers and foundations. However, the effect of the stiffness of the main girders on the distribution of inertial force to each pier is not obvious. Therefore, these main girders were modeled as a reference by shearing springs with a spring constant of 1/10 of that of pier B for the sake of simplicity. Two kinds of experiments were carried out to verify the seismic response behavior of elevated bridges; the dynamic interaction among the piers was considered in Case 1, and the seismic response was considered without the dynamic interaction in Case 2. The experimental and analytical results are shown in the dimensions of these special models.

The natural periods of Pier A and Pier B were 0.892 sec and 0.546 sec, respectively. Figs. 6.5 and 6.6 show the analytical responses of piers A and B subjected to the 20 sec acceleration sine wave record of sine wave without the dynamic interaction among the piers. It is understood from these figures that the amplitudes of the displacement responses are not stable for the first 10 sec, but become stable thereafter. The parallel pseudo-dynamic test was carried out by linking the Pier A model at Osaka City University and the Pier B model at Kyoto University.

6.3.3 Results and Discussion

Figs. 6.7 and 6.8 show the time history of the displacement response of Pier A and Pier B obtained by the proposed system, respectively, for both Case 1 and Case 2. In addition, Figs. 6.9 and 6.10 are drawn for comparison the time history of the displacement response of Pier A and Pier B obtained by numerical simulation for the first 5 sec only. The relations of the horizontal displacement to the horizontal force of Pier A and Pier B obtained by the proposed system are shown in Figs. 6.11 and 6.12, respectively. Finally, the relations of the horizontal displacement to the horizontal force of Pier A and Pier B obtained by the numerical simulations are shown in Fig. 6.13 and Fig. 6.14, respectively.

According to these results, the maximum displacement response obtained by the proposed system agrees well with those by the numerical simulations for both Pier A and Pier B. It is also indicated that the response of Pier A in Case 2, in which the dynamic interaction of the main girders between the piers is considered, is greater than that of Case 1, in which the dynamic interaction is not considered. On the other hand, it is observed that the response of Pier B in Case 2 is smaller than that of Case 1. It is concluded that the proposed system was effective for evaluating the dynamic interaction of bridge systems between the piers.

By checking the communication between experimental facilities and the data transmission control of the experiments are executed correctly throughout the test. The proposed parallel pseudo-dynamic testing system would thus be very useful for evaluating the seismic response of structures with MDOF; e.g., for structural systems consisting of variable material/structural elements that interact

with each other.

6.4 Accuracy in the Response Evaluation

6.4.1 Case I: Effect of Girder Stiffness on the Dynamic Interaction

At first, without consideration of dynamic interaction of main girders with the piers was carried out, the effect of error in stiffness was assessed by varying the stiffness of Pier A from 10% greater than the baseline value to a value 10% less than the baseline value. The variation of the response is summarized in Table 6.2 and Fig. 6.15.

As shown in Fig. 15, the response has no linear relation to the stiffness of the pier; the response must be evaluated based on the natural period determined by the combination of stiffness. So, special care must be taken in regard to the stiffness. Especially, as the design stiffness is not usually obtained owing to the errors in fabrication, variation of material property, it is necessary to assure the stiffness of the model before pseudo-dynamic test.

It is also concluded from Fig. 6.15 that the maximum response increases as the stiffness of the pier increases by +1% to +10%; on the other hand, it decreases as the stiffness of the pier decreases by -1% to -10%. It is obvious that the relation of the natural period of the structural system to the period of excitation may affect the response. The error may be amplified in the case that the natural period of structures is close to the period of excitation.

Secondly, by changing the stiffness of Pier A from 90% to 110%, the effect of the interaction on the response of Pier A and B is assessed. The results are summarized in Fig. 6.16. It can be seen observed that the effect of the stiffness of Pier A is small and the maximum displacement response is not changed in the case that the stiffness of the main girder is the same as that of Pier A. On the other hand, the effect of the stiffness of Pier A becomes significant when the stiffness of the main girder is twice as large as that of Pier A. It is concluded that the inaccuracy of each structural model may distort the response to the others, so that special attention is needed to carry out the test. The accuracy of each experimental procedure of the parallel pseudo-dynamic test must be equally guaranteed.

6.4.2 Case II: Effect of the Displacement-Control Accuracy on the Response

The effect of the accuracy of the displacement control on the response of the structure was assessed by generating the error in the control displacement. The error is assumed by the coefficient to target displacement which is generated by a uniform random number. Here, the random number is generated uniformly as a value between 0.0 and 1.0 by a mixed congruential generator.

At first, the statistics of uniform random numbers generated three-times are summarized in Table 6.3. The average and variance of uniform random number agree well with their theoretical values of 0.5 and 0.0833 (=1/12), respectively in all the cases. The generation random number is verified and can be used for the system assessment.

By generating the uniform random number, 1,000 coefficients with a maximum variation of 10% is shown in Fig. 6.17 as an example. Since it is understood that inaccuracy in any structural members may affect the general response, as described in 6.4.1, this assessment focused on only the response of Pier A.

Fig. 6.18 shows the numerical results in the case that the errors of control displacement were varied to 1%, 3%, and 5%. Table 6.4 summarizes the results. It is understood that the error in the response becomes larger as the error in the control displacement becomes larger. It is also suggested that the error of control displacement should be limited to by at most about 1% in order to evaluate the response within an error of 3%. It is thus necessary to pay attention to ever a small control error of displacement improving in the accuracy experiment. The errors of control displacement were assumed to be random here, but it is necessary to assess the error which has uniform variation such as undershooting /overshooting the target displacement all the time.

6.5 Remote Parallel Analyses between Kyoto University and Other Universities

6.5.1 Purpose and Scheme

For further investigation of the present remote parallel test method through the Internet, additional trials were performed linking Kyoto University with the State University of New York at Buffalo in the U.S.A., with Monash University, Australia and with Osaka City University. In this study, parallel analyses instead of parallel tests were performed on the base-isolated bridge. The elapsed time, the network conditions and the stability of the system were intensively investigated.

In each case, a Client EWS1 and Server EWS2 were set up at Kyoto University, while a Server EWS3 and PC1 were set up at the partner university. The Server EWS2 at Kyoto University has the role of receiving the file the displacement is written in, calculating the restoring force based on a prescribed stiffness, and sending it to the Client EWS1. At the partner university, the PC1 reads the displacement in the prescribed on a hard disk shared with the Server EWS3, calculates the restoring force based on a prescribed stiffness, and then writes it in a prescribed file on the shared hard disk of Server EWS3. Then that Server EWS3 sends the file to the Client EWS1.

Because of the possibility that Kyoto University and the partner university may have different systems, it is helpful to render the data flow visually for the observers at the partner university. In this

system, the received displacement data, the transmitted restoring force data, and the flag files that indicate the existence of other files are displayed as output on the screen of the PC1.

6.5.2 Network Condition and Elapsed Time

The elapsed time for each 1,000 steps of the simulation analyses for the remote parallel pseudo-dynamic tests are tabulated in Table 6.5, Table 6.6 and Table 6.7. It is understood from the tables that the network condition was judged to be stable in each case. It took about 8.2 sec for each step between Kyoto University and SUNY-Buffalo, 8.7 sec for those between Kyoto University and Monash University, and 10.3 sec for those between Kyoto University and Osaka City University. This elapsed time is mainly for communication between two institutions. It is interesting to observe that the elapsed time in the present cases is even shorter than the time required between Kyoto University and Osaka City University, which are located much closer to each other. This indicates that the elapsed time mainly depends on the network condition, not on the distance between the two connected institutions. In addition, an investigation of the connection pathway was also made, and the results are summarized in Tables 6.8, 6.9, and 6.10. It is also mentioned that the pathway seems to be consistent stable during the testing.

6.6 Remote Parallel Test for an Elevated Bridge consisting of Steel and RC Piers between Osaka City University and Kyoto University

6.6.1 Modeling of the Elevated Bridge System

The response characteristics of a single span elevated bridge consisting of steel and RC piers as shown in Fig. 6.19 were evaluated in order to assess the proposed testing system as shown in Fig. 6.1. The equation of the horizontal motion of the elevated bridge was modeled by two degrees-of-freedom systems as shown in Fig. 6.20, and its equation of motion for the modeled elevated bridge can be given by the following equation:

$$\boldsymbol{M}\cdot\ddot{\boldsymbol{X}}+\boldsymbol{C}\cdot\dot{\boldsymbol{X}}+\boldsymbol{F}=-\boldsymbol{M}\cdot\boldsymbol{U}\cdot\ddot{z} \tag{6.2}$$

in which,

$$\boldsymbol{M}=\begin{pmatrix} m_a & 0 \\ 0 & m_b \end{pmatrix},\quad \boldsymbol{C}=\begin{pmatrix} c_a+c_g & -c_g \\ -c_g & c_g+c_b \end{pmatrix},\quad \boldsymbol{F}=\begin{pmatrix} f_a+k_g\cdot(x_a-x_b) \\ -k_g\cdot(x_a-x_b)+f_b \end{pmatrix}$$

$$\ddot{\boldsymbol{X}}=\begin{pmatrix} \ddot{x}_a \\ \ddot{x}_b \end{pmatrix},\qquad \dot{\boldsymbol{X}}=\begin{pmatrix} \dot{x}_a \\ \dot{x}_b \end{pmatrix},\quad \boldsymbol{X}=\begin{pmatrix} x_a \\ x_b \end{pmatrix}$$

Here, M, C, F, ẍ, $\ddot{X}$, $\dot{X}$, X and U designate the mass matrix, damping matrix, restoring force vector, ground acceleration, response acceleration vector, velocity vector, displacement vector of the superstructure relative to the ground surface, and unit vector, respectively. Subscripts a, b and g indicate variables of steel pier, RC pier, and Girder, respectively. The parameters of these structural elements are tabulated in Table 6.11. The stiffness of both bridge piers in this table was based on material testing. The central difference method was utilized for the time integration to solve the equation of motion, Eq. 6.2, with a time increment of 0.01 sec.

In this verification, the restoring forces of two bridge piers were tested by the testing equipment at each university. Namely, steel pier and RC pier were set at Osaka City University and Kyoto University respectively. The response of the girder was assumed to be an elastic system. The ground motion shown in Fig. 6.21 was used.

6.6.2 Test Results

The obtained experimental results of the response displacements and restoring forces of both piers are shown in Fig. 6.22 and Fig. 6.23. The results by the numerical simulation are also shown in these figures in order to verify the validity of this experiment. Here, characteristics of the restoring forces of steel and RC piers were modeled by bilinear and trilinear models in this numerical simulation, respectively.

It is shown that the elastic response within about 1 sec obtained experimentally by using this proposed system is in good agreement with the response by the numerical simulation. Moreover, when both piers begin to be damaged from about 1 sec, it is found that these results deviate gradually. Therefore, this proposed testing system seems to be very effective for evaluating the seismic response of a structural system with different restoring forces.

As for the failure mode, the specimens after the experiment are shown in Photo 6.3. The local buckling of a stiffened flange plate is observed in the steel pier. On the other hand, many cracks near the basement are observed in the RC pier. Compression failure is also seem in the concrete RC pier. Reinforcing bars are also considered to be yield from the monotonic loading test results for the RC pier.

Damages of specimens, steel pier and RC pier, are shown in Photo 6.3, and damages of the actual bridge piers, P353 (steel pier) and P354 (RC pier), due to the Hyogoken-Nambu Earthquake are shown in Photo 6.4. The effectiveness of the proposed testing system was confirmed because these damages are similar well each other.

6.7 Dimension of the proposed Remote Parallel Test for a Base-Isolated Bridge between Kyoto University and KAIST

6.7.1 Model Structure and Equation of Motion

A remote parallel pseudo-dynamic test using the Internet was carried out between Kyoto University and Korea Advanced Institute of Science and Technology (KAIST). The model structure considered herein is the base-isolated bridge model shown in Fig. 6.24. It consists of three piers and a superstructure with three continuous spans. Lead rubber bearings (LRBs) are used as the base isolators (Skinner et al., 1996; Ministry of Construction, 1992; Japan Society of Seismic Isolation, 1995). All of the piers are assumed to be made of steel. Fig. 6.25 shows the modeling of the structure consisting of 4 D.O.F. The primary earthquake load is applied in the longitudinal direction of the bridge axis. Restoring force characteristics of the piers are modeled by linear springs and dashpots; whereas those of the LRB systems are assumed to be nonlinear. The deck is simply modeled as a rigid body with a lumped mass. Masses of the piers are also represented as lumped masses. The structural parameters of each element base-isolated bridge system are shown in Table 6.12.

For the bridge with a conventional bearing arrangement (i.e., one hinge on Pier 2 and rollers on Piers 1 and 3), the primary natural period is obtained as 0.87 sec in the longitudinal direction of the bridge axis, and very close to the period range with high spectral acceleration. LRBs installed on the piers are designed to prolong the primary effective natural period to 2.0 sec. The equivalent stiffness of the bridge with LRBs is given approximately by

$$K_B = m_B \times \left(\frac{2\pi}{T_B}\right)^2 = (36.00) \times \left(\frac{2\pi}{2}\right)^2 = 354.0 \qquad (6.3)$$

where T_B = the target natural period sec; K_B = equivalent stiffness of LRB (kN/cm^2; and m_B = mass of super structure kN·sec^2/cm. The equivalent stiffness (K_B) for all LRBs is assumed to be evenly distributed on three piers, so that the stiffness of the bearing system on each pier is 118.0 kN/cm. From the eigenfrequency analysis on the bridge system with the equivalent LRB stiffness, the primary natural period is computed to be 2.09 sec, which is close enough to the target period of 2.0 sec.

The equation of motion for the bridge model can be written as

$$M\ddot{X} + C\dot{X} + f_{NL}(X) = -MU\ddot{z} \qquad (6.4)$$

in which,

$$\boldsymbol{M} = \begin{bmatrix} m_1 & 0 & 0 & 0 \\ 0 & m_2 & 0 & 0 \\ 0 & 0 & m_3 & 0 \\ 0 & 0 & 0 & m_4 \end{bmatrix}, \quad \boldsymbol{C} = \begin{bmatrix} c_1 + c_4 & 0 & 0 & -c_4 \\ 0 & c_2 + c_5 & 0 & -c_5 \\ 0 & 0 & c_3 + c_6 & -c_6 \\ -c_4 & -c_5 & -c_6 & c_4 + c_5 + c_6 \end{bmatrix} \tag{6.5}$$

and $\boldsymbol{M}$, $\boldsymbol{C}$, $\boldsymbol{K}$, $\ddot{z}$, $\ddot{\boldsymbol{X}}$, $\dot{\boldsymbol{X}}$, $\boldsymbol{X}$ and $\boldsymbol{U}$ designate the mass matrix, damping matrix, stiffness matrix, ground acceleration, response acceleration, velocity, and displacement vector, respectively, of the superstructure relative to the ground motion and unit vector, respectively. $\boldsymbol{f_{NL}(X)}$ is the restoring force vector of the piers and the nonlinear bearings and can be written as follows:

$$\boldsymbol{f_{NL}}(X) = \begin{bmatrix} k_1 x_1 + f_{b1} \\ k_2 x_2 + f_{b2} \\ k_3 x_3 + f_{b3} \\ -f_{b1} - f_{b2} - f_{b2} \end{bmatrix} \tag{6.6}$$

Restoring forces of the bearings on Piers 1 and 2 (f_{b1}, f_{b2}) are obtained from each of the experimental stations at Kyoto University and KAIST, respectively, while the third restoring force on Pier 3 (f_{b3}) is obtained by the simulation using the initial design values by the bilinear hysteretic model. The central difference method was used to evaluate the dynamic response of the total bridge system at the next time step during the pseudo-dynamic testing.

6.7.2 LRB Specimens and Scale Factors during Tests

It is assumed that eight LRB units are installed on each pier, as shown in Fig. 6.26, the general configuration of a manufactured LRB specimen is shown in Fig 6.27 (a). The size of the bearing model tested in the laboratory is taken as one half of the prototype. The relationship between the prototype and the model with a scale factor S (S = 2 in this study) is given by:

$$x_p = S x_m, \quad \dot{x}_p = \dot{x}_m, \quad R_p = S^2 R_m \text{ and } K_p = S K_m \tag{6.7}$$

where, x, $\dot{x}$, R, and K denote the displacement, velocity, restoring force, and stiffness coefficient, respectively. The subscripts m and p indicate the model and the prototype, respectively. Therefore, the vertical load given to the bearing model is calculated as 367.5 kN (=35,280/(2^2×8×3) kN) from Table 6.12

and Eq. 6.7, and the target effective stiffness of the bearing model is obtained as 7.38 kN/cm (= 354.0/(2×8×3) kN/cm) from Eq. 6.3. The initial design stiffness defining the bilinear behavior of the LRB model is approximately estimated as $K_1 = 23.13\ kN/cm$, $K_2 = 5.80\ kN/cm$ and $P_y = 23\ kN$, as shown in Fig. 6.27 (b). This configuration consists of 20 rubber layers, 19 steel layers, a lead core, and 2 steel cover plates. The diameter is 300 mm, the total thickness of the rubber layers is 40 mm, and the total height is 148 mm. During the pseudo-dynamic test, the dynamic response analysis of the bridge was carried out for the prototype. The measured restoring forces from the model were converted to that of the prototype by multiplying S^2 as defined in Eq. 6.7, prior to the execution of the analysis.

6.7.3 Preliminary Test under Monotonic and Cyclic Loading

Photo 6.5 shows the test setup at Kyoto University and KAIST. Before performing the parallel pseudo-dynamic test for the response of the base-isolated bridge under the earthquake excitation, a monotonic loading test was performed at Kyoto University to investigate the characteristics of the bearing model. A vertical load of 367.5 kN was applied to the model as explained previously. The horizontal loading was applied with a loading speed of 0.1 mm/sec at both universities, and the maximum displacement was set to be 4 cm, which corresponds to a shearing strain of 100%.

Then, cyclic loading tests were performed at Kyoto University and KAIST. The magnitude of vertical load and the horizontal loading speed were identical to those for the monotonic loading test. The loading was applied in the following sequence of displacement amplitude: ±1, ±2, ±3 and ±4cm. The hysteresis of the model under the cyclic loading is shown in Fig. 6.28, and the idealized bilinear relation to fit the test results is summarized in Table 6.13, compared with the initial design values.

It can be seen that the monotonic and cyclic test results for the yield load (P_y) and the secondary stiffness after yielding (K_2) are reasonably close to the initial design values. On the other hand, those for the primary stiffness (K_1) are much larger than the design value. The initial design values were approximately estimated based on the target effective stiffness (K_{eff}) before manufacturing the LRBs. The overall response of the bridge mainly depends on the effective stiffness, which relates with the amplitude of the LRB deformation. The effective stiffness with a displacement amplitude of ± 4 cm obtained from the cyclic tests was 10.2 kN/cm and 9.8 kN/cm, respectively, at KAIST and Kyoto University. The stiffness for the initial design value with the same deformation amplitudes is 10.14 kN/cm. The results were good agreement, so that the manufacturing of the LRBs was confirmed to have been precise.

6.7.4 Results of On-Line Parallel Pseudo-Dynamic Testing

The El Centro Earthquake, which had a duration of 15 sec (Fig. 6.29), was used as the input ground motion

in the longitudinal direction of the bridge axis. The time step of the pseudo-dynamic test was set at 0.005 sec by considering the smallest natural period of the structure, which was 0.086 sec, so that the duration of 15 sec was divided into 3,000 steps.

The results of the pseudo-dynamic test are shown in Figs. 6.30-33: They are the displacement and acceleration of the deck (of the prototype) and the horizontal deformations, restoring forces, and hystereses of the LRBs on Piers 1 and 2. It is understood from Fig. 6.30 that the maximum total acceleration of the deck is 79.8 cm/sec^2, which is much smaller than the peak ground acceleration of 300 cm/sec^2. It is also observed that the effect of the base isolation, i.e., the additional damping of the LRBs, made the primary natural period approximately 1.7 sec, which is a little lower than the target design period of 2.0 sec. The discrepancy comes from the higher effective stiffness of the specimen (K_{eff} = 9.9 and 8.7 kN/cm) from the test shown in Fig. 6.33 than the initial design value of 7.38 kN/cm. In addition, the effect of the pier masses, which was not considered in the approximate evaluation of the design period, also contributed to the reduction in the natural period.

The LRBs tested at Kyoto University and KAIST have similar primary initial stiffnesses, but significantly different secondary stiffnesses. In addition, the LRB tested at KAIST shows a comparatively low primary stiffness and high secondary stiffness in shifting direction from the positive direction to the negative direction. This trend was not observed in the results of the cyclic testing, probably because the axial load on the bearings could not be kept constant during the test, unlike in the case of the preliminary test.

Earthquake response analysis was also performed for the purpose of comparison. In the analysis, the hysteretic characteristics of LRB 1 and LRB 2 were taken as bilinear with the properties obtained from the cyclic tests. But the behavior characteristics for LRB 3 were taken as the initial design values, as in the test. The comparisons between the experimental and analytical results are shown in Figs. 6.30-33. The results for the deck acceleration were in very good agreement with the analytical results. However, the test results for the deck displacement and LRB deformations were larger than those by the analysis. The hystereses indicate that the secondary stiffnesses during the pseudo-dynamic test were similar to the results of the cyclic tests, while the yield load for LRB 1 turned out to be lower than the cyclic test results. This discrepancy may have been caused by the difference between the actual hysteretic behavior of the LRB during the test and the idealized bilinear model in the analysis. It may also have been due to the time-dependent properties of the lead cores in LRBs, which are very difficult to simulate by the slowly proceeding pseudo-dynamic test. Further experimental investigations will be needed to determine the time-dependent characteristics of the lead core, and to develop a more efficient pseudo-dynamic testing method for such material. However, the overall responses of the bridge deck obtained by the parallel

pseudo-dynamic test appear to be reasonable to show the feasibility of the remote parallel testing for the large structural system with MODF, even by connecting the corresponding number of institutions in different countries through the Internet.

6.8 Concluding Remarks

This Chapter focused on the development of a remote parallel hybrid test method and its demonstration in an international collaboration among Kyoto University, Osaka City University, KAIST, SUNY-Buffalo, and Monash University. The conclusions from this study can be summarized as follows.

1) The remote parallel hybrid tests are found to be very effective in viewpoint that many testing laboratories in the world can form a network so that they may utilize advanced experimental facilities, technologies, and expertise of other institutions to promote colaborative researches, help understanding partners, and economize their spaces and human powers.
2) The condition of the computer networks through the Internet among the institutions located far apart in the world was generally stable and sufficiently good to carry out remote parallel testing using the Internet.
3) The data communication time between institutions through the Internet took about 3 sec for each data transmission, while it took about 12 sec for data communication between local computers to control the loading operation. On the other hand, it took about 10 sec for pseudo-dynamic testing itself at each step. Therefore, the on-line interactive testing between institutions through the Internet is very feasible.
4) Further improvements should be made to reduce the communication time, to establish methods for on-line monitoring of the test procedures and results, and to protect the computer systems from probable intruders.
5) The parallel pseudo-dynamic testing system was developed in the collaboration with several universities. Based on detailed analyses, it was verified that the reading and writing of the data and the communications between experimental stations and the main computer were properly executed in the proposed system. The demonstration considering the dynamic interaction between structural elements was conducted within the elastic response. It is concluded that this parallel pseudo-dynamic testing system is a versatile system that can be used to evaluate the response of structures consisting of various structural elements with m.d.o.f., in which the dynamic interaction is significant.
6) The assessment of the accuracy of the experiment was made in cases in which errors were made in stiffness and displacement control. According to these numerical results, the effects of these errors on the overall response were significant. For this reason, it will be important to pay attention to the preliminary test in order to eliminate such errors. Since there were many factors ipotentially affecting the errors in this experiment, in future works it will be necessary to inspect the effect of each of these

factors on the experimental accuracy.

7) The errors of control displacement and measurement in the experimental devices in this study may have negatively affected the results of experiment. Therefore, it is necessary to develop manual for the benchmark testing procedure or the evaluation methodology for the accuracy in the experiment in order that the seismic safely of structures is evaluated by using this system. Furthermore, because the proposed experimental system utilizes the Internet, so it is necessary to improve this system for the obstacles on Internet-system in the future.

References

Committee on Roadway Bridges by the Hyogoken-Nanbu Earthquake, (1995), “Investigations on damages of roadway bridges by the Hyogoken-Nanbu Earthquake”, Draft of Interim Report (in Japanese).

Hakuno, M., Okada, T., Takanashi, K., Toki, K., Ikeda, S., Iemura, H. and Katada, T., (1990), “Application manual of pseudo-dynamic testing” (in Japanese).

Japan Society of Seismic Isolation, (1995), “Introduction to Seismically Isolated Structure”, Ohmusha Ltd. (in Japanese).

Kitada, T., Nakai H., and Nakanishi, K., (1998), “Experimental study on method for increasing ultimate strength and ductility of steel box bridge piers against strong earthquake”, Journal of Structural Mechanics and Earthquake Engineering, JSCE, No.591/I-43, pp. 219-232. (in Japanese).

Ministry of Construction, (1992), "Seismic Isolation Design Manual of Highway Bridge (Plan)", Public Works Research Center, (in Japanese).

Nagata, K., Watanabe, E. and Sugiura, K., (1999), “Seismic behavior and dynamic interaction of elevated bridge system consisting of steel and RC piers”, Journal of Structural Engineering, JSCE, Vol.45A, pp.727-736 (in Japanese).

Nakajima, M., (1985), “Relationship between integration time interval and response stability in pseudo dynamic testing”, Journal of Structural and Construction Engineering, No. 353, pp. 29-36.

Research Group on Ductility of Steel Structures of Kansai branch of Japan Society of Civil Engineers, (1991), “Inspection research on evaluation of ductility of steel structures” (in Japanese).

Research Subcommittee on Dynamic Limit State of Steel Structures of Japan Society of Civil Engineers, (1994), “Elasto-plastic behavior and seismic design of steel structures” (in Japanese).

Saizuka, K., Itoh, Y., Kiso, E. and Usami, T., (1995), “A consideration on procedures of hybrid earthquake response test taking account of the scale factor”, Journal of Structural Mechanics and Earthquake Engineering, JSCE, No.507/I-30, pp. 179-190. (in Japanese).

Sharpe R., and Potter T., (2000), “Special Edition: Using Samba”, Que Book.

Skinner, R. I., Robinson, W.H. and Mc Verry, G. H., (1996), "An Introduction to Seismic Isolation", Kajima Institute Publishing Co. Ltd. (in Japanese).

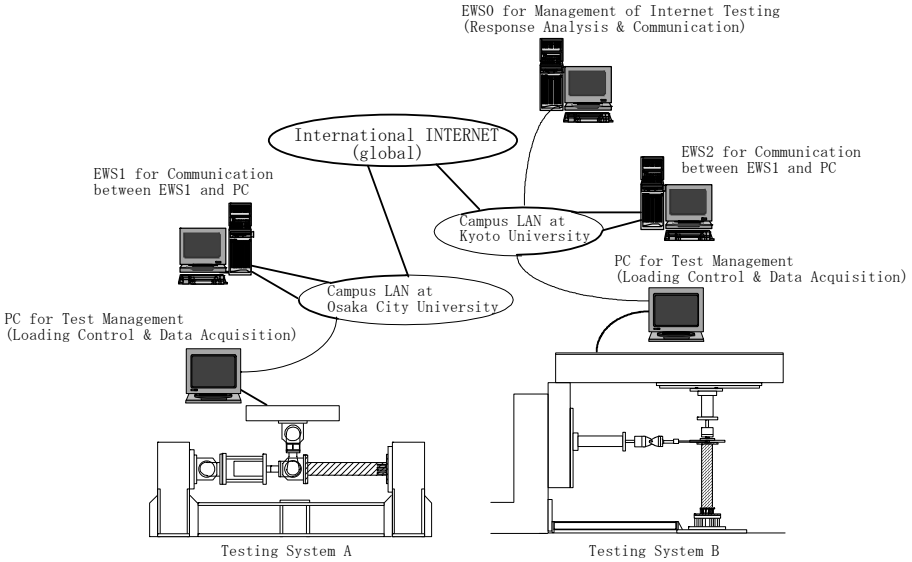

Fig. 6.1 Testing system of Internet testing

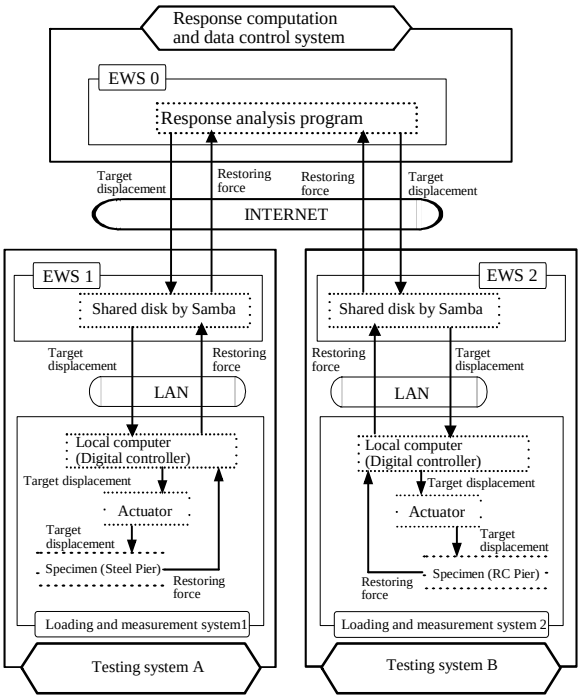

Fig. 6.2 Data flow of the system

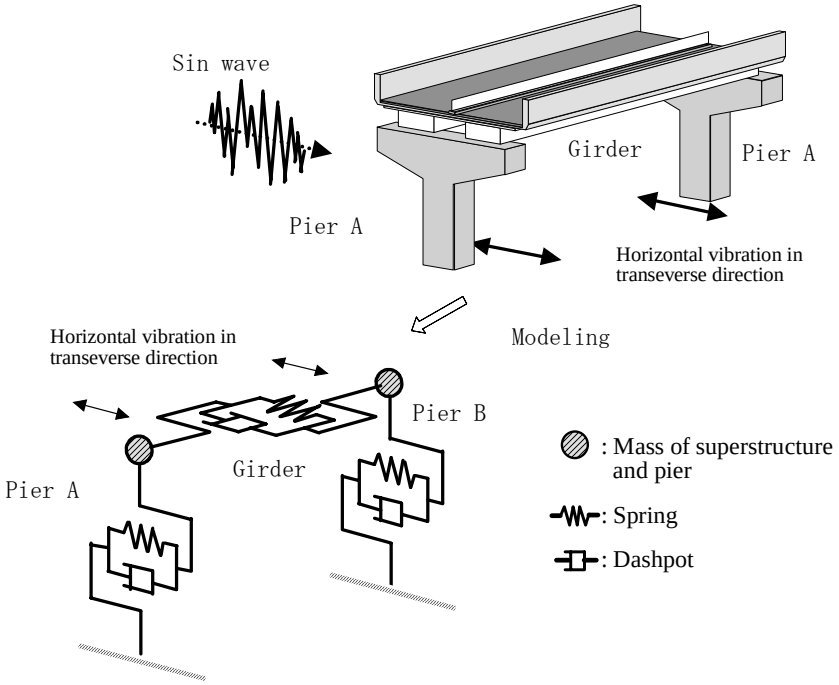

Fig. 6.3 Modeling of elevated bridge

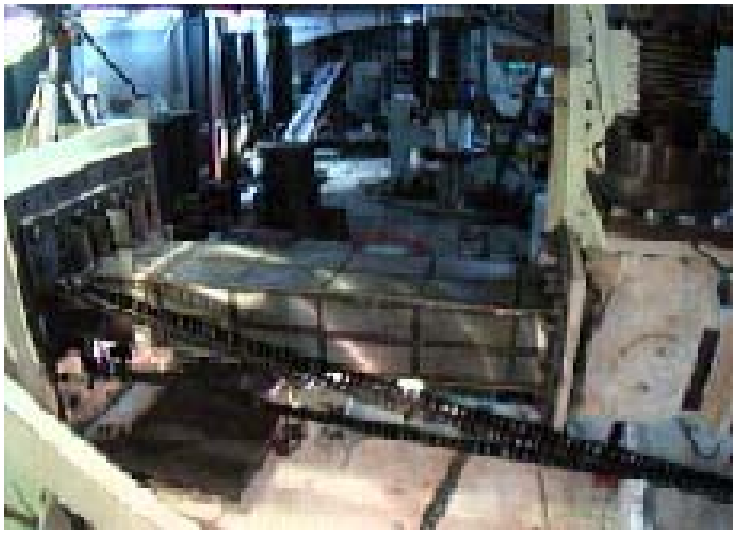

Photo 6.1 Experimental station A

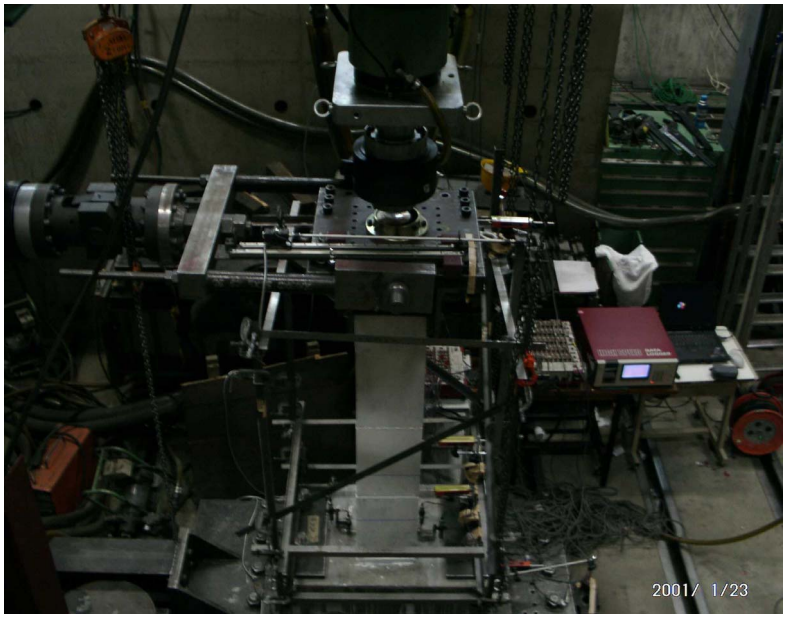

Photo 6.2 Experimental station B

Table 6.1 Structural parameters of structural elements

		Mass (ton)	Stiffness (kN/mm)	Damping factor
Pier-A		592	29.4	0.05
Pier-B		370	49	0.05
Girder	Case1	0	0	0
	Case2	777	4.9	0.03

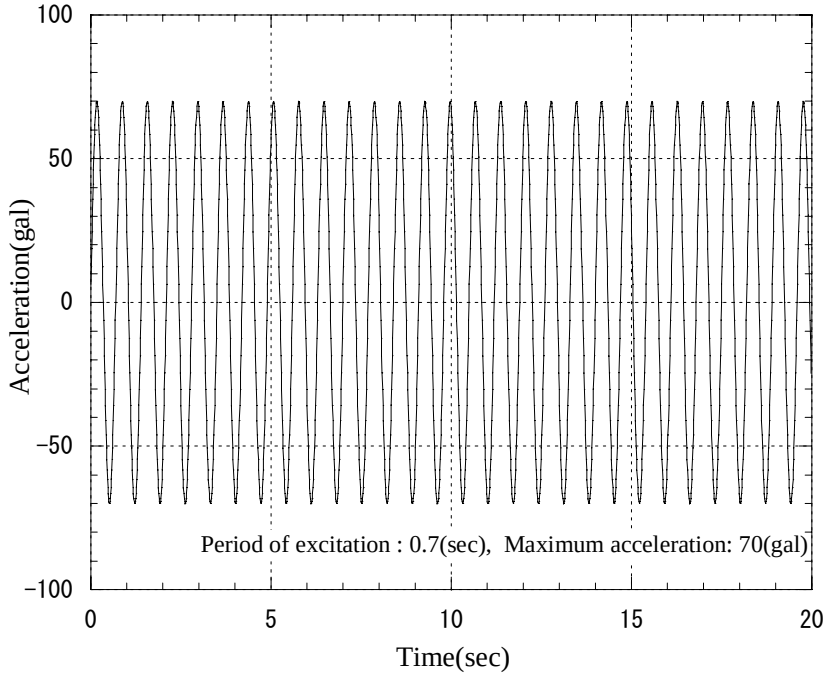

Fig. 6.4 Ground motion

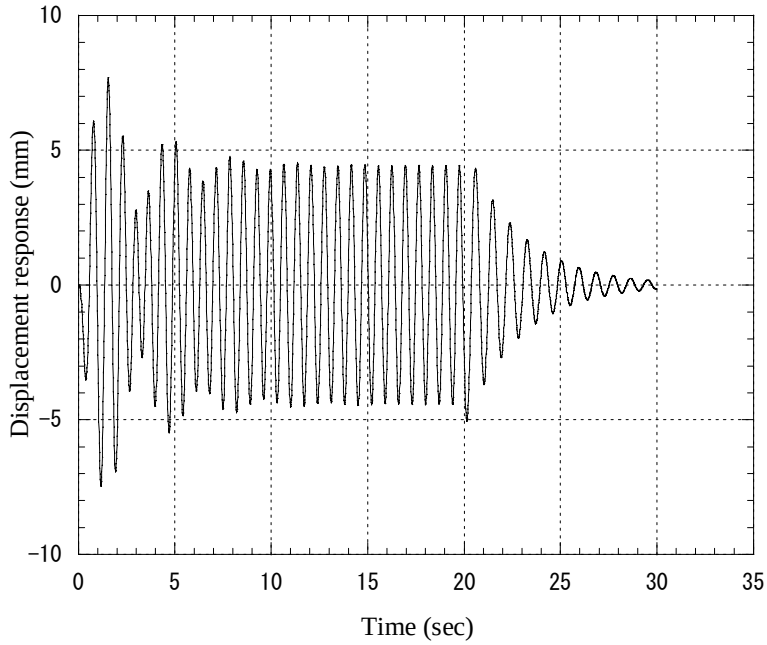

Fig. 6.5 Displacement response of Pier-A

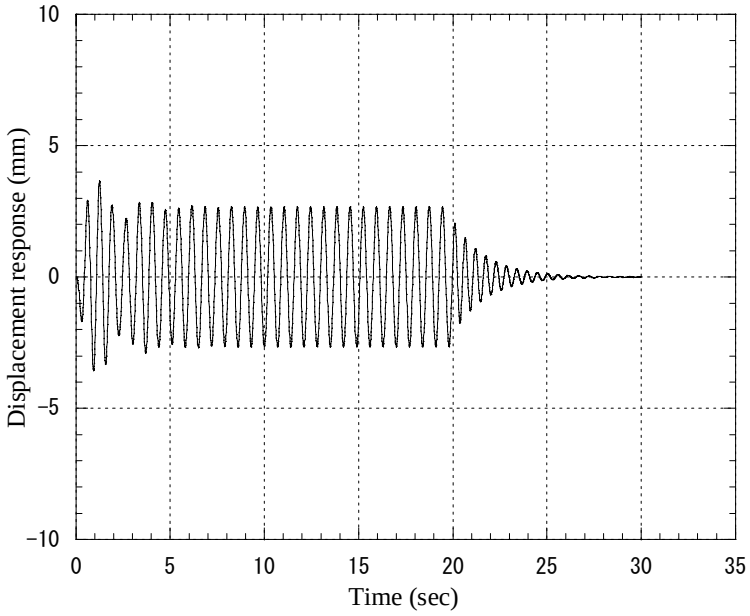

Fig. 6.6 Displacement response of Pier-B

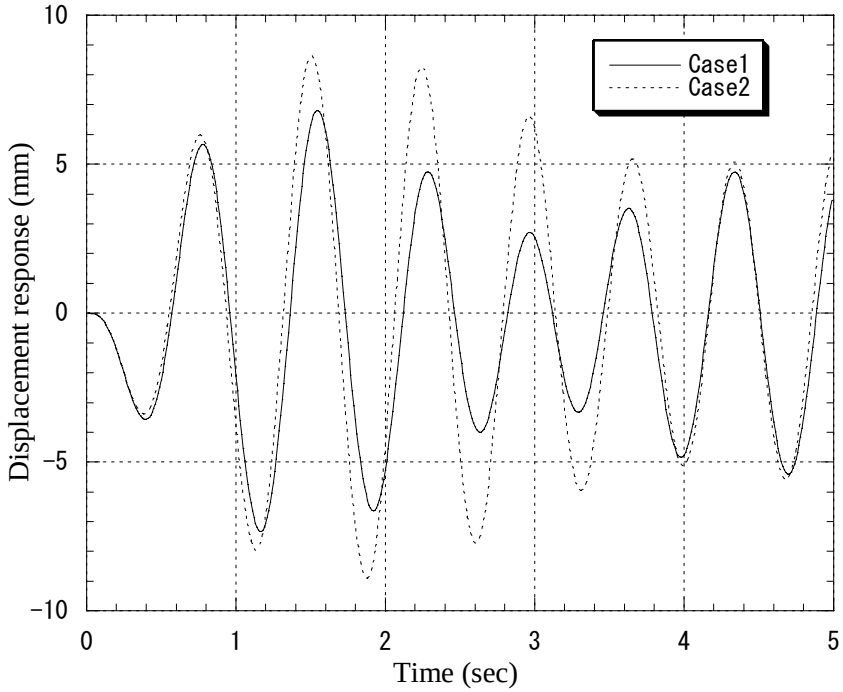

Fig. 6.7 Displacement response of Pier-A

(Test result)

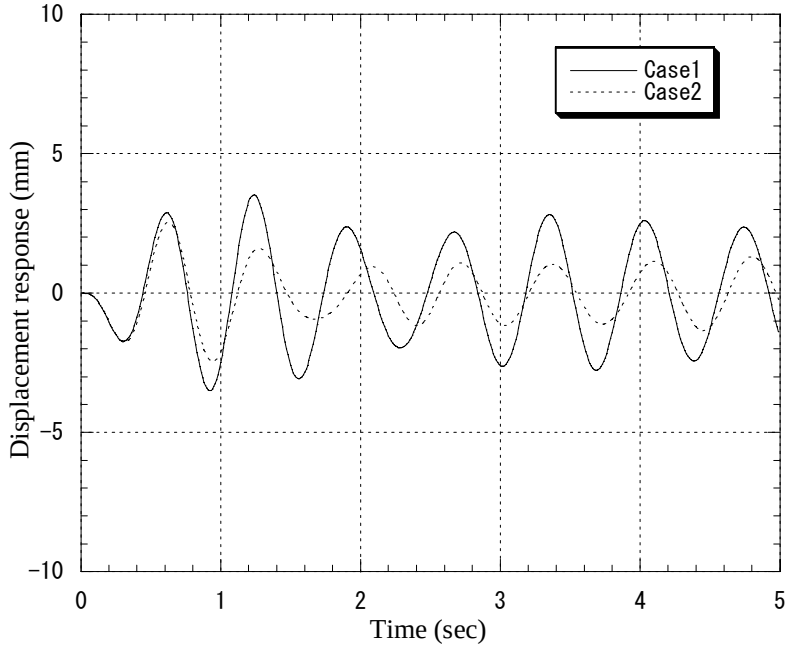

Fig. 6.8 Displacement response of Pier-B

(Test result)

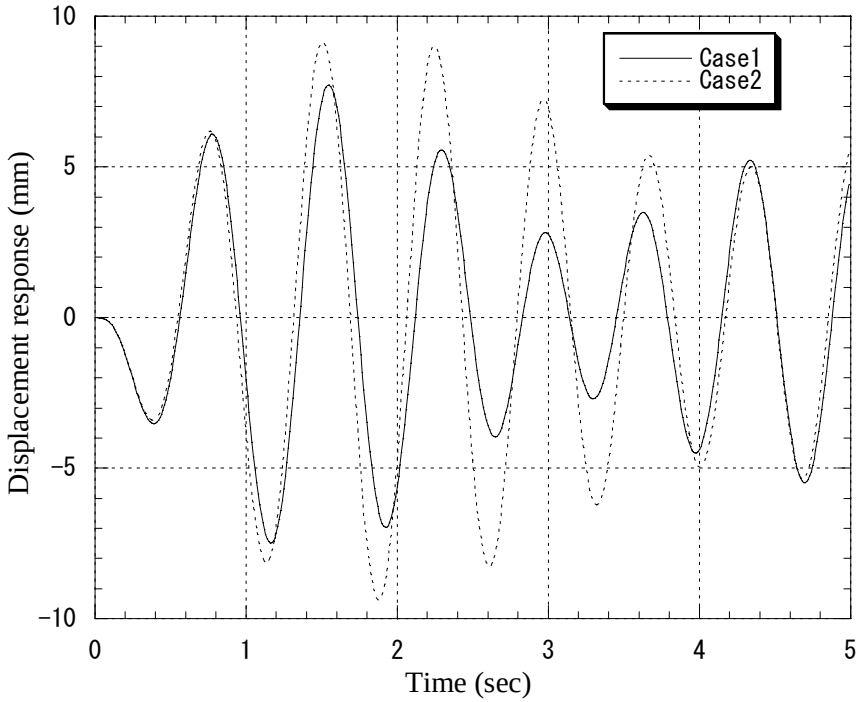

Fig. 6.9 Displacement response of Pier-A

(Analytical result)

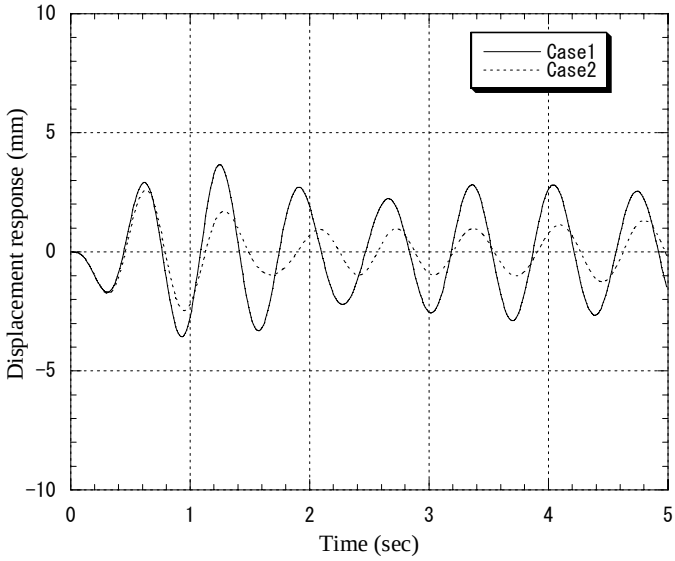

Fig. 6.10 Displacement response of Pier-B

(Analytical result)

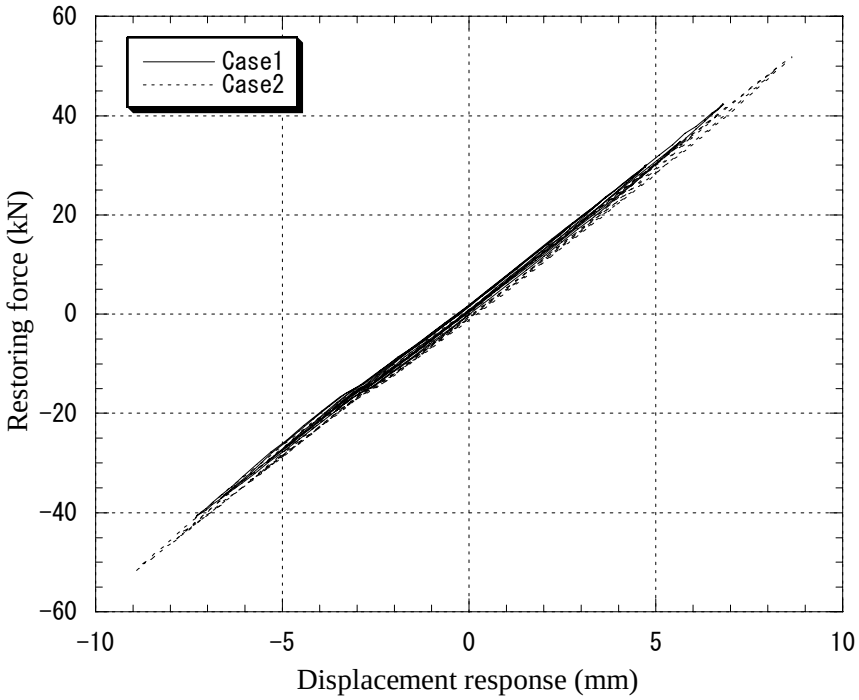

Fig. 6.11 Hysteresis curve of Pier-A

(Test result)

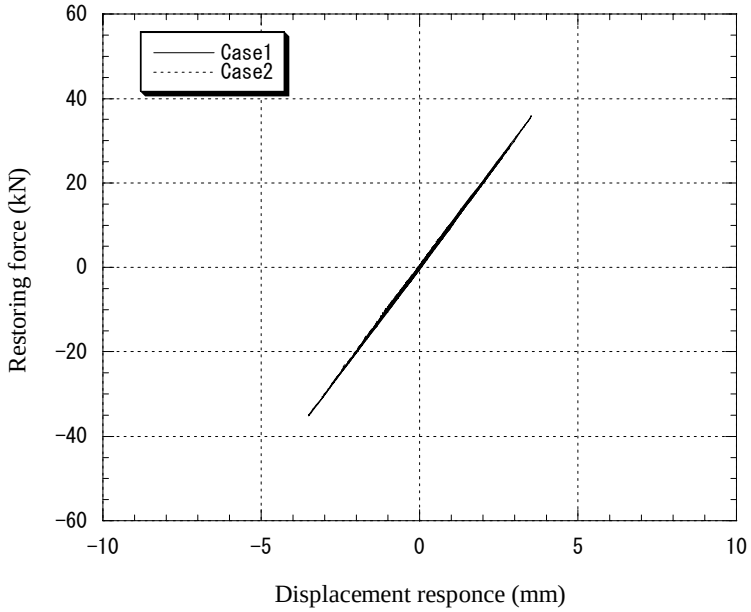

Fig. 6.12 Hysteresis curve of Pier-B

(Test result)

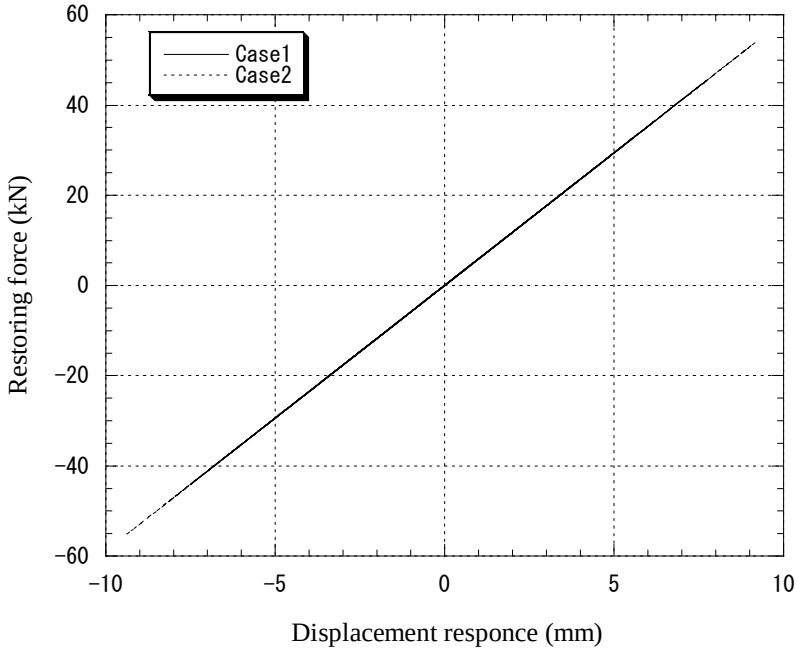

Fig. 6.13 Hysteresis curve of Pier-A

(Analytical result)

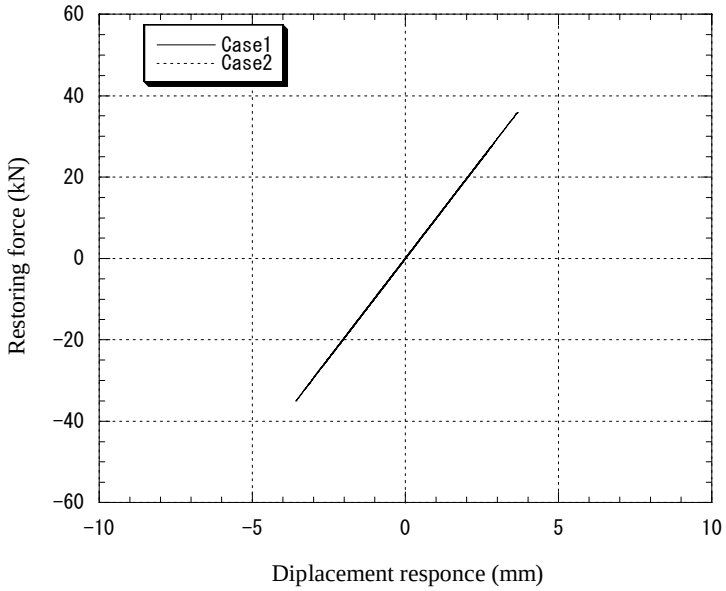

Fig. 6.14 Hysteresis curve of Pier-B
(Analytical result)

Table 6.2 Natural period and response ratio of single pier (Pier-a)

Ratio of stiffness (%)	Natural period (sec)	Response ratio
-10	0.940	0.872
-5	0.915	0.930
-1	0.896	0.986
0	0.892	1.000
+1	0.887	1.018
+5	0.870	1.083
+10	0.850	1.178

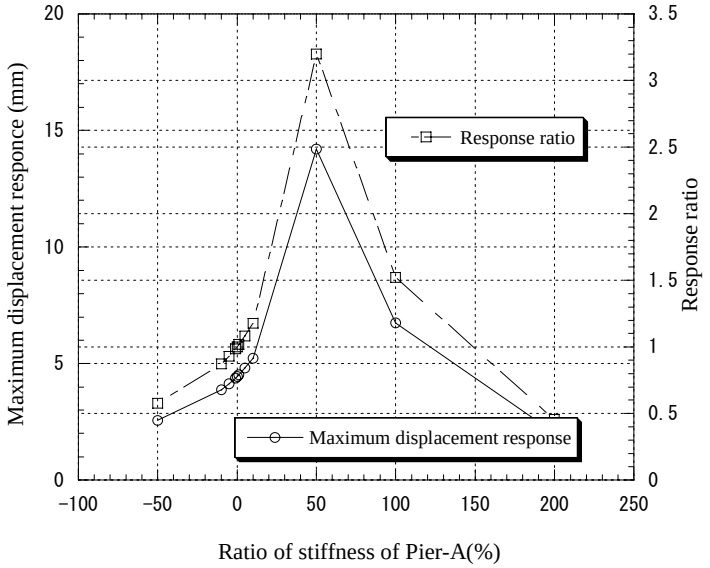

Fig. 6.15 Maximum displacement response for change ratio of stiffness

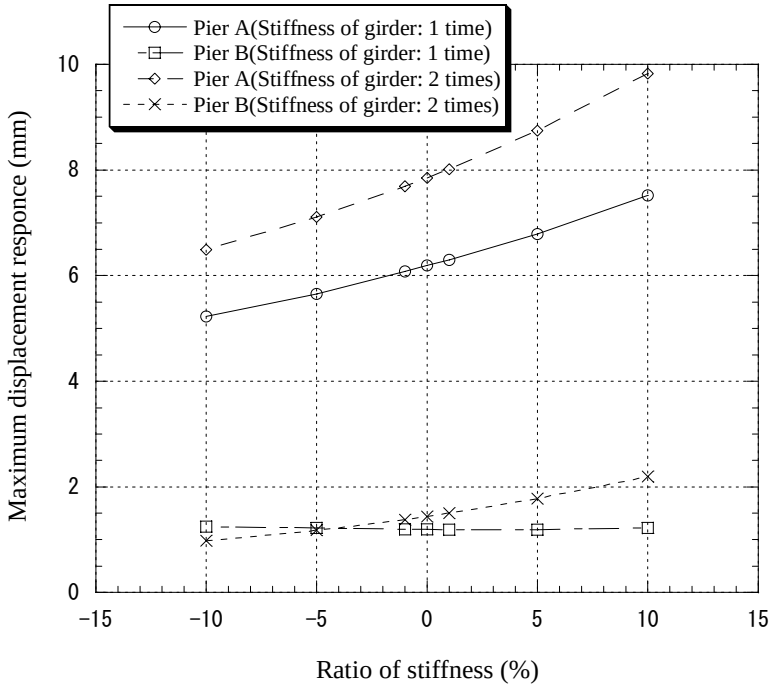

Fig. 6.16 Effect for structural element

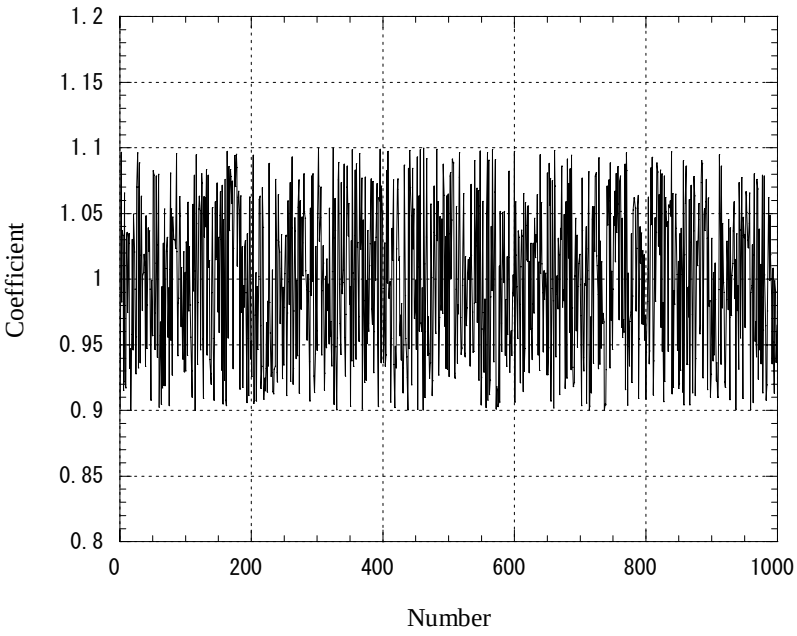

Fig. 6.17 Uniform random number (Unevenness : 10%)

Table 6.3 Statistic value of 1.000 random number

	1st	2nd	3rd
Minimum value	0.0007	0.0012	0.0002
Maximum value	0.9995	0.9998	0.9989
Average value	0.5052	0.4993	0.4851
Dispersion	0.0832	0.0828	0.0838

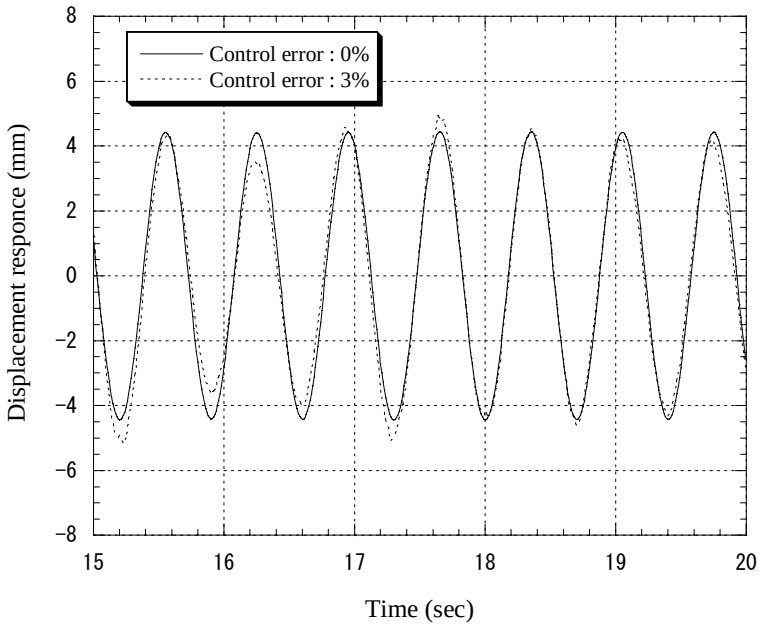

Fig. 6.18 Distortion of response (example)

Table 6.4 Unevenness of maximum displacement response

Displacement control error		1%	3%	5%
Displacement response (mm)	1st	4.63	5.18	5.67
	2nd	4.57	4.98	5.42
	3rd	4.56	4.96	5.45
	Average	4.59	5.04	5.51
	Response error	3.30%	13.5%	24.2%

In the case of uniform：4.44mm

Table 6.5 Elapsed time for 1000 steps between Kyoto University and State University of New York at Buffalo (sec)

Cases	1st trial	2nd trial	3rd trial	Average
Total Elapsed Time	8245.8	8240.8	8243.5	8245.8
Elapsed Time per 1 Step	8.2548	8.2408	8.2435	8.2458

Table 6.6 Elapsed time for 1000 steps between Kyoto University and Monash University (sec)

Cases	1st trial	2nd trial	3rd trial	Average
Total Elapsed Time	8939.9	8635.5	8459.1	8678.2
Elapsed Time per 1 Step	8.9399	8.6355	8.4591	8.6782

Table 6.7 Elapsed time for 1000 steps between Kyoto University and Osaka City University (sec)

	1st trial	2nd trial	3rd trial	Average
Total Computation time	985.0	1031.5	1078.7	1031.7
Computation time per 1 step	9.850	10.315	10.787	10.317

Table 6.8 Traced route from client WS in Kyoto University to server WS in State University of New York at Buffalo

Node No.	Node Name	IP Address	Ping Time (ms)			
0	strxp.kuciv.kyoto-u.ac.jp	130.54.24.201	-	-	-	-
1	y15-c01.gw.kyoto-u.ac.jp	130.54.24.254	2	2	2	2
2	K04-FS02-LIS21.gw.kuins.kyoto-u.ac.jp	130.54.1.62	7	7	7	7
3	130.54.130.185	130.54.130.185	9	5	5	6
4	CR0-1.gw.kuins.kyoto-u.ac.jp	130.54.130.161	3	3	3	3
5	FR0.gw.kuins.kyoto-u.ac.jp	130.54.131.171	3	6	7	5
6	cisco1-kyoto.osaka.itrc.net	192.50.7.1	5	5	5	5
7	tppr-atm0-0-0-13.jp.apan.net	203.181.248.218	23	22	22	22
8	tpr3-ge0-0-0.jp.apan.net	203.181.249.118	22	25	22	23
9	192.203.116.33	192.203.116.33	137	137	137	137
10	Abilene-PWAVE.pnw-gigapop.net	198.32.170.43	137	137	137	137
11	sttlng-sttl.abilene.ucaid.edu	198.32.11.124	137	137	138	137
12	dnvr-sttl.abilene.ucaid.edu	198.32.8.50	165	165	166	165
13	198.32.11.111	198.32.11.111	165	166	167	166
14	kscy-dnvr.abilene.ucaid.edu	198.32.8.14	176	176	179	177
15	kscyng-kscy.abilene.ucaid.edu	198.32.11.117	190	202	193	195
16	iplsng-kscyng.abilene.ucaid.edu	198.32.8.80	188	189	191	189
17	chinng-iplsng.abilene.ucaid.edu	198.32.8.76	188	189	191	189
18	buf-m20-abilene-chin.nysernet.net	199.109.2.1	201	201	202	201
19	sunyab-buf-m20.nysernet.net	199.109.2.25	202	202	201	202
20	l3sw-cc9-82.cc.buffalo.edu	128.205.9.82	341	210	229	260
21	l3sw-bell9-1.cc.buffalo.edu	128.205.9.1	219	233	248	233
22	pollux.eng.buffalo.edu (PC1)	128.205.19.28	201	202	202	202

Table 6.9 Traced route from client WS in Kyoto University to server WS in Monash University

Node No.	Node Name	IP Address	Ping Time(ms)			
			1st	2nd	3rd	Ave.
0	strxp.kuciv.kyoto-u.ac.jp	130.54.24.201	-	-	-	-
1	y15-c01.gw.kyoto-u.ac.jp	130.54.24.254	2	2	2	2
2	K04-FS02-LIS21.gw.kuins.kyoto-u.ac.jp	130.54.1.62	7	6	17	10
3	130.54.130.185	130.54.130.185	7	6	6	6
4	CR0-1.gw.kuins.kyoto-u.ac.jp	130.54.130.161	3	3	3	3
5	FR0.gw.kuins.kyoto-u.ac.jp	130.54.131.171	3	3	3	3
6	cisco1-kyoto.osaka.itrc.net	192.50.7.1	5	5	5	5
7	tppr-atm0-0-0-13.jp.apan.net	203.181.248.218	24	23	23	23
8	tpr3-ge0-0-0.jp.apan.net	203.181.249.118	23	22	23	23
9	192.203.116.33	192.203.116.33	150	143	143	145
10	AARNet-PWAVE.pnw-gigapop.net	198.32.170.45	144	143	148	145
11	pos2-0.sccn1.manoa.aarnet.net.au	192.231.212.161	299	299	299	299
12	pos2-0.sccn1.broadway.aarnet.net.au	192.231.212.41	289	289	290	289
13	nswrno2-gbe10-0-0-916.nswrno.net.au	192.231.212.18	304	290	291	295
14	nsw-vic.atm.net.aarnet.edu.au	192.12.76.2	310	307	308	308
15	monash-gw1.vrn.edu.au	203.21.130.40	318	318	317	317
16	clay2-gw-28.net.monash.edu.au	130.194.28.13	319	318	318	318
17	civ-sugiura.eng.monash.edu.au (PC1)	130.194.129.139	319	318	319	319

Table 6.10 Traced route from client WS in Kyoto University to server WS in Osaka City University

Node No.	Node Name	IP Address	Ping time (ms)			
			1st	2nd	3rd	Ave.
0	strxp.kuciv.kyoto-u.ac.jp	130.54.24.201	-	-	-	-
1	y15-c01.gw.kyoto-u.ac.jp	130.54.24.254	3	3	2	3
2	K04-FS02-LIS21.gw.kuins.kyoto-u.ac.jp	130.54.1.62	8	8	7	8
3	130.54.130.185	130.54.130.185	5	5	*	5
4	130.54.130.161	130.54.130.161	2	3	3	3
5	FR0.gw.kuins.kyoto-u.ac.jp	130.54.131.171	3	3	3	3
6	kyoto-S1-G1-0.sinet.ad.jp	150.99.197.201	3	3	4	3
7	JT-osaka-S1-P4-0.sinet.ad.jp	150.99.197.65	4	4	4	4
8	osaka-S1-P5-0.sinet.ad.jp	150.99.197.74	5	5	4	5
9	osaka-1-F0-1-0.sinet.ad.jp	150.99.7.3	5	5	4	5
10	osaka-cu.gw.sinet.ad.jp	150.99.207.53	5	5	5	5
11	atmgw.gw.osaka-cu.ac.jp	160.193.8.253	7	7	6	7
12	160.193.2.220	160.193.2.220	7	7	7	7
13	160.193.178.252	160.193.178.252	11	7	7	8
14	160.193.159.89 (Dynabook)	160.193.159.89	11	7	8	9

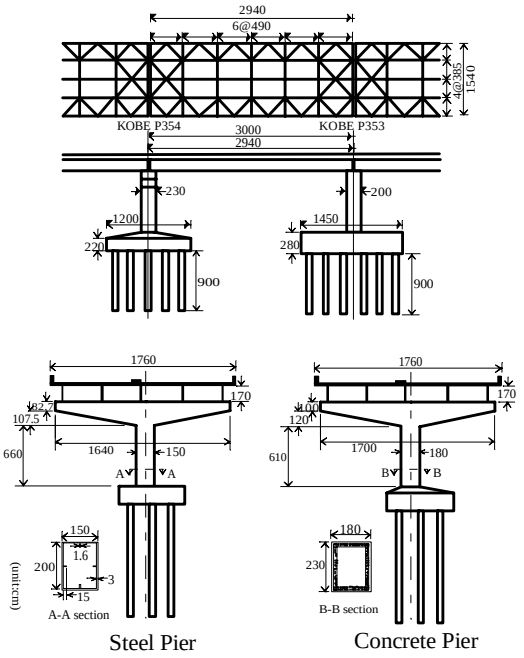

Figure 6.19 Proto-type of elevated bridge
(Third Kobe line of Hanshin Expressway)

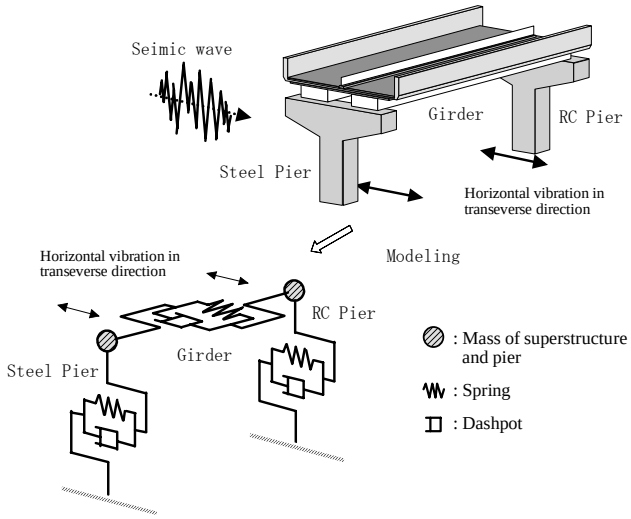

Fig. 6.20 Modeling of elevated bridge

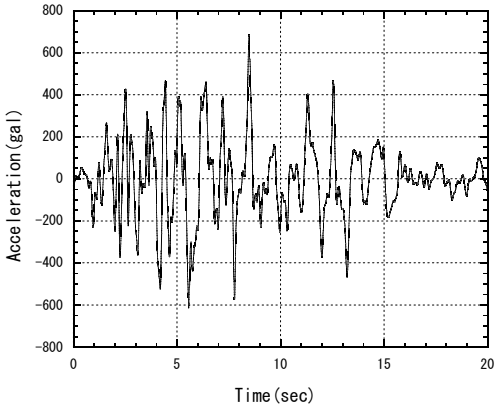

Fig. 6.21 Ground motion

Table 6.11 Parameters of structural elements

Structural element	Mass (ton)	Damping factor	Stiffness (kN/cm)
Steel Pier	492	0.02	521
RC Pier	558	0.05	377
Girder	482	0.03	2176

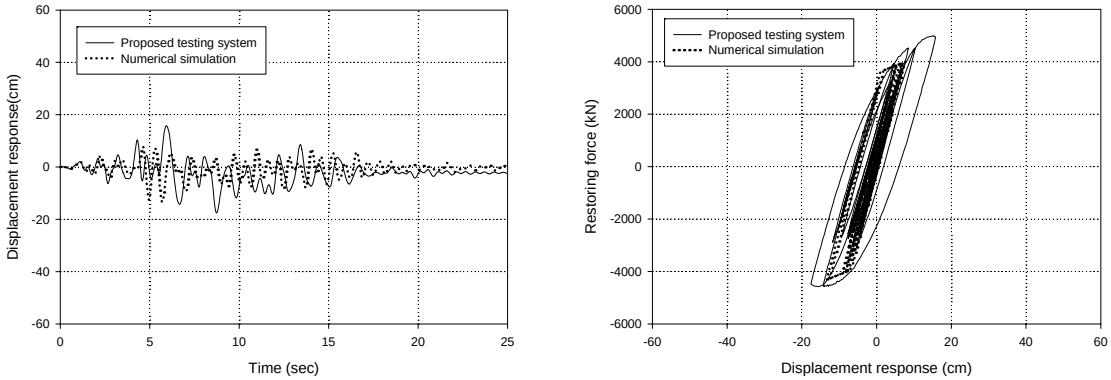

(a) Time history of displacement response (b) Restoring force vs. displacement response

Fig. 6.22 Testing results (Steel Pier)

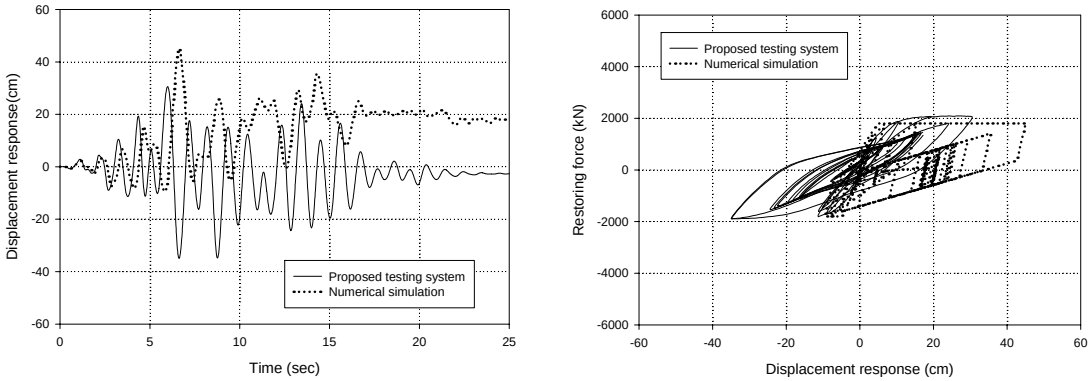

(a) Time history of displacement response (b) Restoring force vs. displacement response

Fig. 6.23 Testing results (RC Pier)

(a) Steel pier with local buckling

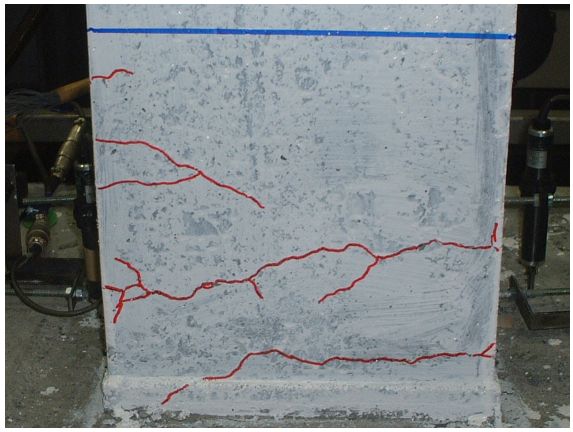

(b) RC pier with cracks

Photo 6.3 Damaged piers after the experiment

(a) Pier P353 with local buckling

(b) Pier P354with cracks

Photo 6.4 Damaged actual bridge piers after Hyogo-ken Nambu Earthquake

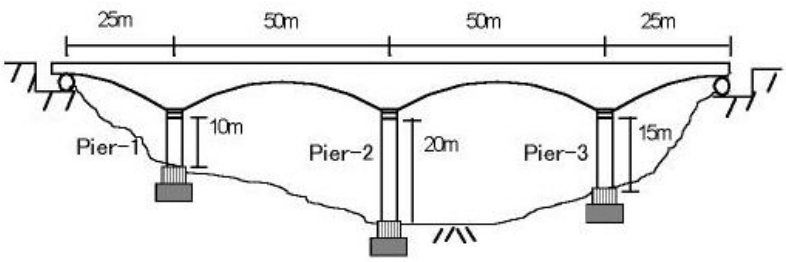

Fig. 6.24 Base-isolated bridge model

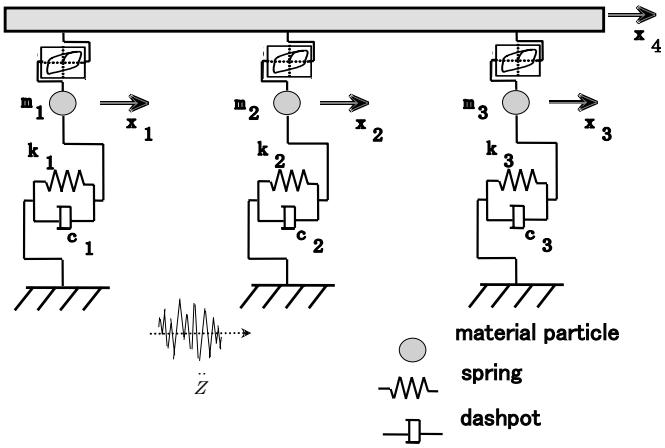

Fig. 6.25 Structural model for base-isolated bridge by mass-spring-dashpot

Table 6.12 Structural parameters of structural elements

Structural element	Weight（kN）	Stiffness（kN/cm）	Damping factor
Pier- 1	645.8	3439.8	0.05
Pier- 2	1274.0	860.0	0.05
Pier- 3	980.0	1379.8	0.05
Deck & Girder	35280.0	（Rigid body）	（Rigid body）

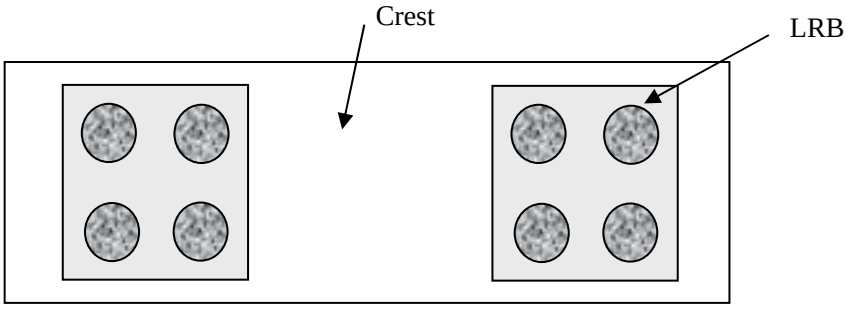

Fig. 6.26 LRB arrangement on each pier

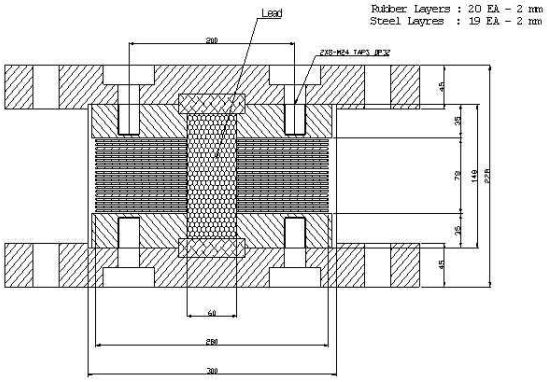

(a) Dimensions (unit: mm)

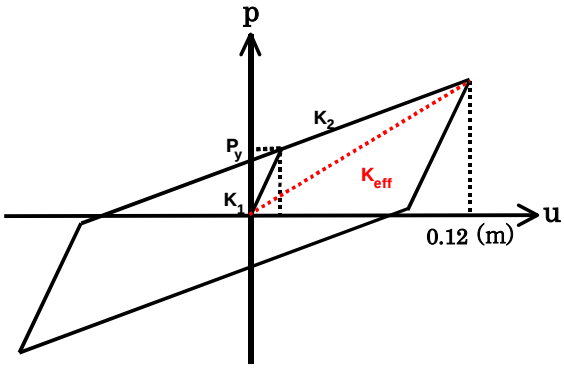

$K_{eff} = 7.38kN/cm$; $K_1 = 23.13kN/cm$

$K_2 = 5.80kN/cm$; $P_y = 23kN$

(b) Bilinear properties of initial design of LRB

Fig. 6.27 Lead rubber bearing specimen: 1/2 model

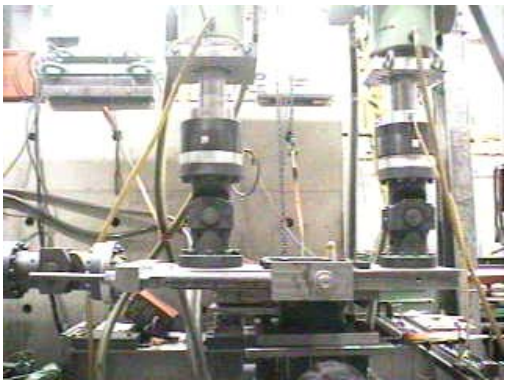

(a) Facility at Kyoto University

(b) Facility at KAIST

Photo 6.5 Testing setup

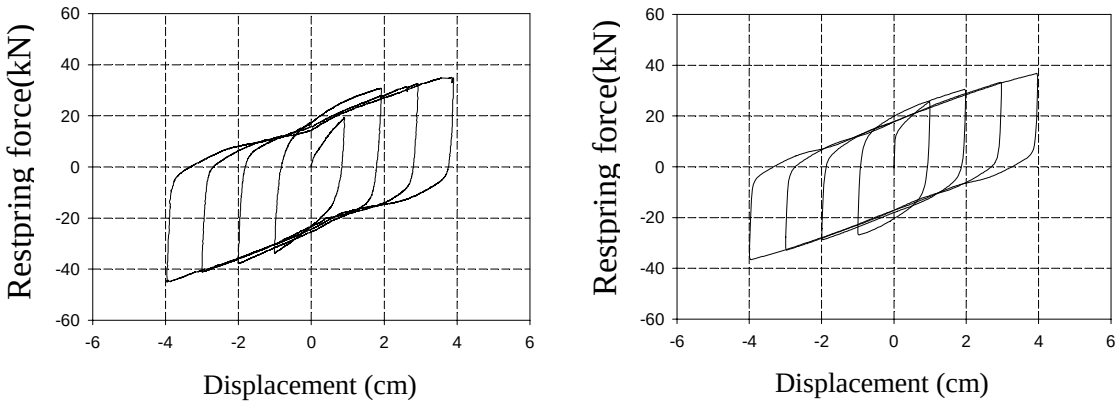

(a) LRB 1 at KAIST (b) LRB 2 at Kyoto University

Fig. 6.28 Hystereses obtained by cyclic loading tests on LRB specimens

Table 6.13 Bilinear properties of cyclic loadings

Cases	LRB 1	LRB 2	Initial Design Values
Primary Stiffness（kN/cm）	226.6	247.3	23.13
Secondary Stiffness（kN/cm）	6.5	5.8	5.8
Yield load（kN）	21.4	18.2	23.13

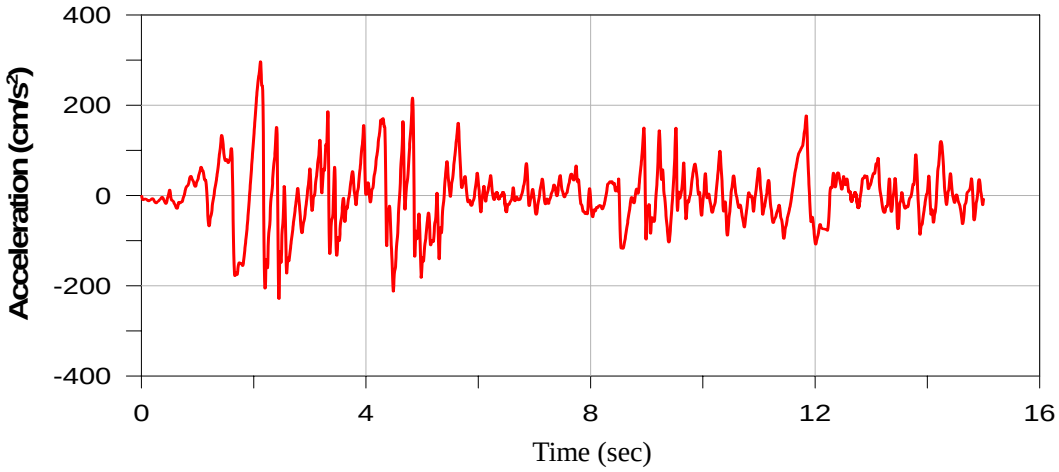

Fig. 6.29 Acceleration of El Centro Earthquake

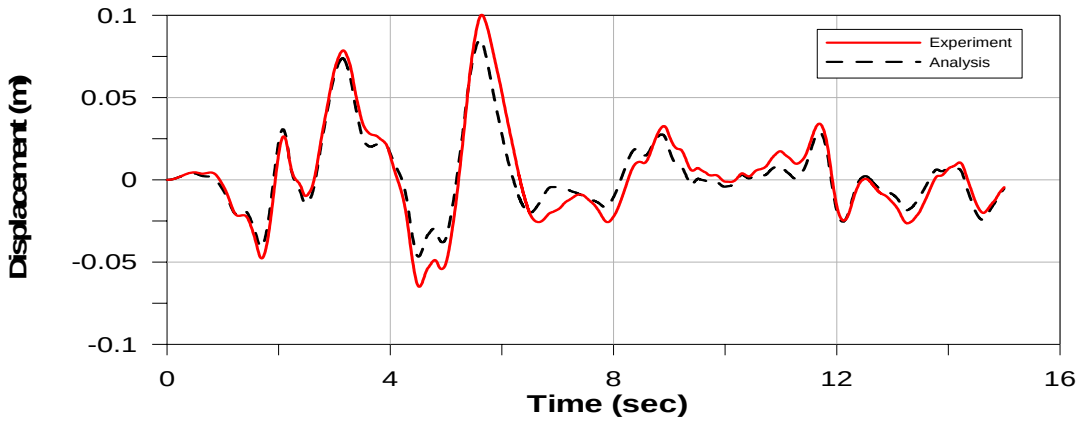

(a) Relative displacement response

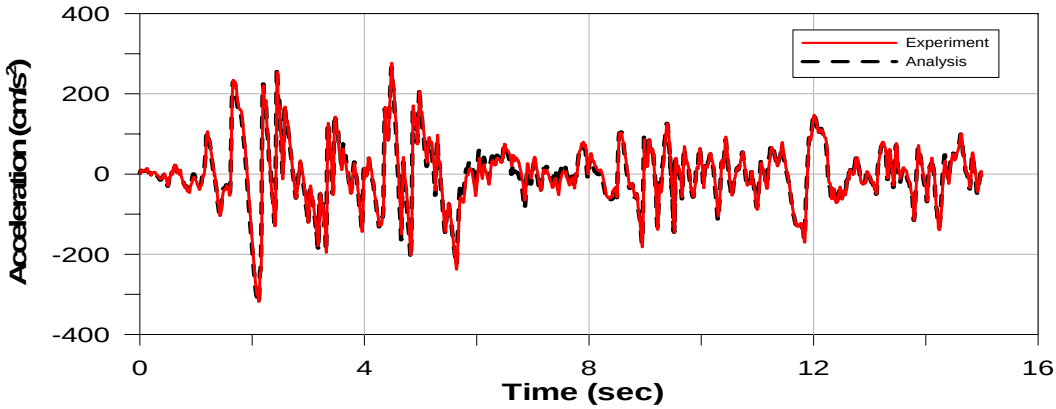

(b) Relative acceleration response

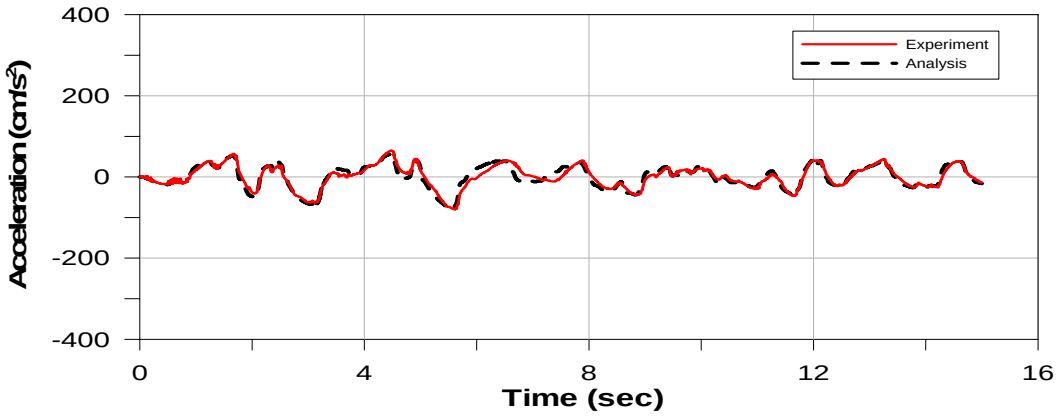

(c) Absolute acceleration response

Fig. 6.30 Horizontal displacement and acceleration of superstructure (Prototype)

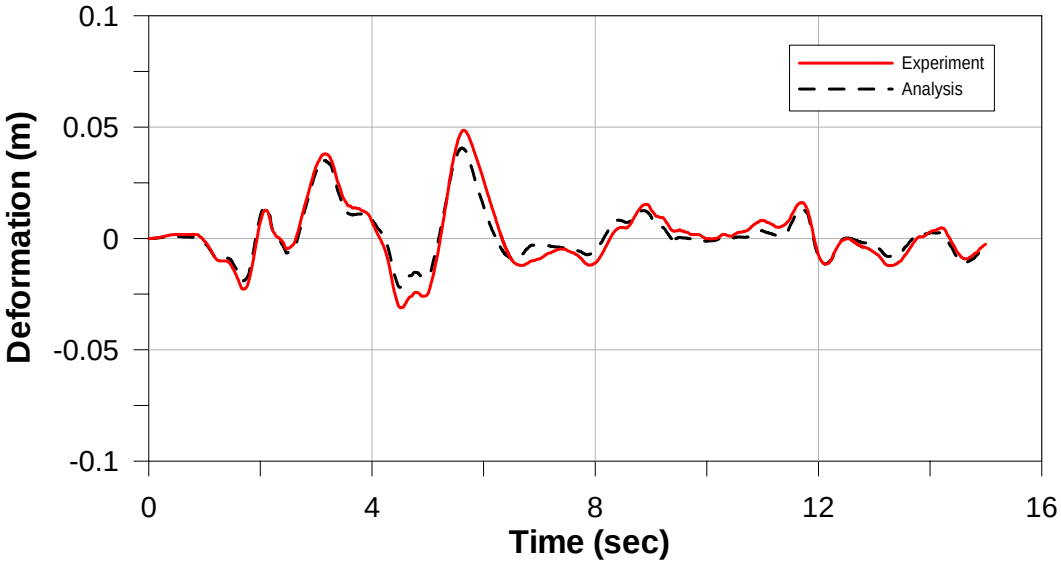

(a) Displacement response at LRB specimen 1

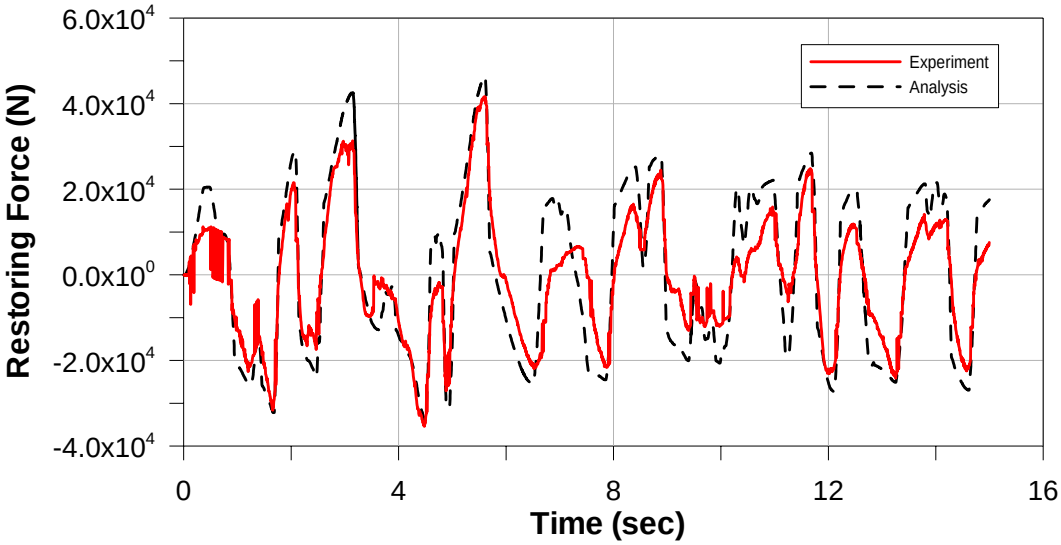

(b) Restoring force at LRB specimen 1

Fig. 6.31 Displacement response and restoring force of bearing specimen: LRB 1

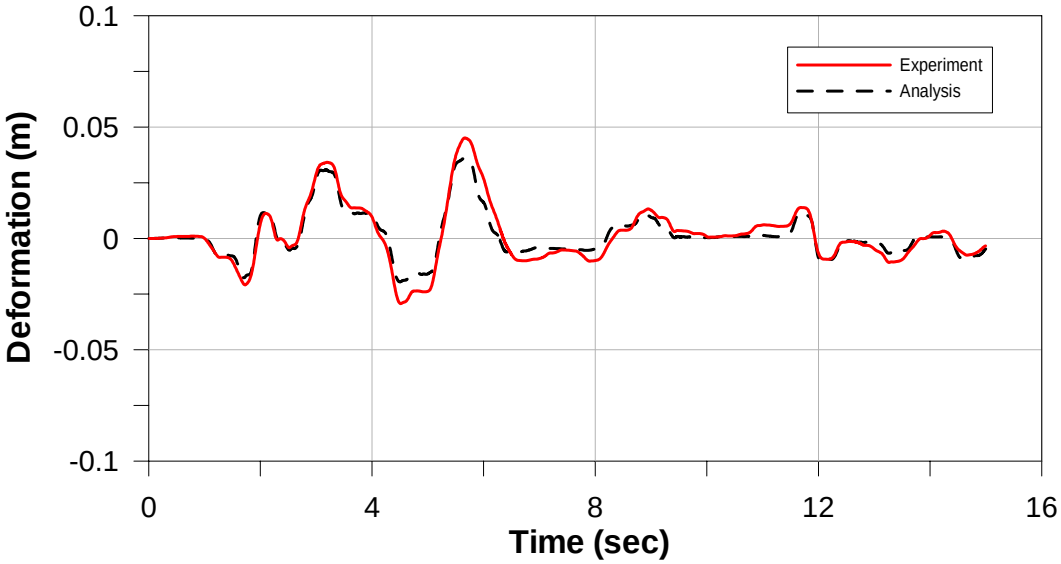

(a) Displacement response at LRB specimen 2

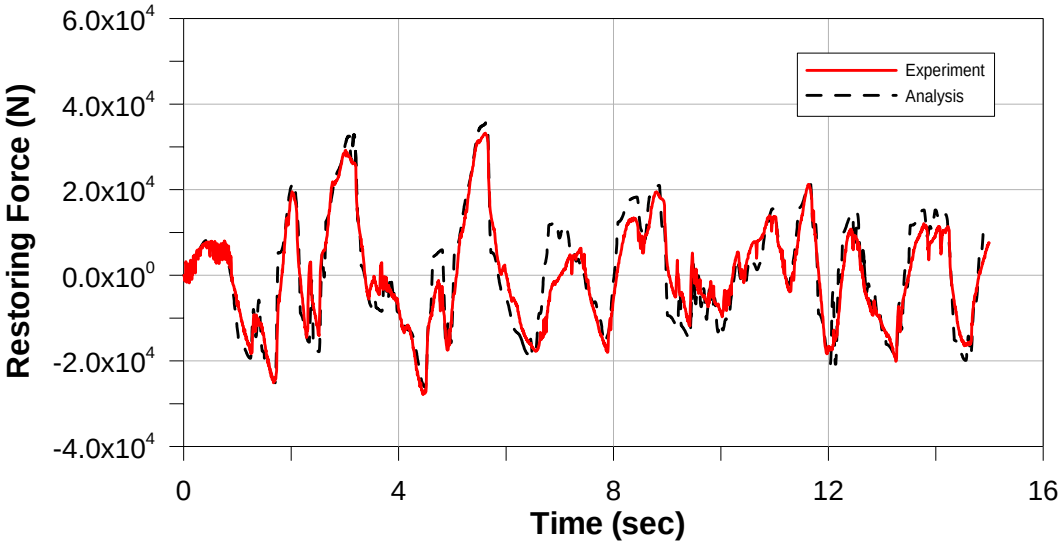

(b) Restoring force at LRB specimen 2

Fig. 6.32 Displacement response and restoring force of bearing specimen: LRB 2

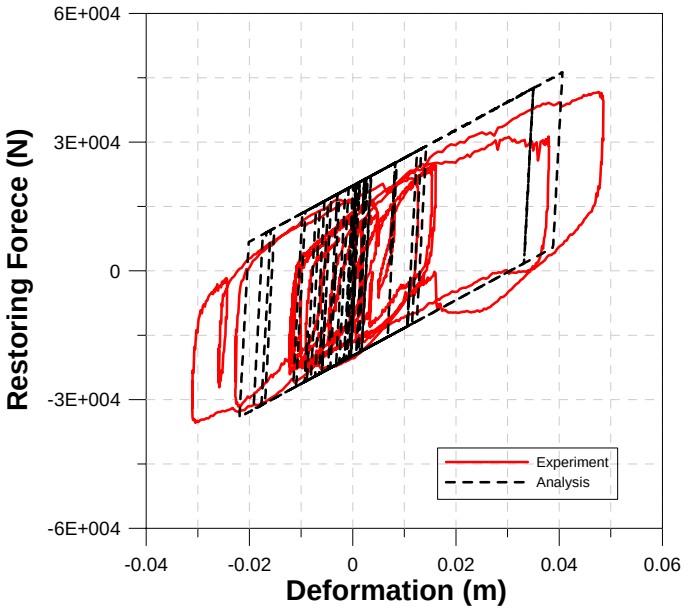

(a) LRB 1 at KAIST (K_{eff} = 9.9kN/cm)

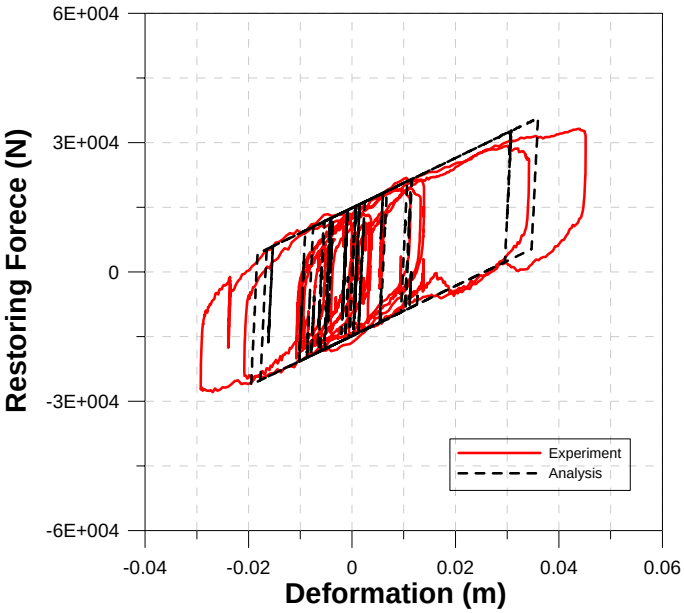

(b) LRB 2 at Kyoto Univ. (K_{eff} = 8.7kN/cm)

Fig. 6.33 Hysteretic restoring forces vs. deformation curves of bearing specimens

Chapter 7

Summary and Conclusions

This study deals with the dynamic interaction problems that arise in the design of elevated bridges subjected to strong ground motions. Although the dynamic interaction of structures is not a new research topic, it should be understood that a seismic design methodology that considers dynamic interactions has not been quantitatively developed. In order to quantify the dynamic interaction, elasto-plastic response analyses, elasto-plastic finite displacement analyses, static loading tests and pseudo-dynamic tests were carried out in this study. In addition, a new testing method was also proposed for evaluation of the seismic response of multi-degree-of freedom system.

The following dynamic interactions were investigated.

(1) The response of an elevated bridge system consisting of different types of piers, such as steel and PC piers.

(2) The response of an elevated bridge considering the degree of freedom of foundation and its pacification.

(3) The response of rigid-frame steel piers where the interaction of beam member and column member.

(4) The strength and ductility interaction of steel bridge piers under multi-axial earthquake loads, particularly the response against strong ground motions in horizontal two directions.

The primary results of this study can be summarized as follows.

In Chapter 2, the seismic response characteristics of a continuous elevated bridge system were assessed; in particular, special emphasis was placed on the dynamic interaction of the elevated bridge consisting of different types of piers, such as steel piers and RC piers. The characteristic vibration mode of the continuous elevated bridge made of different types of piers is found to be completely different from that of the continuous elevated bridge made of the same type of piers. Therefore, if elevated bridges consist of piers having restoring forces with different characteristics, it is necessary to make the seismic design by considering the whole elevated bridge as a vibration unit. In general, the response characteristics of steel piers differ from those of RC piers in terms of the restoring force characteristics, natural period and allowable displacement response. Therefore, the effect of the dynamic interaction becomes significant somewhere adjacent each other of the steel piers and the RC piers. The vibration mode varies with the number of continuous spans of the elevated bridge, that is, the number of piers and the stiffness of the girders. It is thought necessary to assure the safety of the elevated bridge as a system for the seismic design. In addition, attention is found to be paid not only to the stiffness of the girders but also to the arrangement of the bearings.

In Chapter 3, the influence of the dynamic interaction of the foundation-structure system is investigated. A simple system of three degrees-of-freedom considering foundation and superstructure is considered for the response analysis, and the numerical assessment is made by varying the type of soil, the level of seismic force, the yield restoring force, and the tangent stiffness in the plastic range for each degree of freedom. By employing a three degrees-of-freedom system that takes into account the sway and rocking motion of the foundation instead of the general one mass system for response analysis of the bridge pier, the influence of the dynamic interaction between the motion of the superstructure and the foundation can be clarified from the viewpoint of the vibration energy and ductility factor. It is found that the interaction between the horizontal motion of the superstructure and the rocking motion of the foundation is the most significant. Comparing the case of no degree of freedom with the foundation to the case of two degree of freedom in the foundation, the difference in response is more significant in the model using type III soil than in the model with type I soil. Therefore, in the case that the foundation is constructed on soft ground, the response analysis with one degree of freedom might be insufficient, and the motion of the foundation should be modeled. By assessing the energy balance of the vibration and hysteresis in the elasto-plastic response of the foundation-structure system, the response characteristics of three degree-of-freedom can be evaluated by the scalar quantity by energy. In addition, the effect of the dynamic interaction is also clarified considering the proportion of vibration energy in each degree of freedom. Therefore, to use the scalar quantity of vibration energy as the index for evaluating of the response of multi-degree-of-freedom system is very effective. The analysis considering the yielding strength ratio and tangent stiffness in the plastic range is carried out in conjunction with the index of ductility factor. It is concluded that the yield strength ratio and tangent stiffness are very important factors for the elasto-plastic response behavior of the foundation-structure system. It is also proven that the ductility factor is affected by the wave form of input acceleration. Therefore, to set the allowable displacement response considering the restoring force is rational for the seismic design. Furthermore, it is confirmed that the plastic deformation is concentrated in structural element with relatively lower strength. It is found possible, however, that the plastic deformation of the foundation is effectively reduced by decreasing the yield strength ratio of the superstructure when the foundation-structure system is subjected to very large seismic force that makes the foundation deform plastically.

In Chapter 4, the collapse processes and seismic performance of steel rigid-frame piers subjected to in-plane loading are discussed. The steel rigid-frame pier investigated in this study has the a maximum horizontal load-carrying capacity of 2.3 times the yield horizontal load, and it has a superior load-carrying capacity and ductility ratio compared to those of a single-column pier. It is found that the steel rigid-frame pier can keep the stiffness as high as initial elastic one until two plastic hinges were formed, and that the ultimate state may be obtained when four plastic hinges were formed. The steel rigid-frame pier investigated in this study can resist up to a maximum displacement of $3.3\delta_y$, and no significant damage was

observed even when the pier was subjected to a ground acceleration as large as that recorded in the Hygoken-Nanbu Earthquake, indicating the good seismic performance. It is necessary to develop a well-balanced earthquake-resistant design for a steel rigid-frame pier by investigating the correlations among various parameters, including the strength ratio between the beam and column, the ratio of the yield load to the maximum load, and the ductility ratio, because in the steel rigid-frame pier, one plastic hinge will not cause a collapse of the entire structural system.

Chapter 5 summarizes the static loading test and the pseudo-dynamic test for the inelastic response of the T-shaped single-column steel bridge piers subjected to earthquake loads with variable loading direction. The elasto-plastic finite displacement analysis as well as the response analysis by the simple mass-spring-dashpot model are also discussed. Secondly, as for the rigid frame-type steel bridge piers, detailed structural models are made for the elasto-plastic finite displacement analysis by ABAQUS, paying attention to the effect of the loading direction on the strength and ductility. The significant strength degradation due to bidirectional and nonproportional load is identified, and compared to the stable hysteretic response under unidirectional loading. The dynamic response of the bridge pier subjected to bidirectional ground motions was also found to be larger than that in the case of unidirectional acceleration input; in particular, the increase of the response with respect to the weak axis was more significant. A simple mass-spring-dashpot model for evaluating the response of structures subjected to bidirectional ground motions was proposed, wherein the elasto-plastic stiffness was defined based on the strength interaction curve in conjunction with the basic principles of the theory of plasticity. The proposed simple model was verified to be sufficient to accurately predict accurately the bidirectional response of structures. The variation in strength and ductility dependent on the loading direction was found to be more remarkable in the case of the rectangular cross; in addition, the structural indeterminacy makes this variation even larger. Therefore, the frame-type bridge piers should be carefully designed by considering these differences of strength and ductility for the proper load combinations. The current research only picked up the particular steel bridge. By considering the plate slenderness, column slenderness, and ratio of vertical load, the seismic design specifications should be provided.

In Chapter 6, a parallel pseudo-dynamic testing system was proposed and its feasibility was investigated by a collaboration among several universities. It is validated that the remote parallel hybrid tests are found to be very effective in view of the fact that many testing laboratories in the world can form a network so that they may utilize advanced experimental facilities, technologies, and expertise of other institutions to promote cooperative researches, help understanding partners, and economize their spaces and human powers. The condition of the computer networks through the Internet among the institutions located far apart in the world was generally stable and sufficiently good to carry out remote parallel testing using the Internet. This proposed testing technique using the Internet is strongly recommended for the effective utilization of experimental facilities all over the world.

Finally, the current study has confirmed the effect of the dynamic interaction of elevated bridges and developed an evaluation method by parallel pseudo-dynamic testing through the Internet. However, in order to establish a rational seismic design that incorporates the dynamic interaction, it will be necessary to conduct further tests using full-scale bridge systems, and to compare the results with those derived from smaller models. The construction of E-Defense system, which can scale large structures of up to 12,000 tons, will be completed by the end of 2004. I wish that near future, the dream to save lives and structures against destructive earthquake comes true.

Author's Research Activities

Journal papers with reviewing

Nagata, K., Watanabe, E. and Sugiura, K., (1996), "Non-linear dynamic interaction of foundation-structure system, Journal of Structural Engineering", JSCE, Vol. 42A, pp. 593-602 (in Japanese).

Watanabe, E., Sugiura, K., Nagata, K. and Kitane, Y., (1998), "Performances and damages to steel structures during the 1995 Hyogoken-Nanbu Earthquake", Engineering Structures, ELSEVIER, Vol. 20, pp. 282-290.

Nagata, K., Watanabe, E. and Sugiura, K., (1999), "Seismic behavior and dynamic interaction of elevated bridge system consisting of steel and RC piers", Journal of Structural Engineering, JSCE, Vol.45A, pp.727-736 (in Japanese).

Kishimoto, Y., Suzuka, Y., Watanabe, E., Kitada, T., Yamaguchi, T., Nagata, K. and Sugiura, K., (2000) "Development of parallel pseudo-dynamic testing system using Internet", Journal of Civil Engineering Information Processing Symposium, JSCE, Vol. 9, pp. 111-120 (in Japanese).

Nagata, K., Watanabe, E., Kitada, T., Sugiura, K. and Yamaguchi, T., (2002), "Assessment on error propagation in response evaluation by parallel pseudo-dynamic testing system", Journal of Structural Engineering, JSCE, Vol. 48A, pp. 35-42 (in Japanese).

Nagata, K., Watanabe, E., Sugiura, K., Adachi, Y. and Okashiro, S., (2003), "Collapse processes of steel rigid-frame piers subjected to in-plane horizontal loads", Journal of Structural Engineering, JSCE, Vol. 49A, pp. 427-434 (in Japanese).

Yamaguchi, T., Nagata, K. and Kishimoto, Y., (2003), "Simulation up to collapse of a simply supported elevation bridge supported by two piers made of different materials using network technology", Journal of Structural Engineering, JSCE, Vol. 49A, pp. 47-56 (in Japanese).

Nagata, K., Watanabe, E. and Sugiura, K., (2004), "Elasto-plastic response of box steel piers subjected to strong ground motions in horizontal 2 directions", Journal of Structural Engineering, JSCE, Vol. 50A, pp. 1427-1436 (in Japanese).

Conference, Symposium, Colloquium and Seminar papers

Nagata, K., Watanabe, E., Sugiura, K. and Utsunomiya, T., (1995), "Non-linear dynamic interaction of foundation-structure system", Proceedings of the 23rd JSCE Earthquake Engineering Symposium, pp. 1021-1024 (in Japanese).

Nagata, K., Sugiura, K. and Watanabe, E., (1996), "Parallel computing for non-linear dynamic interaction of foundation-structure system", XIXth International Congress of Theoretical and Applied

Mechanics, p. 828.

Watanabe, E., Sugiura, K. and Nagata, K., (1996), “Parallel computing for non-linear response of large structural systems”, Proceedings of the Sixth NTU-KU-KAIST Tri-Lateral Seminar/Workshop on Civil Engineering, pp. 143-148.

Watanabe, E., Sugiura, K., Nagata K., Niwa, K. and Kotani N., (1996), “Parallel computing for seismic response of structure-foundation system by AVS”, Proceedings of the 2nd Visualization Conference, pp. 55-57 (in Japanese).

Watanabe, E., Sugiura, K., Nagata, K. and Kitazawa, M., (1997), “Seismic behavior of highway bridge systems”, Proceedings of the Second International Conference of Behavior of Steel Structures in Seismic Areas, pp. 885-896.

Watanabe, E., Sugiura, K. and Nagata K., (1997), “Seismic behavior of elevated bridge system consisting of piers with different restoring force characteristics”, Proceedings of the 24th JSCE Earthquake Engineering Symposium, pp. 1021-1024 (in Japanese).

Watanabe, E., Sugiura, K., Nagata K., Kitazawa M. and Horie Y., (1997), “Seismic response of elevated bridge systems consisting of steel and RC piers”, Proceedings of Nonlinear Numerical Analysis and Seismic Design of Steel Bridge Piers, pp. 295-300, (in Japanese).

Watanabe, E., Sugiura, K. and Nagata, K., (1997), “Multi-phase dynamic testing system at Kyoto University, Research Prospects on Multi-Phase Dynamics”, The 100th commemoration Symposium of Department of Civil Engineering, Kyoto University, pp. 1-6 (in Japanese).

Nagata, K., Watanabe, E., Sugiura, K. and Suzuka, Y., (1998), “Development of remote parallel pseudo-dynamic testing system by using Internet”, Proceedings of Fifth Pacific Structural Steel Conference, pp. 589-594.

Nagata, K., Watanabe, E., Sugiura, K. and Suzuka, Y., (1998), “Seismic behavior of elevated bridge consisting of steel and RC piers”, Journal of Constructional Steel, JSSC, Vol. 6, pp.93-100 (in Japanese).

Sugiura, K., Nagata, K., Suzuka, Y. and Watanabe, E., (1998), “Internet related structural testing”, Proceedings of the Eighth KKNN Seminar on Civil Eng., pp. 65-70.

Suzuka, Y., Watanabe, E., Sugiura, K. and Nagata, K., (1998), “Evaluation of non-linear seismic behavior of structural system by remote parallel pseudo-dynamic testing system”, Proceedings of the Second Symposium on Nonlinear Numerical Analysis and its Application to Seismic Design of Steel Structures, JSCE, pp .207-212 (in Japanese).

Watanabe, E., Sugiura, K., Nagata, K. and Suzuka, Y., (1998), “Development of parallel pseudo-dynamic testing system and its verification”, Proceedings of the 10th Earthquake Engineering Symposium, Vol. 2, pp. 2205-2210 (in Japanese).

Watanabe, E., Sugiura, K., Nagata, K. and Oyawa, W.O., (1998), “Strength and ductility of steel piers for

bridges", Proc. of the 3rd German-Japanese Colloquium for Steel and Composite Bridges, pp.11-26.

Kunishi, R., Nagata, K., Watanabe, E., Sugiura, K. and Okashiro S., (1999), "A study on modeling and earthquake resistance of rigid-frame pier", Journal of Constructional Steel, JSSC, Vol.7, pp.125-130 (in Japanese).

Nagata, K., Watanabe, E., Sugiura, K., Yamaguchi, T. and Niwa, K., (1999), "International on-line interactive testing system through the Internet", Proceedings of the 12th KKNN Seminar/Workshop on Civil Engineering, pp.189-195.

Watanabe E., Sugiura K., Nagata, K., Yamaguchi, T. and Niwa, K., (1999), "Multi-phase interaction testing system by means of the Internet", Proceedings of the First International Conference on Advances in Structural Engineering and Mechanics, Vol.1, pp.43-54.

Watanabe, E., Sugiura, K., Nagata, K., Koike, M. and Okashiro, S., (1999), "A experimental study on elasto-plastic in-plane behavior of steel rigid-frame piers", Proceedings of the Third Symposium on Ductility Design Method for Bridges, pp.195-200 (in Japanese).

Kunishi, R., Watanabe, E., Nagata, K., Sugiura, K. and Mizutani H., (2000), "Study on in-plane behavior of steel rigid-frame piers", Journal of Constructional Steel, JSSC, Vol. 8, pp. 269-276 (in Japanese).

Watanabe, E., Sugiura, K., Nagata, K., Kunishi, R., Takei, M. and Mizutani, H., (2000), "Study on in-plane behavior of steel rigid-frame piers", Proceedings of the Thirteenth KKNN Symposium on Civil Engineering, pp. 125-130.

Watanabe, E., Sugiura, K., Yamaguchi, T. and Nagata, K., (2000), "International cooperative pseudo-dynamic testing system through the Internet", Proceedings of the Seminar on Integrated Engineering, Engineering Advances at the Dawn of the 21st Century, pp. 71-78.

Watanabe, E., Nagata, K., Sugiura, K., Mizutani, H. and Okashiro, S., (2000), "Seismic response by pseudo-dynamic testing and seismic-resistant design", Proceedings of the Third Symposium on Ductility Design Method for Bridge, pp. 299-306 (in Japanese).

Adachi, Y., Yoshihara, S., Uchida, S., Okashiro, S., Watanabe, E. and Nagata, K., (2001), "Seismic design of a rigid framed bridge pier", Proceedings of the Fourteenth KKNN Symposium on Civil Engineering, pp. 159-164.

Nagata, K., Watanabe, E., Sugiura, K., Takei, M. and Adachi, Y., (2001), "Seismic behavior of steel rigid-frame piers", Journal of Constructional Steel, Vol. 9, JSSC, pp.353-358 (in Japanese).

Watanabe, E., Yun, C.-B., Sugiura, K., Park, D.-U. and Nagata, K., (2001), "On-line interactive testing between KAIST and Kyoto Universty", Proceedings of the Fourteenth KKNN Symposium on Civil Engineering, pp. 369-374.

Watanabe, E., Kitada, T., Sugiura, K. and Nagata, K., (2001), "Parallel pseudo-dynamic seismic loading test on elevated bridge system through the Internet", Proceedings of the Eighth East Asia-Pacific Conference on Structural Engineering and Construction, Paper No. 1245 (CD-ROM).

Hata, K., Adachi, Y., Yoshimura, S., Okashiro, S., Uchida, S., Nagata, K. and Watanabe, E., (2002), “Study on load-carrying capacity of actual rigid-frame steel pier under seismic load”, Proceedings of the Forth Symposium on Nonlinear Numerical Analysis and its application to Seismic Design of Steel Structures, pp. 217-221 (in Japanese).

Nagata, K., Watanabe, E., Sugiura, K., Adachi, Y. and Okashiro, S., (2002) “Seismic performances and collapse processes of steel rigid-frame piers”, Journal of Constructional Steel, Vol.10, Japanese Society of Steel Construction, pp. 413-418 (in Japanese).

Takei M., Watanabe, E., Sugiura, K., Nagata, K., Adachi, Y. and Okashiro, S., (2002), “Collapse process of steel rigid-frame piers”, Proceeding of the Forth Symposium Nonlinear Numerical Analysis and its Application to Design of Steel Structures, pp. 145-152 (in Japanese).

Yamaguchi, T., Kishimoto, Y., Kitada, T., Nagata, K., Watanabe, E. and Sugiura, K., (2002), “Development and practical application of multi-phase pseudo-dynamic testing system by using the Internet”, Proceedings of IABSE 2002 Symposium, CD-ROM.

Watanabe, E., Nagata, K., Takei, M., Sugiura, K. and Adachi, Y., (2002), “In-plane behavior and collapse processes of steel rigid-frame piers”, Proceedings of Second International Conference on Structural Stability and Dynamics, pp. 207-212.

Watanabe, E., Sugiura, K., Nagata, K., Adachi, Y. and Okashiro, S., (2002), “Collapse processes of steel rigid-frame piers subjected to in-plane horizontal loads”, Proceedings of the Fifteenth KKCNN Seminar on Civil Engineering, pp.S169-S174.

Nagata, K., Park, D.-U., Watanabe, E., Yun C.-B. and Sugiura, K., (2003), “On-line interactive testing between KAIST and Kyoto University”, Proceedings of the Sixteenth KKCNN Symposium on Civil Engineering, pp. 115-120.

Okamoto, H., Watanabe, E., Sugiura, K. and Nagata, K., (2003), “Load-carrying capacity of steel rigid-frame piers in the arbitrary horizontal direction, Journal of Constructional Steel”, Vol. 11, JSSC, pp. 373-378 (in Japanese).

Watanabe, E., Yun, C.-B., Kitada, T., Sugiura, K., Yamaguchi, T. and Nagata, K., (2003), “International collaborative testing by using the Internet”, Proceedings of the International Civil engineering Conference on Sustainable Development in the 21st Century, pp. 587-592.